The Effects of Molecular Weight Variation of Polystyrene on its SFG spectra

Wasef Bzeih

A Thesis

in

The Department

of

Mechanical and Industrial Engineering

Presented in Partial Fulfillment of the Requirements

for the Degree of Master of Applied Science (Mechanical Engineering) at

Concordia University

Montreal, Quebec, Canada

November 2013

CONCORDIA UNIVERSITY

School of Graduate Studies

This is to certify that the thesis prepared

By: Wasef Bzeih

Entitled: The Effects of Molecular Weight Variation of Polystyrene on its SFG spectra

and submitted in partial fulfillment of the requirements for the degree of

Masters of Applied Science in Mechanical Engineering

complies with the regulations of the University and meets the accepted standards with respect to originality and quality.

Signed by the final examining committee:

_____Dr. S. Rakheja_____ Chair

_____Dr. V. Zazubovits_____ Examiner

_____Dr. M. Pugh_____ Examiner

_____Dr. P. Wood-Adams_____ Supervisor

Approved by _____

Chair of Department or Graduate Program Director

_____

Dean of Faculty

Date _____

Abstract

The Effects of Molecular Weight Variation of Polystyrene on its SFG spectra

Wasef Bzeih

Understanding the behaviour of materials at interfaces is critical for improving manufacturing processes. Interfaces can be the decisive factor in the application of materials. Several properties can be obtained from studying the interfaces such as friction, roughness, heat conductivity, reactivity, corrosion resistance, surface energy and surface tension. A very powerful technique that allows the study of interfaces is Sum Frequency Generation (SFG).

SFG is a second order, nonlinear, optical technique which is specific to interfaces. Its principle is the combination of two incident photons with different frequencies (infrared and visible) into one SFG photon with frequency equal to the sum of the incident frequencies. When the frequency of the IR photon is equal to that of the molecule's bond vibration, SFG is strongly enhanced, and its intensity increases significantly. The intensities of the collected SFG photons are graphed into a spectrum, and every peak in the spectrum is characterized by three parameters: amplitude, width and frequency center.

In this work, we intend to determine the effect of molecular weight variation of polystyrene (PS) on its SFG spectra. The peak intensities in normalized SFG spectra with respect to the product of intensities of incident IR and visible photons increase with the molecular weight. The parameters generated from fitting the experimental data into the theoretical relationship did not seem to follow the same trend like the intensities due to the complexity of this relationship. Similarly, upon calculating the orientation angle of the phenyl groups in the PS molecules, it did not seem to have any consistent pattern. However, we do not infer that there is

no relationship between the variation of parameters and orientation angle, and molecular weight. We suggest that the relationship is complicated and beyond the scope of this work.

Acknowledgements

I would like to express my deep and sincere gratefulness to my supervisor Prof. Paula M. Wood-Adams for her continuous guidance, support, generosity and wise advice in this work and in my professional future.

Special thanks to Dr. Alexei Lagoutchev in Birck Nanotechnology Center at Purdue University for his patience and efforts in helping me get a better understanding of the subject.

Thanks to Dr. Valter Zazubovits in the physics department of Concordia University and Dr. Patrick Hayes in the chemistry department of Université de Montreal for the valuable discussions that we had.

Finally, I would like to thank my parents, my siblings, my wife and my lovely son for their support and encouragement.

Table of Contents

List of Figures

List of Tables

Chapter 1

1.1 Introduction:

The science of optics has evolved so widely that it has been incorporated in various other fields of science like chemistry, biology and engineering. Spectroscopy, the study of the interaction between matter and radiated energy, has proven very effective in studying physical, chemical and even mechanical properties of materials, which in turn is improving the quality of industrial production.

Electromagnetic radiation has wavelike properties as well as particle-like properties. The wavelike properties mean that the radiation propagates at certain frequencies ranging from as low as a few kilohertz for radio waves up to the order of 10^{20} hertz for gamma waves. The choice of the type of radiation in spectroscopy depends on the nature of the application. For example, some techniques utilize infrared photons, others utilize ultraviolet photons, and other studies combine two or more types of photons.

Currently, there is a broad range of techniques available in spectroscopy, including nuclear magnetic resonance spectroscopy, x-ray spectroscopy and vibrational spectroscopy. In nuclear magnetic resonance spectroscopy, nuclei placed in a magnetic field absorb and re-emit electromagnetic radiation in the radio frequency region. X-ray spectroscopy observes the difference in energy between the excited inner electron and the replacing electron from outer orbitals. This energy difference is emitted as an x-ray photon. In vibrational spectroscopy, the vibrations of intra-molecular bonds in a molecule that occur at specific frequencies are the point of interest. Infrared photons with identical frequencies to those of bond vibrations are usually shed on interfaces, and reflected photons with different energies are collected. This collected photon provides information about the material's physical and chemical properties[1]. A major

vibrational spectroscopic application is Sum Frequency Generation (SFG), which combines infrared and visible photons, and is the topic of this thesis.

Before going deeply into SFG, it is important to briefly explain the theory of molecular motion. This theory was explored many times over the past few centuries, but the first publication to contribute effectively to the modern understanding of molecular behavior was the work of Brown in 1827[2]. His microscopical observations on particles contained in the pollen of plants gave a preliminary visualization of the theory of molecular motion. This kinetic theory states that a molecule is in continuous motion and is never at rest due to the collisions of the fast-moving particles. The molecular motion can be translational where a molecule moves from a place to another, rotational where a molecule rotates around itself, or vibrational where the molecule's bonds move within the molecule. The vibrational motion itself has various types including symmetrical stretching, asymmetrical stretching, scissoring, rocking, wagging and twisting. According to the geometry of the molecule, any combination of these types of motion can occur. SFG is based on the vibrational motion of molecules.

The kind of vibrational motion varies widely depending on the chemical composition and the structural geometry of the molecule. In other words, the type and energy of a vibrational motion in a molecule is highly dependent on its environment. As a simple example, besides the translational and rotational motions, a diatomic molecule like HCl performs stretching vibrational motion, where hydrogen and chlorine atoms move towards and away from each other[3]. More importantly, this vibration, like any other vibrational motion, occurs at a very specific frequency. This property allows almost any compound to react to electromagnetic radiation by absorption and emission of photons. An interesting variety of absorption/emission processes is shown in Figure 1.1. For example, Rayleigh scattering occurs when the molecule is

excited from the ground vibronic state (electronic state 0, vibrational state 0) up to a virtual energy state. This excitation is followed by a relaxation which brings the molecule back to the same initial state (ground vibronic state). In Stokes Raman scattering, the same thing happens, but the relaxation brings the molecule to a slightly different state: an excited vibrational state within the ground electronic state. The anti-Stokes Raman transition on the other hand starts from an excited vibrational state within the ground electronic state up to a virtual energy state, and relaxes down to the ground vibronic state. Resonance Raman scattering is similar to the Stokes Raman scattering, except that the molecule is excited to a real energy state rather than a virtual state. Sum Frequency Generation utilizes two incident photons, one from the infrared region (IR) and the other from the visible region (VIS). It is a combination of an IR absorption followed by a Raman anti-Stokes transition[4].

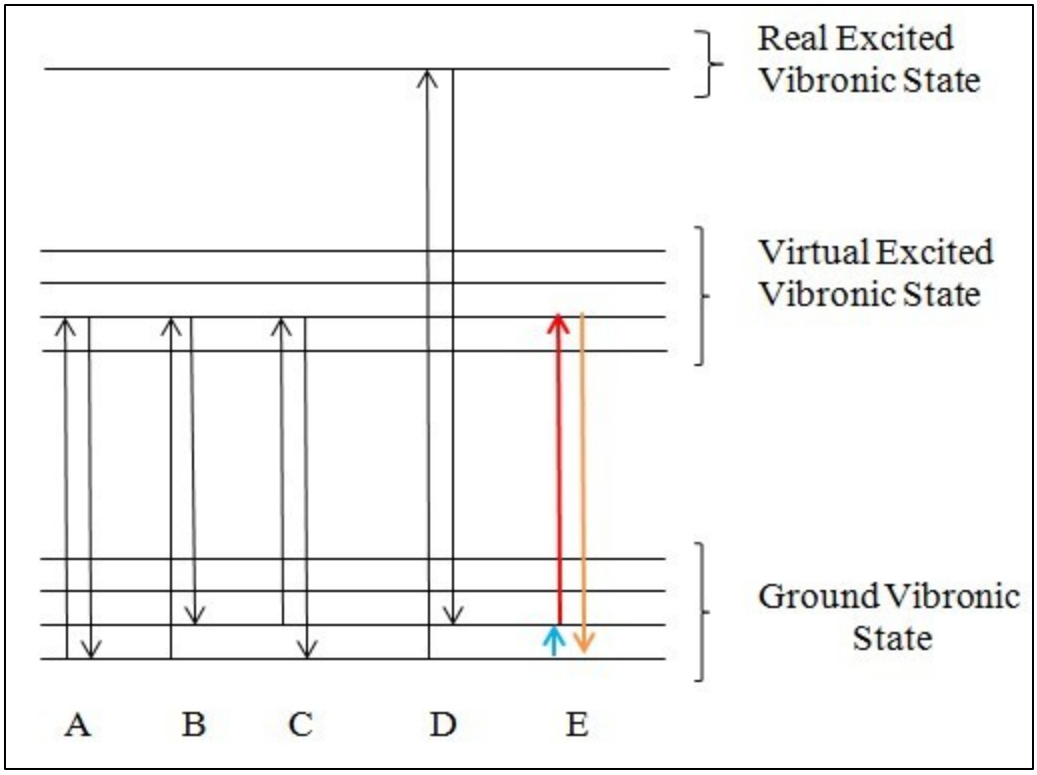

Figure 1.1: Different types of vibrational transitions. A – Rayleigh Scattering. B – Stokes Raman Scattering. C – Anti-Stokes Raman Scattering. D – Resonance Scattering. E – Sum Frequency Generation (IR Absorption + Anti-Stokes Raman Scattering).

As shown in Figure 1.2, these transitions take place between vibronic states rather than electronic or vibrational states of a molecule. A vibronic state is a vibrational state within an electronic state. A vibrational state in turn is a quantum energy level which corresponds to the behaviour of a molecular bond in a vibratory motion. An example of the vibrational state is a diatomic molecule acting as a simple harmonic oscillator. The solution to its respective Schrodinger's equation would allow us to determine the energy level and the electric dipole moment, fulfilling the selection rules that are $\Delta\nu = \pm 1$, $E = h\omega_0(\nu + \frac{1}{2})$ and $\nu = 0, 1\ldots$ This solution will include the characteristics and the physical meaning of this specific vibrational state4.

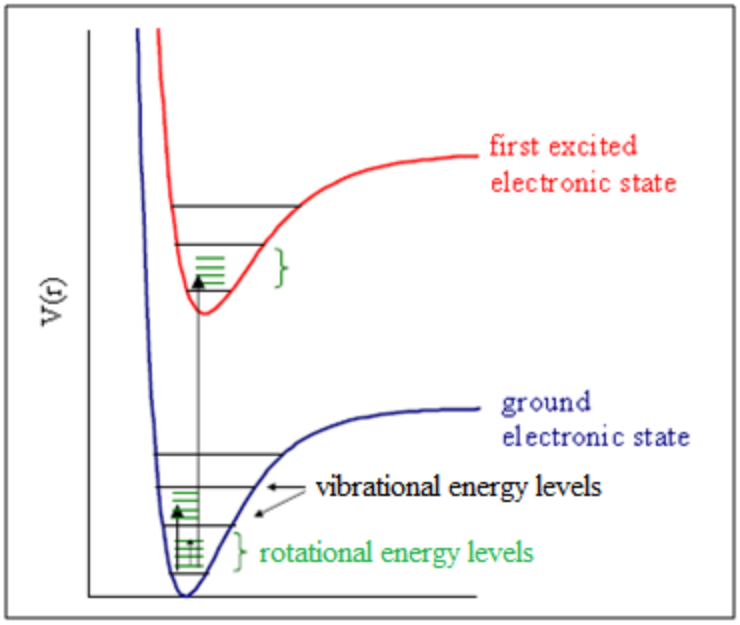

Figure 1.2: Schematic drawing of vibrational transitions between vibronic states.

Unlike diatomic molecules, vibrational motions of larger molecules are much more complicated. The types of bonds formed in the molecule, the chemical composition and the geometrical structure of the molecule all play significant roles in the vibrational behaviour. Polystyrene (PS) for example, the molecule of interest in this research, is one of the most widely used thermoplastics. It is a synthetic, aromatic polymer made from the monomer styrene according to the following chemical reaction:

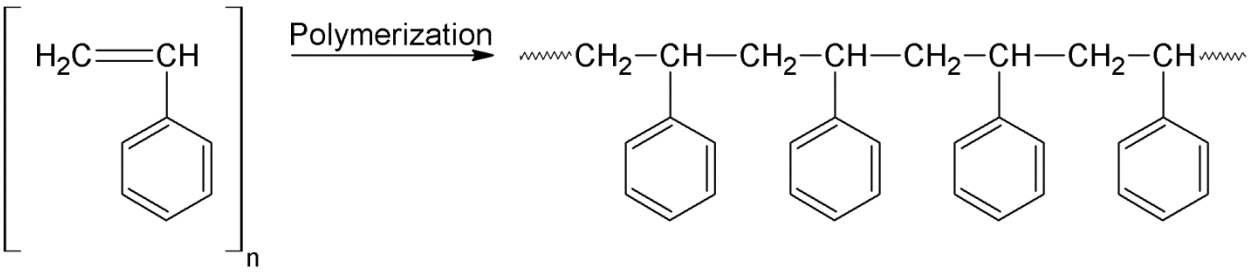

Styrene Polystyrene

It has the chemical formula $(C_8H_8)_n$ and it can form long chains with enormous molecular weights. It is in a glassy state at room temperature, with a glass transition temperature of 105 °C.

The polymerization process is simple; polystyrene is the product of numerous interconnecting styrene monomers. The carbon-carbon double bond in the vinyl group breaks and new carbon-carbon single bond forms, which links the monomer to another one. Polystyrene is stable and difficult to depolymerize because of the strength of the newly formed intermolecular sigma bond. Typically, several thousand monomers form chains of polystyrene with molecular weight of 100,000–400,000 kg/mol[5].

Polystyrene was chosen in this research project for two main reasons. First, it is easy to find, inexpensive and available as nearly monodisperse samples of a broad range of molecular weights. The second reason and most importantly, is that it is a solid at room temperature, but has a moderate glass transition temperature (~105 ^{O}C) which is suitable for annealing of the specimens5.

As shown above, polystyrene consists of a hydrocarbon backbone chain with pendant phenyl groups. The five carbon-hydrogen bonds of the phenyl groups of polystyrene have been found to have five strong vibrational modes when excited with infrared radiation[6]. Based on the group theory of molecules, these modes of vibration are assigned and sketched in Figure 1.3.

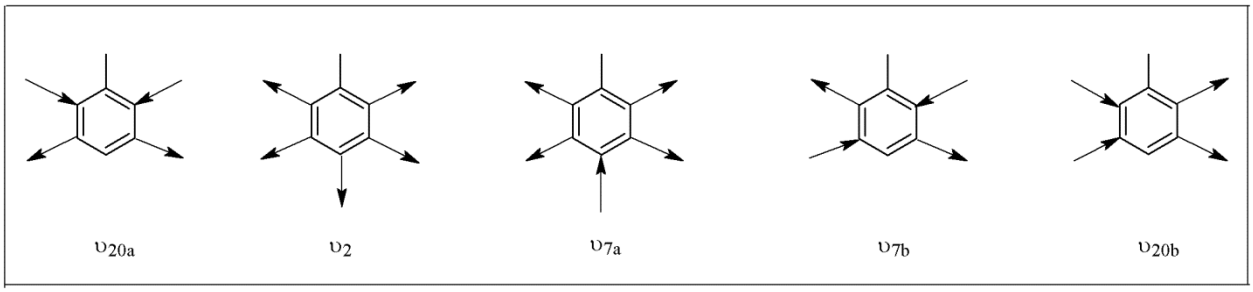

Figure 1.3: Vibrational modes of C-H bonds in phenyl groups of polystyrene.

Every one of those vibrations occurs at a specific frequency. So for example, the ν_2 vibration would be excited when the molecule is exposed to IR radiation with angular frequency

equivalent to 3069 cm^{-1}. However, if the molecule were exposed to IR radiation of frequency 3038 cm^{-1}, the ν_{7a} vibration would be excited[6].

This phenomenon of molecular vibration has been used in many different fields of spectroscopy for the sake of better understanding of various properties of materials, and especially polymers. One of the important applications is Sum Frequency Generation. Sum Frequency Generation (SFG) is a second order, non-linear, optical process that utilizes the principle of quantized vibrational behaviour of molecular bonds within the molecule on interfacial levels of materials. It is based on the interference of two photons, one from the IR range and the other from the visible range in both space and time. In other words, the photons have to arrive at the same spot on the interface, and at the same time. The result will be the generation of a photon with a frequency equal to the sum of the frequencies of the incident photons, emitted away from the sample. The reflected photons can be detected, and the output spectrum can be analyzed for information related to physical properties of the studied material[7].

1.2 Literature Review:

The work of Franken et al. in 1961[8] is considered the base from which non-linear optics has developed. The authors stated that when an intense beam of monochromatic light is shed onto a dielectric material, it can generate a second harmonic. Second harmonic generation (SHG) is the process of combining two photons with the same energies and frequencies into one photon with the sum of the initial frequencies. The authors first determined the mathematical relationship between the polarization of the dielectric and the applied electric field to be

$$P = \chi E\left(1 + \frac{E}{E_1} + \frac{E^2}{E_2^2} + \cdots\right) \qquad [1.2.1]$$

where P is the polarization, χ is the dielectric susceptibility and E is the electric field. More interestingly, the authors described how the structure of the molecule of interest affects the second harmonic generation specifically, and the frequency mixing in general. For example, the authors describe how the quartz crystal geometry governs its response to electric field, depending on the direction of the incident beam. This response is presented in the form of a combination of coordinates of the quadratic electric field and independent coefficients α and β. These coefficients are the piezoelectric coefficients, meaning the coefficients that quantify the change in the volume of the piezoelectric material once subject to an electric field.

The process of second harmonic generation is a special case of sum frequency generation (SFG). In SFG, two photons with different frequencies and energies are combined into a single photon with a frequency that equals the sum of frequencies of the two incident photons. The first IR-vis SFG spectrum was collected by Shen et al.[9] in 1986. Shen et al.[9] used SFG to observe the C-H stretching behaviour of methanol and pentadecanoic acid adsorbed on glass and water. SFG appeared to be the solution to the critical limitation of SHG which is its lack of molecular selectivity. With the ability to use a tunable infrared laser, ranges of wavelengths can be shed on

the monolayer interface, and molecular selective responses can be collected. Shen et al.[9] formulated the mathematical description of polarization for SFG as follows:

$$P^{(2)}(\omega_{SF} = \omega + \omega_{IR}) = \chi^{(2)}: E(\omega)E(\omega_{IR}) \quad [1.2.2]$$

The polarization is a function of electric fields and second order susceptibility($\chi^{(2)}$), which is in turn the summation of two parts, the resonant (from PS) and the nonresonant (from substrate):

$$\chi^{(2)} = \chi_R^{(2)} + \chi_{NR}^{(2)} \quad [1.2.3]$$

Shen et al.[9] also explained that the angle of reflection of the SF beam can be determined from the following equation:

$$\omega_{SF}\sin(\theta_{SF}) = \omega\sin(\theta) + \omega_{IR}\sin(\theta_{IR}) \quad [1.2.4]$$

This equation holds if the change in index of refraction from a medium (usually air) to another medium (usually the dielectric) is insignificant, which is what Shen et al.9 assumed to be the case. In addition, an explanation of the relationship of this equation to the critical angle, or the total internal reflection of the dielectric is not presented. This means that the SF beam can be reflected and collected up to certain geometrical limits, after which the phenomenon of total internal reflection might occur.

Shen et al.[9] also made a very important note about the second order nonlinear susceptibility, which is that the collected spectra include the resonant signal, as well as a non-resonant signal. Being the first SFG work performed, it was essential to explain how the non-resonant background from the substrate affects the SFG signal, and how it manifests in a SFG spectrum. In other words, detecting a SFG signal will allow the experimenter to identify and designate vibrational peaks, but it is very important in the process of identification to account for the signal coming from the substrate. A mathematical procedure that allows the background

signal to be identified and accounted for currently exists, but was not available in the initial work of Shen et al[9]. The importance of this factor will be explained later in this thesis.

Finally, the spectra that Shen et al.[9] were able to collect confirmed the quantization of frequency for every vibrational mode, and the capability of the SFG technique to identify the specific molecules. The major factor in determining that SFG is an efficient technique for molecular identification is the fact that SFG can be applied on dielectric materials that are IR and Raman active. In his work, however, Shen did not present the IR and Raman spectra of the materials that he performed SFG on, methanol and pentadecanoic acid. It was very important to show the IR and Raman spectra of these two chemicals, and employ them to prove that these vibrational peaks identified here actually exist and can be used in the chemical structure and compositional analysis.

Shen et al's work[9] opened the gates wide in front of many scientists to utilize this new technique for various kinds of studies. SFG started becoming popular when it proved efficient in studying interfaces with molecular selectivity, which was a major limitation. As a commonly used polymer, polystyrene has been studied using SFG numerous times, leading to very important results about its structure at interfaces.

The work of Dhinojwala et al. in 2000[10] is considered one of the important studies of polystyrene (PS) using SFG, because it includes spectra collected from the free PS/Air interface, as well as from the buried PS/substrate interface. The first significant contribution of this work was clarifying the dependence of SFG signal on incident angles of visible and IR beams. This partially solved the limitation of the equation of Shen et al.[9] [1.2.4] which was presented earlier, and gave an example of the effect of incident angles on the SFG signal. With the assistance of a prism on top of the polymer film, it was determined that the strongest SFG signals for both

PS/Air and PS/substrate are generated when the angle between the incident IR beam and the surface normal line was equal to the critical angles; 36 degrees for PS/Air and 64 degrees for PS/sapphire. A schematic of the setup is shown in Figure 1.4. This conclusion is limited, with acceptable range of accuracy, to some conditions like temperature, humidity and the index of refraction of the materials.

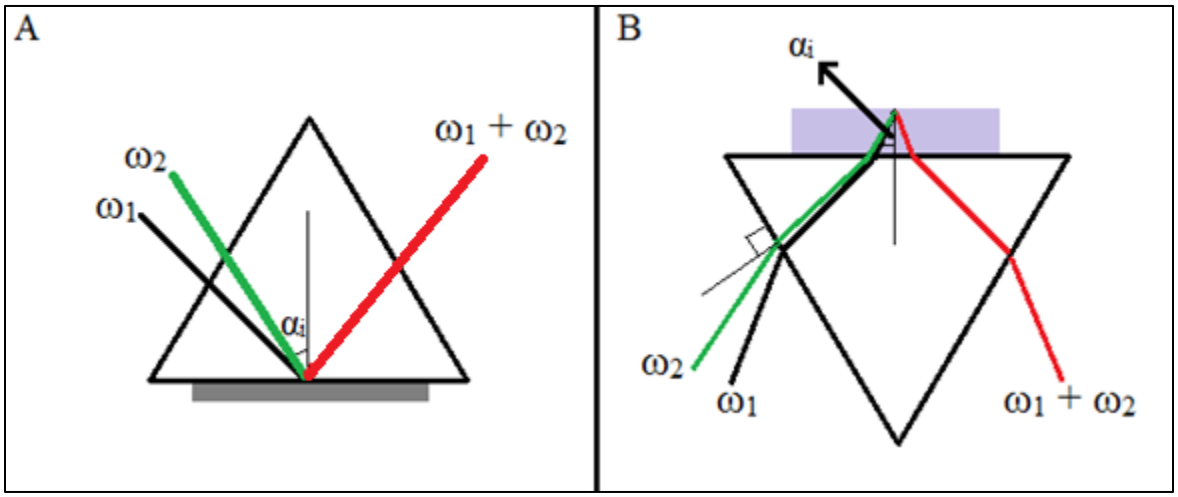

Figure 1.4: Schematic of total internal reflection at A: buried interface and B: polymer/air interface

Moreover, SFG spectra from both interfaces were collected at two polarizations: ssp (S-SFG, S-VIS, and P-IR) and ppp. For PS/Air interface, five different peaks were identified at five different frequencies: ν_{20b}, ν_{7a}, ν_{7b}, ν_2, and ν_{20a} at 3027 cm^{-1}, 3038 cm^{-1}, 3058 cm^{-1}, 3069 cm^{-1} and 3082 cm^{-1} respectively. The same peaks existed for PS/sapphire interface, but at slightly different frequencies: ν_{20b}, ν_{7a}, ν_{7b}, ν_2, and ν_{20a} at 3023 cm^{-1}, 3037 cm^{-1}, 3059 cm^{-1}, 3069 cm^{-1} and 3081 cm^{-1} respectively. The same issue that was explained when discussing Shen et al.'s work9 applies here. As a unique work, an explanation and presentation of deciding the peak frequency centers of polystyrene SFG spectra are based on IR and Raman spectra. However, these data were neither presented nor tabulated for comparison. In fact, these peaks have been reported by

other scientists, and different designations and frequencies were presented elsewhere. Even the number of peaks was not the same sometimes. The IR and Raman spectra allow us to determine this information.

The Lorenzian form of the SFG intensity equation relates this intensity to the peak center (ω_q), amplitude (A_q), and damping factor (Γ_q). Using the collected SFG data, Dhinojwala et al.[10] were able to fit this data to the equation, and generate a table of parameters. This table includes amplitudes of the five peaks mentioned above, their peak center and their damping factor for ssp and ppp polarizations.

After performing the fitting, the amplitudes of every peak were used to determine the orientation angle of the polystyrene molecules using a technique that they developed. We will be using this technique in determining the tilt angle of the phenyl groups of the PS molecules on the PS/air interfaces of the films that we formed in our study. The conclusion of Dhinojwala et al.[10] was that the tilt phenyl rings of the polystyrene are almost parallel to the surface normal at the PS/Air interface, and they are almost perpendicular to the surface normal at the PS/sapphire interface. It is significant to note that this conclusion regarding the determination of orientation angle of phenyl groups in PS cannot be generalized. It is important to understand that the length of the chains, governed by the molecular weight of the polymer, may be an important factor in this behaviour, as we explore in this work. As the molecular weight increases, the chain length increases. This change in molecular chain length might in turn be responsible for orientation angle changes as well. In fact, the point of this thesis is to explain, if any, the effect of molecular weight of polystyrene on its SFG spectra, via analyzing the vibrational behaviour of the chains on the interfaces. In addition, we will present an accurate, quick and simple qualitative experimental approach of sample preparation and SFG spectra collection which takes into

consideration various factors that might affect the process of SFG. This will allow future researchers to have a detailed and easy guide to follow while preparing samples and collecting SFG spectra, which was never presented before.

The final contribution of Dhinojwala et al's work[10] was collecting SFG spectra for polystyrene at 200 ^{O}C, which is about 100 ^{O}C above its glass transition temperature. These spectra were very similar to those collected at room temperature, which allowed Dhinojwala et al.[10] to deduce that the molecular surface structure of polystyrene when in its glass state is not different than when PS is in the melt state.

Another significant piece of SFG work on PS was that done by Richter et al. in 2001[11]. Since a dielectric material must be Raman and IR active in order to be studied by SFG, Richter et al.[11] used and presented the Raman and IR spectra of polystyrene to determine the peak frequencies and designations for his SFG data. This is considered an important step, because as explained earlier, the designations primarily depend on IR and Raman spectra of the material. The IR spectrum of PS showed five peaks around 3000 cm^{-1}, 3027 cm^{-1}, 3060 cm^{-1}, 3083 cm^{-1}, and 3104 cm^{-1}. The Raman spectrum, on the other hand showed four peaks at 3000 cm^{-1}, 3034 cm^{-1}, 3050 cm^{-1} and 3060 cm^{-1}. Using this information, it was concluded that the SFG spectrum of PS will have 5 peaks with frequencies very close to those. Upon completing the fitting of the spectrum, five vibrational modes were detected at frequencies 3024 cm^{-1}, 3035 cm^{-1}, 3054 cm^{-1}, 3066 cm^{-1} and 3078 cm^{-1}., and two combination bands at 3004.2 cm^{-1} and 3101 cm^{-1}. A combination band is an absorption band that appears at $\nu_1+\nu_2$ where ν_1 and ν_2 are fundamental frequencies.

Another contribution of Richter et al.'s work[11] was a study of the effect of film thickness on SFG intensity. The SFG intensity coming from the free PS/Air interface was determined to be

maximized when the film thickness is around 130 nm. The study was carried out at the frequency of the highest PS peak (ν_2), 3066 cm^{-1}. The graph that shows the variation of Fresnel weight (line) and the experimental SFG intensity (dots) as a function of film thickness is shown in Figure 1.5, which is copied from Richter et al.'s work[11]. It is important to note here that because other vibrational modes appear with different intensities on the PS spectrum, it is also very possible that they might behave differently with different thicknesses. This was not explained in Richter et al.'s work[11].

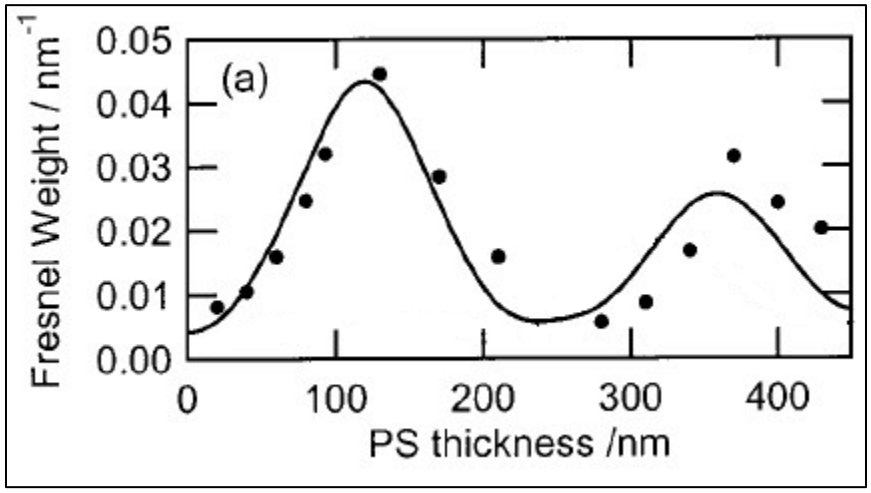

Figure 1.5: Cropped and modified from [11]: Variation of SFG intensity at ν_2 and calculated Fresnel weight for SSP as a function of film thickness. Solid line: Calculated Fresnel weight. Dots: SFG intensity

Richter et al.[11] also offered theoretical interpretation to his experimental results, by providing the calculations of the Frensel weight, which is a mathematical indicator of the intensity of SFG. Interestingly, the values of Frensel weights varied with thickness in a way that qualitatively agreed with the experimental results. The results were not very different when the study was done at the buried SiO_2 interface. The highest SFG intensity and highest Frensel

weight values were when the film thickness was around 130 nm. The Fresnel weight for the bulk of the PS film was different in that it increased and had a maximum at around 400 nm.

Another important contribution of Richter et al.'s work[11] was the determination of the molecular orientation of the phenyl rings of PS. They were shown to make an average angle of 57° with the surface normal, on the free interface. It was shown, however, that if the orientation angle were based on ratios of different peaks, the value might change, so some uncertainty as to its value and the approach for its determination remains.

As explained so far, the infrared and Raman spectra are very important in SFG studies, especially for assigning the fundamental vibration modes detected in SFG. For this reason, the work of Liang and Krimm in 1958[12] is important for our work. It presents the IR and Raman spectra of polystyrene, and explains the assignment of the modes.

Liang and Krimm[12] start with a critical assumption which is to treat each monomer in the polystyrene polymer as a monosubstituted benzene ring. This allowed them to choose C_{2v} as the point group for the molecule. Point group is a chemical system of differentiation based on the geometry of the molecule. In other words, the geometry of the molecule governs what kinds of symmetry operations can take place in this molecule. The allowed symmetry operations are those that when applied, the molecule will be in a form that is undistinguishable from its original form. The group of symmetry operations that a molecule can undergo defines the point group to which it belongs. As a result, Liang and Krimm[12] expected that there are 30 vibrational modes for polystyrene between 70 cm^{-1} and 3200 cm^{-1}, which based on calculations, are distributed as follows: $11A_1 + 3A_2 + 10B_1 + 6B_2$. In the A_1 fundamentals, they assign three of the 11 modes as C-H stretching, while the rest are C-C stretching, H bending and C-H that is moving as a whole unit. They assign these 3 C-H stretching units as follows: ν_{20a} at 3029 cm^{-1}, ν_{7a} at 3056 cm^{-1} and

ν_2 at 3066 cm^{-1}. As for the 10 B_1 fundamentals, there are two C-H stretching modes assigned as ν_{7b} at 3038 $cm^{-1}$and ν_{20b} at 3083 cm^{-1}. The remaining 25 vibration modes do not relate to the C-H bonds in which we are interested in this work.

Interestingly, the assignments of vibration modes on C-H bonds in the phenyl group of PS molecules are not unique. So far, we have seen three different designations. This is because of the methodology that every group follows in determining the vibration mode characteristics. For example, Richter et al.[11] referred to the "ab initio Hartree-Fock (HF) and density functional theory (DFT) calculations for toluene" in order to determine the assignments for the vibrational modes of PS [13]. Liang and Krimm[12] used Wilson's methodology of vibrational mode numbering[14]. On the other hand, Dhinojwola et al.[10] used Varsanyi's method to determine the assignments[15]. In our work, we follow Dhinojwola's mode assignments and orientation angle determination methodologies because of the availability of all required information from both literature and experiments.

The previous discussion has been focused on works done on untreated PS thin films on different substrates. It is interesting, however, to see the effect of some kinds of surface treatment on SFG spectra of PS. The work of Yeganeh et al. in 2000[16] studied the effect of UV irradiation and plasma treatment on SFG spectra of polystyrene.

Yeganeh et al.[16] started by presenting SFG spectra of PS before any treatment on three polarizations: SSP, SPS and PPP, and then showed the spectra of treated surfaces. Throughout their study, they focused on the main peaks which had detectible intensities rather than all peaks that had been identified previously. This makes the study more qualitative than quantitative, and focused on the visible effects of treatments. However, nonlinear fitting of spectra could have

been done, and sets of parameters could have been collected, compared and contrasted and could have a more in depth understanding of the molecular structure.

In their work, Yeganeh et al.[16] presented spectra of PS after UV irradiation and plasma treatment, which show several changes when compared to the untreated PS. These changes are basically a decrease in intensity of some peaks, absence of others, and appearance of new peaks. The explanation that they have provided is that the polymer was undergoing chemical reactions that produced new functional groups, which have different vibrational modes. The plasma treatment, for example, increased the level of oxidation on the surface, producing carbonyl/carboxyl groups, also confirmed with XPS and contact angle studies.

Another work that studies the effects of changes in the environment on the SFG spectra is that done by Opdahl and Somorjai in 2002[17]. SFG spectra from polystyrene/air and pure toluene/air interfaces were collected for later comparison with treated polystyrene films. After polystyrene films were placed under toluene vapor pressure for 30 minutes, SFG spectrum of PS/air interface was similar to that of toluene/air interface, suggesting that the toluene placed itself on the interface and disturbed the order of the phenyl groups of polystyrene. In order to confirm this conclusion, deuterated toluene (toluene-d_8) was used with the same experimental setup. The absence of C-H vibrational modes in toluene-d_8 means that there should be no C-H vibrational peaks from the toluene-d_8. That was exactly what they observed. After the toluene was allowed to evaporate, the SFG spectrum of PS/air interface looked exactly like the spectrum from PS/air interface without treatment. This means that the phenyl groups on PS/air interface rearranged themselves to their original orientation, close to the surface normal.

The significance of this work for our work is that it is a reliable proof that the solvent that we used, toluene, is not affecting our SFG spectra. However, again, it would have been more

valuable to determine the sets of parameters from the nonlinear fitting, and study the effect of toluene vapor quantitatively. This will allow the reader to analyze and calculate the orientation angle change. In addition, determining the orientation angle depends on the ratios of A_q values from different peaks. In the work of Opdahl and Somorjai[17], the only peak that was investigated was the symmetric ν_2 stretch at ~ 3060 cm^{-1}, and the methodology of determining the orientation angle which normally requires at least two peaks was not explained.

Many other works focused on the PS/solid and PS/liquid interface, or what is called a buried interface. The work of Yang et al. in 2004[18] studies the SFG spectra of interfaces of deuterated PS with various liquids. The aim of this study was to understand the effect of interfacial energy on PS interface structure. The IR range studied was between 2100 cm^{-1} and 2350 cm^{-1}. The spectra of interfaces from the PS/methanol, PS/ethanol and PS/hexane interfaces were quite similar, and those from the PS/water and PS/glycerol interfaces were also similar, but completely different from the first group. Upon investigating the orientation angles of the phenyl groups of the PS molecules at the buried interfaces, it was found also that the angle of the first group was close to that of PS/air and the angle of the second group was close to that of PS/Au. The suggested explanation lays in the difference of the surface tension of the liquids. For the first group, the surface tension is low, which makes the PS spectra at their interfaces similar to that of PS/air. The liquids in the second group have high surface tension making their spectra comparable to SFG spectra of PS/Au performed in previous works.

Yang et al.[18] focused on the vibrational modes of the hydrocarbon backbone chain of polystyrene like discussed above, and did not investigate the vibrational modes of the aromatic phenyl group lying in the IR range between 3000 cm^{-1} and 3100 cm^{-1}. The orientation of phenyl groups must be determined from the vibrational modes of the phenyl groups using the parameters

obtained from the fit. Studying this IR range could have provided valuable information about the behaviour of aromatic phenyl groups and their vibrational modes at the buried interfaces with liquids that have different surface energies. The industrial importance of this study is that it can improve synthesis, mixing, storage and transportation of polymers with higher efficiency and lower cost.

SFG is getting more popular every year because it has proven to be a powerful tool in numerous fields, especially in chemical analysis. Nevertheless, it is important to know how this tool can be helpful in real life, and what the extracted chemical information can offer to industry. First, it is important to understand that surfaces and interfaces of materials are very critical and give great amounts of information about the behaviour of the material in important applications. For example, surfaces and interfaces are very critical in corrosion, electrochemical reactions, adsorption, wetting/dewetting, and friction. All of these properties are affected by the local molecular structure. This is what makes SFG, an effective tool for studying surfaces, important.

Advanced applications of SFG have become available. Flörsheimer et al. in 1999[19] and Kuhnke et al. in 2003[20] have utilized the sum frequency generation technique in sum frequency microscopy, and were able to perform chemical imaging of several chemicals. It is based on the utilization of a SF technique with an optical microscope, which is capable of collecting and displaying the photons into a physical image with exposure time of about 2-3 hours. The interesting thing about sum frequency imaging is that, like shown in Figure 1.6, the images collected for the same material under different IR frequency are different. This is because at different IR frequencies with the visible frequency fixed, different vibrational modes are detected. This means that the collected and observed sum frequency photons will have amplified intensities at different frequencies, leading to different detectable images.

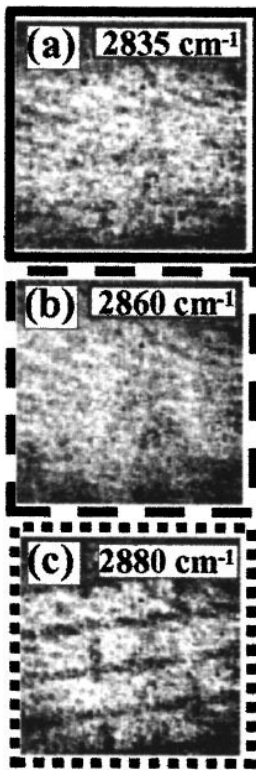

Figure 1.6: Cropped from [19] showing SF images of self-assembled monolayer of thiolates at different IR frequencies.

SFG has found its way through biology as well. For example, the work of Thirty et al. in 2004[21] utilized the SFG technique to study and model biosensor systems. Biosensors are very critical in biology, because they are the devices that detect biological phenomena by physical signals. With the extensive usage of biosensors on many unicellular and multicellular organisms, including human beings, the study of interaction of these devices with intracellular environments on the interfacial levels is quite important. Their work focused on artificial interfaces between the vitamin biocytin and substrates instead of focusing on the interfacial behavior of this vitamin with real cellular environment. It is understandable that the interaction will occur between the electrode of the biosensor and the body, but the choice of biocytin could have been improved if replaced by blood for instance. In other words, rather than studying biocytin/metal interface, it

could have been more interesting to study cellular plasma/metal interface or biocytin/amniotic fluid interface for example.

Sartenaer et al., on the other hand, studied different interfaces of DNA monolayersin 2006[22]. This work has provided a brief and simple understanding of the nature of interaction between the DNA and buffers from the nuclear culture in the cell. The most important conclusion of this work is the disordered arrangement of the oligonucleotide chains. This was observed by the lack of SFG contribution from the DNA strands. Since the cell is much more complicated than a simple DNA strand in a buffer, it is important to note that this conclusion might not be true. This conclusion can only be confirmed when the study is performed in situ with all organelles active and chemical compounds present.

The significance of any SFG spectrum is contained within the chemical information that can be extracted from it. However, extracting the correct and meaningful information from any SFG spectra can be complicated and not at all trivial. For example, performing comparisons and contrasts between absolute SFG spectra is difficult and needs more advanced SFG systems. The way that most researchers have been doing it is to normalize the collected SFG spectra of interest. Subsequent to normalization, many researchers then use nonlinear curve fitting to get a set of parameters that will be used to formulate conclusions about the material. The work of Busson et al. in 2009[23], however, explained that the collected set of parameters - or generator as they call it - is not necessary unique. In other words, there might be several sets of parameters that can lead to the exact fit, but to different chemical information.

According to Busson et al.[23], any SFG spectrum with N resonant vibrational modes can have up to 2^Nparameters. In order to collect these parameters, they have formulated a mathematical algorithm. This mathematical algorithm assumes that the frequency peak center

and the damping factor of the vibrational modes are constant, and that the only variable is the amplitude of the peak, A_i. The assumption that the peak center must remain the same for all parameters is legitimate, based on the IR and Raman spectra of the studied material. However, the assumption that the damping factor must be the same is not necessarily appropriate. Based on the analysis of Busson et al.[23] they have written the most general formula for the second order susceptibility with a reduced denominator, where the resonant frequency center and the damping factor have been combined into one term (ω_i). This reduction is the base from which the fixed damping – or peak width – assumption started. In other words, when the fitting procedure is performed, set of (3N + 1) parameters can be collected. These parameters are the nonresonant susceptibility, peak amplitudes, widths and frequency centers. During the fittings, sets of parameters can be generated, but some have meaningless values. This is when other fits are performed, and new iterations are done. Although the fit might look perfect, the set of parameters can seem wrong and not make physical sense.

Using this logic, it is important to understand that when new set of parameters are found using the fitting procedure, damping factor values change as well as amplitudes. Fixing the width as Busson el al.[23] have done necessarily means that this is its true value. It is important, nevertheless, to try to generate other sets of parameters with different values of the damping factor. It is possible that this might improve the reliability of the chemical information extracted from the spectra. Regardless of this assumption, and assuming that the fixed frequency and widths are correct, following the algorithm of Busson et al.[23] generates new and improved parameter sets from which chemical information can be extracted.

1.3 Theory

Sum Frequency Generation (SFG) is a second order, non-linear optical process. It is a more general form of the second harmonic generation phenomenon where two photons of equal frequencies generate one photon with double the frequency of the incident beam ($\omega_{SHG} = 2\omega_i$). SFG is a frequency mixing process, where the incident photons do not have the same frequency:

$$(\omega_{SHG} = \omega_{vis} + \omega_{IR}) \qquad [1.3.1]^{24}$$

The electrical fields of the incident beams induce electrical dipole moments in the nonlinear material (dielectric). The induced dipoles modify the incident beam and for strong optical fields lead to the generation of new photons (SFG) with new frequencies. Like Figure 1.7 demonstrates, an infrared (IR) photon and a visible (VIS) photon intersect both temporally and spatially on the interface of the sample, to generate a single photon (SFG) with frequency equalling the sum of frequencies of the IR and VIS photons.

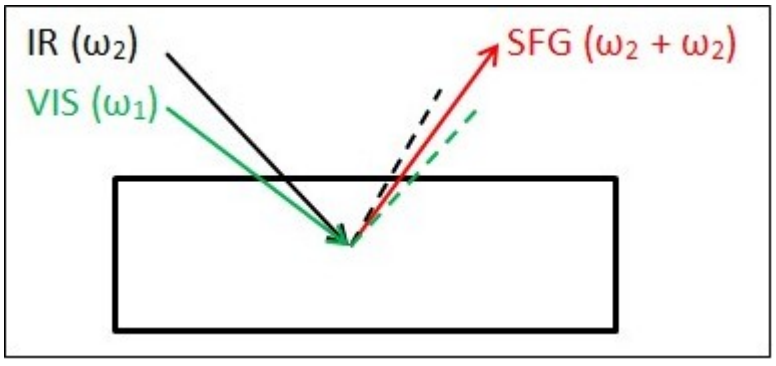

Figure 1.7: Demonstration of SFG phenomenon

Dielectrics are different from conductors and insulators in that when they are exposed to an electric field, the electric charges do not flow through the material, but move a little from their equilibrium position. This state that they are in when under the effect of an electric field is called

dielectric polarization[25]. This polarization in the absence of any external electric field is approximated to be $P = \varepsilon_0 \chi E$, which is linear. In this case, the only electric field that the dielectric feels is the weak intermolecular electric field of the electrons. However, with the strong field created by the incident beams during sum frequency generation, this approximation does not hold, because it does not show the contribution of the strong electric field; i.e. where there are two incident beams creating an electric field on the dielectric[24]. The polarization of the sum frequency generating dielectric is corrected to be

$$P_k = \varepsilon_0\left(\chi_{ik}^{(1)} E_i + \chi_{ijk}^{(2)} E_i E_j\right) \qquad [1.3.2]^{24}$$

So this is where the phenomenon of sum frequency generation gets its non-linearity and its second order. In SFG, when the two incident beams with frequencies ω_1 and ω_2, and with respective amplitudes $E_{0,1}$ and $E_{0,2}$ intersect, the first nonlinear term appears and leads to mixing.

But

$$E_i = E_{0,1} \cos(\omega_1 t) \qquad [1.3.3]^{24}$$

and

$$E_j = E_{0,2} \cos(\omega_2 t) \qquad [1.3.4]^{24}$$

then the first nonlinear term in Equation [1.3.2] becomes as follows[18]:

$$P^{(2)} = \chi^{(2)} : E_{0,1} \cos(\omega_1 t)\, E_{0,2} \cos(\omega_2 t) \qquad [1.3.5]^{24}$$

where each term corresponds to the energy of one of the input beams (IR and vis).

Equation 1.3.5 shows the nonlinear form of the polarization of a dielectric under the effect of a strong external electric field. Susceptibility (χ) is the proportionality constant between dielectric polarization (induced dipole moment per unit volume) and electric field. It represents the macroscopic response of the dielectric material to the applied electric field. In the case of second order processes of nonlinear optics, it is a third rank tensor with 27 elements[24].

The elements of the susceptibility tensor are governed by the molecule's symmetry. Where there is inversion symmetry, the elements of susceptibility vanish because dipole contribution is forbidden by symmetry. Where this symmetry breaks, the corresponding elements have non-zero values[24].

In order to understand the meaning of inversion (or centro-) symmetry, Figure 1.8 shows a simple schematic of the bulk of water with air molecules on top. Taking any smaller portion of the bulk (red hexagon) and performing inversion on any axis passing through the center molecule, the resulting conformation will be identical and indistinguishable from the original conformation. However, on the interface, where molecules of different nature adsorb, this inversion symmetry is broken. For example taking the top layer of molecules on the surface of the water medium in contact with the air molecules as shown in Figure 1.8 (blue hexagon) and trying to perform vertical inversion will result in air molecules inside the water bulk and vice versa. This means that the final conformation is not identical to the original one, and inversion symmetry is broken.

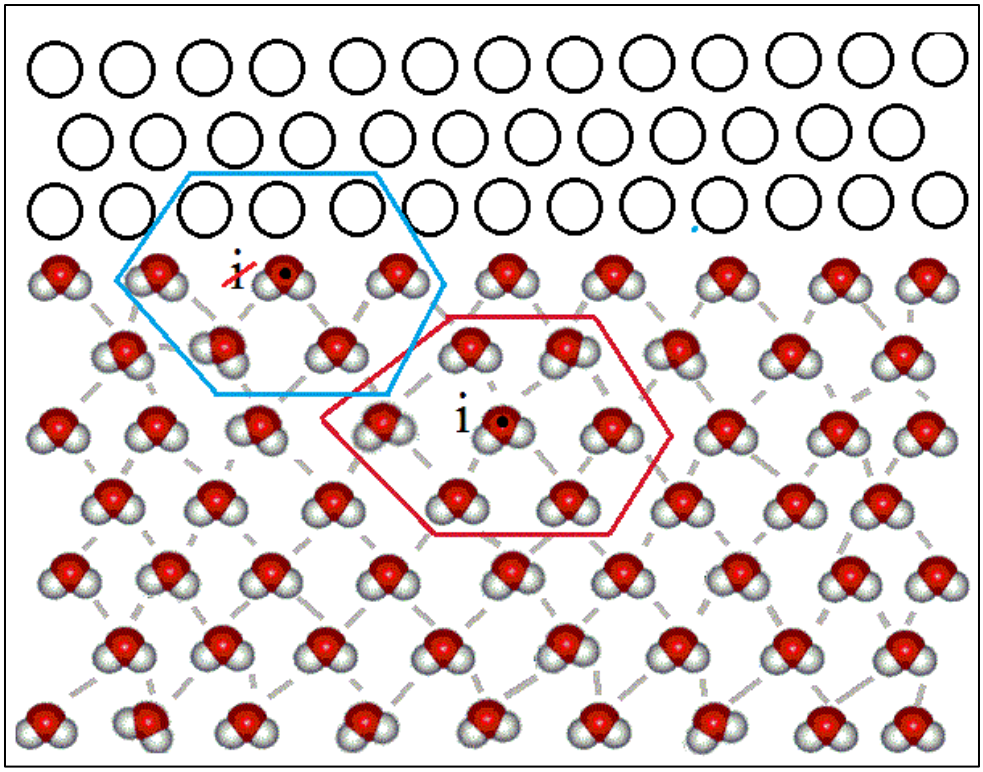

Figure 1.8: Schematic representing inversion symmetry in the bulk and how it is broken on interface.

In the bulk of material due to its centro-symmetric nature, molecular bonds can either be IR active or Raman active, but not both. However, on surfaces, breaking the inversion symmetry allows the molecules to be both IR and Raman active. One of the primary conditions for SFG is that the dielectric must be both Raman and IR active. This is why sum frequency generation is interface selective[24].

The inversion symmetry in the bulk leads to zero elements in the susceptibility tensor. However, this symmetry is broken on surfaces, meaning that there are non-zero elements in the tensor. This is what allows SFG to be surface specific on the order of few angstroms. In addition, the susceptibility consists of two fractions: resonant and non-resonant. The resonant susceptibility is the part that was explained above, which is the result of molecular vibrations at

the interface. The non-resonant is that coming from the substrate and it does not change very much within the tuneable spectral infrared range investigated.

The sum frequency generation process is an IR excitation followed by anti-Stokes Raman transitions. As shown in Figure 1.9, the process starts at the ground vibronic state which is the state of molecular electronic and vibrational relaxation. After the IR photon bombards the molecular vibration at $\upsilon_{vib} = 0$, the vibration gets excited to a new level, $\upsilon_{vib} = 1$ within the same electronic state. Then, the visible photon excites the electron from this vibrational state into a new vibrational state within a new electronic state that can be real or virtual. Finally, the energy absorbed from both exciting photons (IR and VIS) gets emitted as a single SFG photon with energy equaling the sum of the energies of both incident photons, returning the molecule to its initial vibronic ground state. The transition from $\upsilon_{vib} = 1$ of the ground electronic state up to the virtual (or real) electronic state, and then back to the ground vibronic state is the anti-Stokes Raman scattering transition[26].

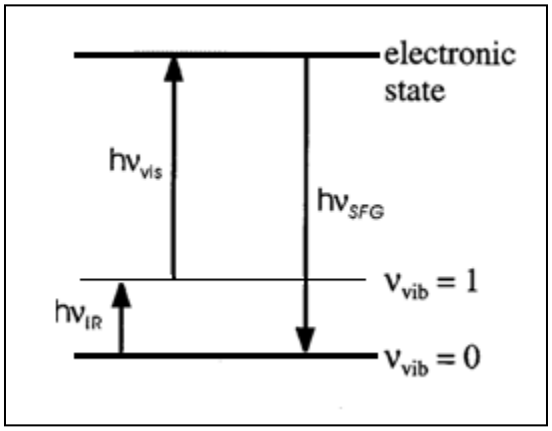

Figure 1.9: Schematic of the SFG process (involves IR and Raman transitions).

The sum frequency generation process requires two major conditions to happen efficiently. The first condition is spatial and temporal superposition of IR and visible photons on

the interface. This ensures that the frequency coupling is taking place between all possible incident photons, generating as many sum frequency photons as possible. If the superposition is not accurate, many incident photons will be lost, and the possibility of frequency coupling will decrease dramatically[24, 26].

The second condition is that the frequency of the IR incident beam should be as close to the resonant vibrational frequency of the molecule as possible. In other words, the tunable frequency of the IR beam should be identical to the frequency at which the intramolecular bond is vibrating. If this is not the case, no sum frequency photon can be generated because the vibration will not be enhanced, and its intensity will not increase. Again, this can be explained in the energy level diagram shown in Figure 1.9. The energy states are quantized, and the vibrational states take place at certain frequencies. To enhance the vibration and raise it to a higher level, the exact energy is required. Otherwise, no SFG takes place[24, 26].

In order to relate the SFG intensity and the dielectric polarization, it is important to note that the susceptibility (χ) is equal to the product of hyperpolarizability (β) and the number of molecules in a specific volume (N); i.e. $\chi = N\beta$[24]. The importance of this relation is that the polarization (P) is directly proportional to susceptibility, and the susceptibility is dependent on the molecular hyperpolarizability. This ideal situation is true assuming no interaction between molecular fragments. The equation that relates susceptibility and SFG intensity is:

$$I(\omega_{SF}) \propto \left|\chi^{(2)}\right|^2 = \left|\chi_{eff,NR} + \sum_q \frac{A_q}{\omega_2 - \omega_q - i\Gamma_q}\right|^2 \qquad [1.3.6]9, 10, 11, 23, 24, 26$$

where A_q, ω_q and Γ_q are the amplitude, peak center frequency and peak width of every vibrational mode (q). This relation shows that the SFG intensity is directly proportional to the second order susceptibility, which is in turn divided into two parts

$$\chi^{(2)}_{eff,ijk}(\theta) = \chi^{(2)}_{sub,ijk} + \chi^{(2)}_{int,ijk}(\theta) \qquad [1.3.7]^{24}$$

where $\chi_{sub,ijk}$ is the effective non-resonant susceptibility appearing in equation [1.3.7].

Equations [1.3.6] and [1.3.7] assume that these two signals are perfectly coherent, meaning that the phase shift between the signals is not changing. If the signal intensities of the resonant (I_R) and the non-resonant (I_{NR}) are written in their general complex forms, they will be

$$I_R = Ae^{i\varphi} \qquad [1.3.8]$$

and

$$I_{NR} = Be^{i\theta} \qquad [1.3.9]$$

A and B are the amplitudes of the resonant and non-resonant signals respectively, and φ and θ are the phase shift angles of the resonant and non-resonant signals respectively. The modulus of these two signals is

$$Modulus = \left|Ae^{i\varphi} + Be^{i\theta}\right| \qquad [1.3.10]$$

Since the SFG signal is proportional to the square of the modulus, then it can be written in the following form:

$$I_{SFG} = \left[Ae^{i\varphi} + Be^{i\theta}\right]\left[Ae^{-i\varphi} + Be^{-i\theta}\right] \qquad [1.3.11]$$

which is equal to:

$$I_{SFG} = \left[A + Be^{i(\varphi-\theta)}\right]\left[A + Be^{-i(\varphi-\theta)}\right] \quad [1.3.12]$$

After multiplying we get:

$$I_{SFG} = A^2 + B^2 + AB\left[e^{-\mathrm{i}(\varphi\,-\,\theta)} + e^{\mathrm{i}(\varphi\,-\,\theta)}\right] \quad [1.3.13]$$

Using Euler's formula:

$$e^{ix} = \cos(x) + i\sin(x) \quad [1.3.14]$$

we end up with what is called the cosine theorem:

$$I_{SFG} = A^2 + B^2 + 2AB\cos(\varphi\ -\ \theta) \quad [1.3.15]^{27}$$

The derivation presented above is necessary and important in the process of the spectrum analysis. In particular, it will allow us to understand the physical meaning of a skewed peak and a dip in a SFG spectrum.

For further elaboration, we present one unique example. Consider the particular case when the phase of resonant, $\varphi = \pi$ (180 ^{O}), and that of non-resonant, $\theta = 0$ ^{O}. Analyses of other phase angle combinations are possible, but very complicated and out of the scope of this work. The result of equation [1.3.15] will be

$$I_{SFG} = A^2 + B^2 + 2AB\cos(\pi) = A^2 + B^2 - 2AB \quad [1.3.16]$$

There are three conditions that this equation can be in. The first condition is when the amplitudes of the resonant and non-resonant signals are equal ($|A| = |B|$). In this case, the SFG signal will be cancelled, and will go to zero. This is when a "dip" appears in the SFG spectrum, because the resonant and non-resonant signals cancelled each other, and the SFG signal goes below the non-

resonant background. The SFG spectrum of PS/air interface can have a dip at 3027 cm^{-1} as indicated by the red circle in Figure 8. It is important to note that this dip will be represented by a negative value of amplitude for the corresponding vibrational mode in the fitting parameters, as shown below:

$$Ae^{i.\pi} = A[\cos(\pi) + i\sin(\pi)] = -1A \qquad [1.3.17]$$

The second condition is when the resonant amplitude A is much bigger than the non-resonant amplitude B. The square of non-resonant amplitude, B^2, becomes negligible, and the cross term 2.A.B reduces the resonant peak by skewing it. Thus, the dip will turn into skewed peak because of the cross term. An example of this case is the second peak at 3037 cm-1 in the SFG spectrum from PS/air interface which can have a skewed peak as indicated by the blue circle in Figure 1.10.

The third condition is when the non-resonant amplitude B is much bigger than the resonant amplitude A. In this case, A^2 becomes negligible, and the cross term 2.A.B reduces the non-resonant signal, creating a less steep dip. In other words, the resonance will still show as a dip, but its amplitude will be predominantly due to the cross term, not A^2. In this way, the background signal B amplifies the weak dip due to A through the cross-term.

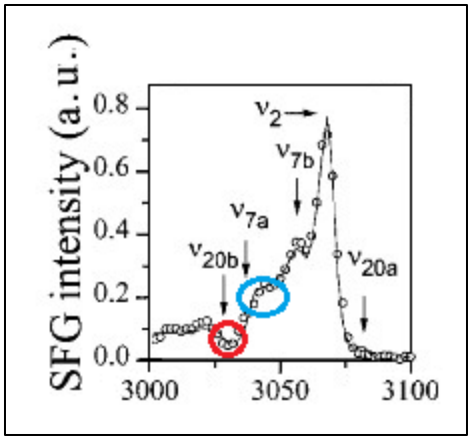

Figure 1.10: Cropped from [10] – SFG spectrum for PS/air interface showing a dip and a skewed peak.

The conditions that were presented above are 3 of countless other conditions that can occur. We focused on these three conditions only to explain the reasoning behind a dip or skewed peak that might appear in a spectrum.

Chapter 2

SFG system operational details

Figure 2.1 is a schematic of the optical layout of the Sum Frequency Generation system used in the research project discussed in this thesis[28]. The system is composed of five major compartments: power center, laser, optical parametric generator, sample stage, and monochromator.

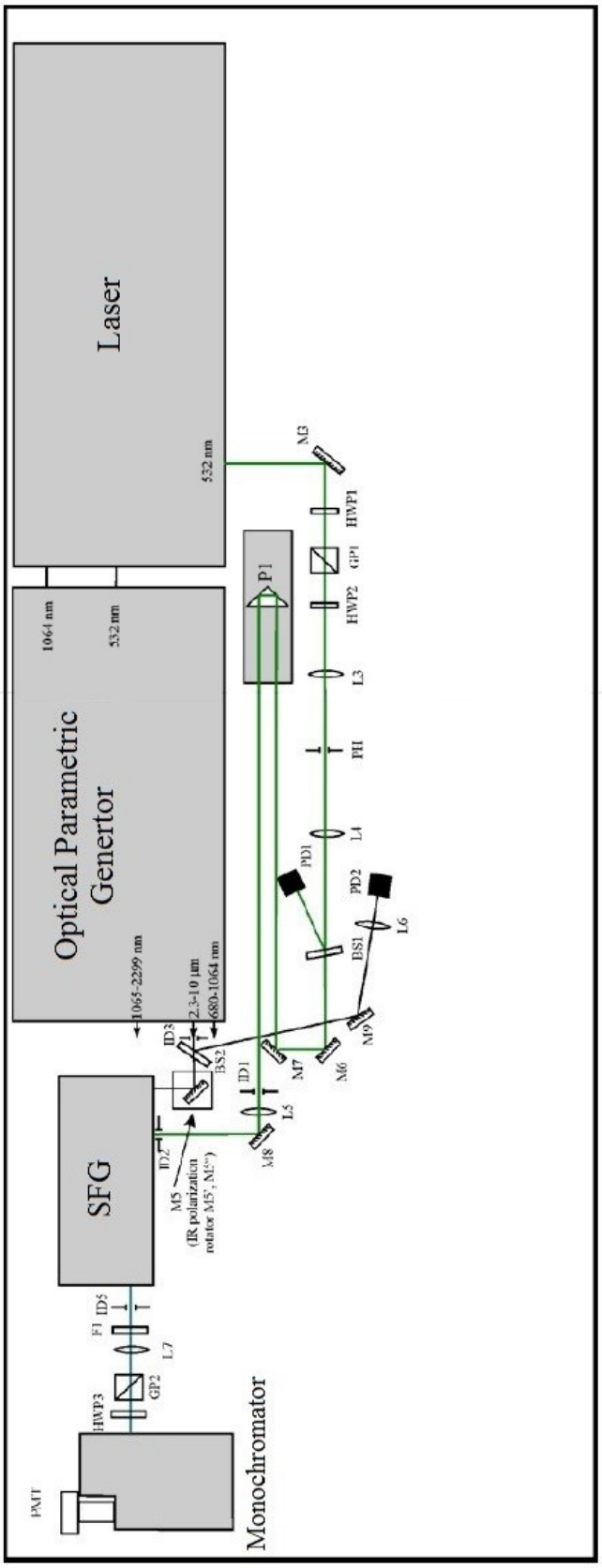

Figure 2.1: Schematic of optical layout of SFG system[28]

The power supply center is the cabinet that allows the electric controlling of the laser. It ensures that the voltage across the flash lamps of the laser is sufficient. Using this voltage, the energy output of the laser is monitored and controlled. In addition, the power cabinet includes a cooling system that will ensure that the temperature of the laser is within the safe range[28].

The second component of the system is the PL2241 series laser. It is a picosecond mode-locked Nd:YAG laser with a control pad. It is connected to the power cabinet via a flexible umbilical. It is the compartment that provides the incident photons for sum frequency generation. It is composed of the master oscillator, regenerative amplifier and the amplification stage[28].

The master oscillator is a diode pumped passively mode-locked employing Nd:YVO_4 laser material. It is a cavity which allows the oscillation of 532 nm visible photons between mirrors M1 and M8 after being pumped from the pump source. Two beams exit the master oscillator, one towards the regenerative amplifier and the second towards an optical fibre for system monitoring[28].

The regenerative amplifier is a cavity in which the photons oscillate and amplify their energy to about 1.5 mJ. The output visible beam enters the amplification stage where the level of amplification can be raised between 1 and 99 steps. The output visible beam enters the optical parametric generator PG501/DFG[28].

The optical parametric generator PG501/DFG is the compartment that allows the generation of the two incident beams (IR and VIS) starting from the single output beam of the laser. After the visible beam arrives from the laser into the PG501/DFG compartment, it gets divided into two beams, 532 nm and 1064 nm by harmonic generation at DHG crystals. The visible 532 nm beam is used as one incident beam, while the 1064 nm travels to the OPG, where

it can be tuned up to 10,000 nm. This tuned IR beam is the second incident beam, which along with the fixed visible beam will generate the sum frequency photon[28].

The fourth part of the apparatus is the sample stage, where the IR-VIS overlapping takes place. It contains optical objects that ensure that the beams are in temporal and spatial overlap, as shown in Figure 2.2. The red beam is a red light which helps direct the IR incident beam.

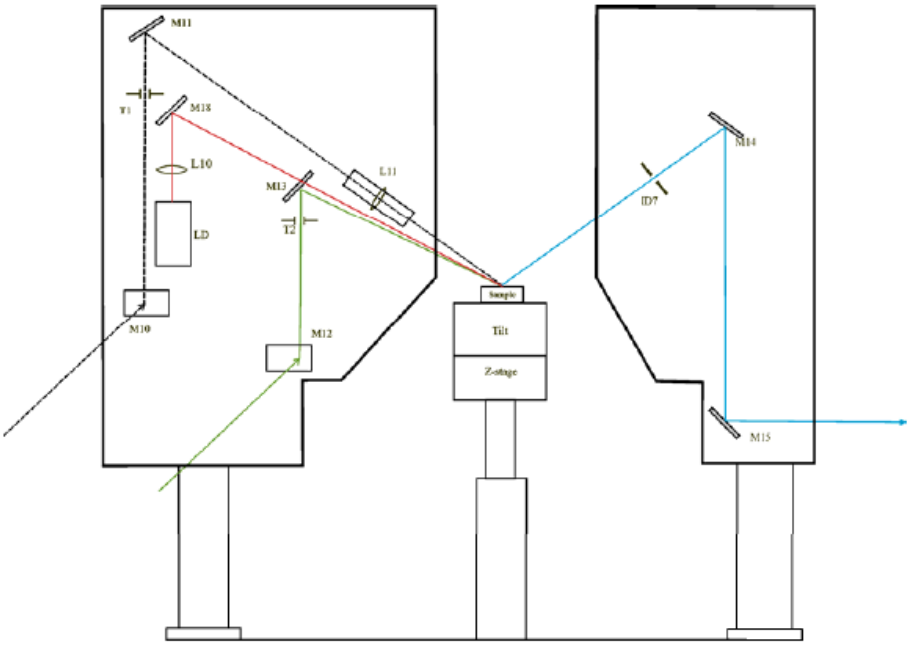

Figure 2.2: Schematic of sample stage[28]

After the SF beam is generated, it is sent to the monochromator MS2001 to select a narrow bandwidth of wavelength of the SFG range.

Finally, there is the optical signal detector which includes a photomultiplier tube (PMT). The PMT's sensitivity detects the energy of the SFG signal, and finally sends a corresponding electric signal which will be displayed on the screen as the observed SFG signal[28].

Chapter 3

3.1 Experimental procedure

The most important issue that has to be considered carefully in this research is that the experimental conditions need to be "unique" and uniform for all trials. Otherwise, it is very possible that inaccurate data will be generated and will result in misleading conclusions.

2% weight solutions of the different monodisperse polystyrene products with low index of dispersion (M_W/M_N) were formed in toluene. The polystyrene products (Table 3.1) were purchased from Scientific Polymer Products, Inc.

Table 3.1: Properties of polystyrene products used in experiments.

Polymer designation	**MW g/mol**	**Mw/Mn**
6K	6,300	1.05
13K	13,700	1.06
18K	18,000	1.01
29K	29,300	1.09
48K	48,900	1.01
59K	59,500	1.07
76K	76,200	1.17
102K	102,700	1.04

After the polystyrene solutions were prepared, thin films were formed using spin coater placed in a clean room. The substrates used were plain uncoated glass microscope slides from Bio Nuclear Diagnostics Inc. (catalogue number LAB-033). These slides were cleaned by pressurized deionized water after manufacturing, and well-sealed for minimum contamination. Fresh slides were used, and the slide box was opened immediately before spin coating inside the clean room to minimize substrate contamination. The spin coating was done at 2000 RPM speed for 1 minute for every slide. Following spin coating, the samples were carefully transferred to a vacuum oven, and annealed in vacuum for 4-5 hours at temperature 110 ^{O}C (T_g of PS = 105^{O}C). SFG experiments were done on the samples within a few days from their preparation to avoid any sample aging effects.

The geometry of the SFG stage area was fixed with IR beam forming a 55^{O} angle with the surface normal, and the visible beam forming 60^{O} with the surface normal of the film. We attempted to keep the laser pump rate constant by monitoring the pulse energy and keeping it at ~ 500 μJ. The IR and visible OPG output energies were also kept as constant as possible (E_{IR} = 7.7mJ and E_{VIS} = 6.6mJ).

Upon preparing the system and warming it, the samples were scanned in the IR range between 3000 cm^{-1} and 3100 cm^{-1} with 1 cm^{-1}/step and 100 acquisitions/step. Two distant spots on every slide and multiple slides of the same molecular weight were studied. The SFG spectra were normalized with respect to the product of the I_{IR} and I_{VIS} signals to account for any possible pump rate differences. These differences can be because of experimental variables that we will discuss in the following section.

3.2 Non-functional experimental procedures and other difficulties

The experimental procedure described above was developed after many failed attempts at collecting meaningful data. There are several experimental procedures available in literature, but are either very dangerous because of the cleaning methodologies that they follow, or very complicated in order to assure no contamination on the substrate. For example in one of the procedures, the substrates were rinsed in boiling piranha solution for 2 hours, rinsed with ultrapure water several times, rinsed with spectroscopically pure isopropanol and finally dried under nitrogen flow. In our experiments, we were trying to avoid risky procedures and to develop a simple approach that allowed us to keep the experiments as quantitative as possible.

3.2.1 Film casting technique

The experiments were started with a polydisperse polystyrene because it serves as a good, inexpensive model while developing procedures. A 2% weight solution of polydisperse polystyrene (M_W = 200 Kg/mol) was formed in toluene. After the polymer dissolved, the "dip" method was used to form thin films. The dip method is simply to clean the coated glass microscope slide (substrate) with acetone, wait until it dries, and dip it vertically into the solution for few seconds. Acetone was used as a generally agreed simple cleaning solvent. Afterwards, the slide is taken out of the solution and held horizontally until the solvent evaporates. Then, the dry samples are placed in a vacuum oven for annealing at 110 ^{O}C for 4-5 hours. Finally, the samples are removed from the oven and left to cool.

This is a quick and easy method to form polymer films, but is not reliable for several reasons. The dip method includes placing the substrate vertically in the solution, and then inverting it into the horizontal position. This means that there are not well-controlled factors

acting on the polymer solution (like effect of gravity and adsorption) which alter the homogeneity of the film, and the thickness of the polymer film is not uniform. This was characterised using an atomic force microscope (AFM) which is a very powerful technique that allows the study of the profile of the surface of the material. Figure 3.1 is a typical AFM section analysis of a film prepared in this manner, as well as another film prepared by spin coating. The blue curve is the thickness profile of the polymer film prepared by dipping, and the red curve is the thickness profile of the polymer film prepared by spin coating. A scratch using a sharp and thin blade was gently made on the films in order to determine their thickness. The sharp increase in thickness at around 2 microns is where the scratch ends. The little bump after a couple of microns from the scratch is due to polymer build-up on the edges of the scratch. It is obvious that the thickness of the film formed by dipping is increasing from left to right by about 250-300 nm, or 85% over 40 μm. On the other hand, the thickness of the film spin coated at 2000 RPM for 1 minute is ~130 nm. The variation in the film thickness is ~20 nm, which is less than 20%. In fact, according to Richter et al.[11] the maximum Fresnel weight and SFG intensity for PS/air interface is when the film thickness is 130 nm.

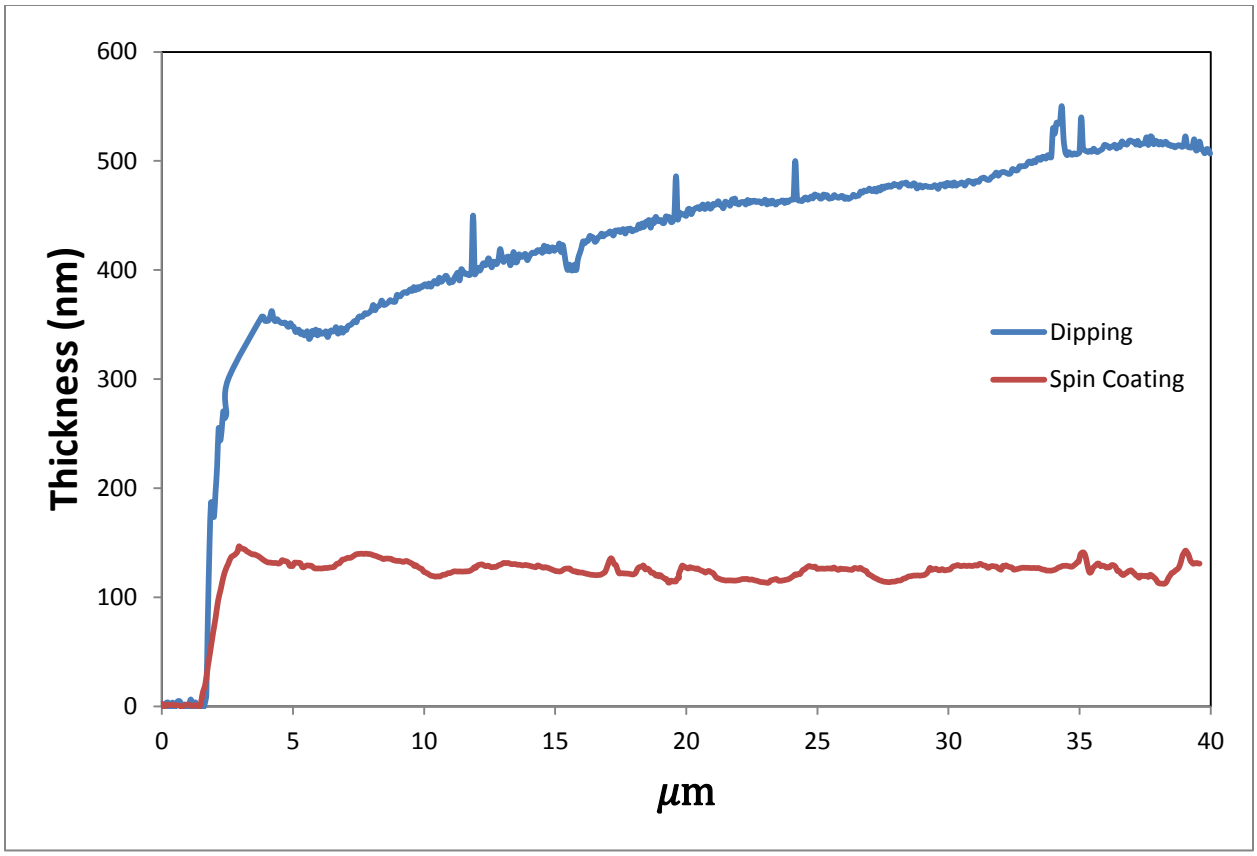

Figure 3.1: Thickness profile done by AFM for PS films formed by dipping and spin coating.

After the samples were annealed, they were subjected to SFG analysis in order to evaluate the signal to noise ratio and the repeatability. Although a good signal was obtained, the spectra were not repeatable. Figure 3.2 shows spectra collected for different spots of polydisperse PS/air interfaces prepared by the dip method, and normalized with respect to $I_{IR}*I_{VIS}$.

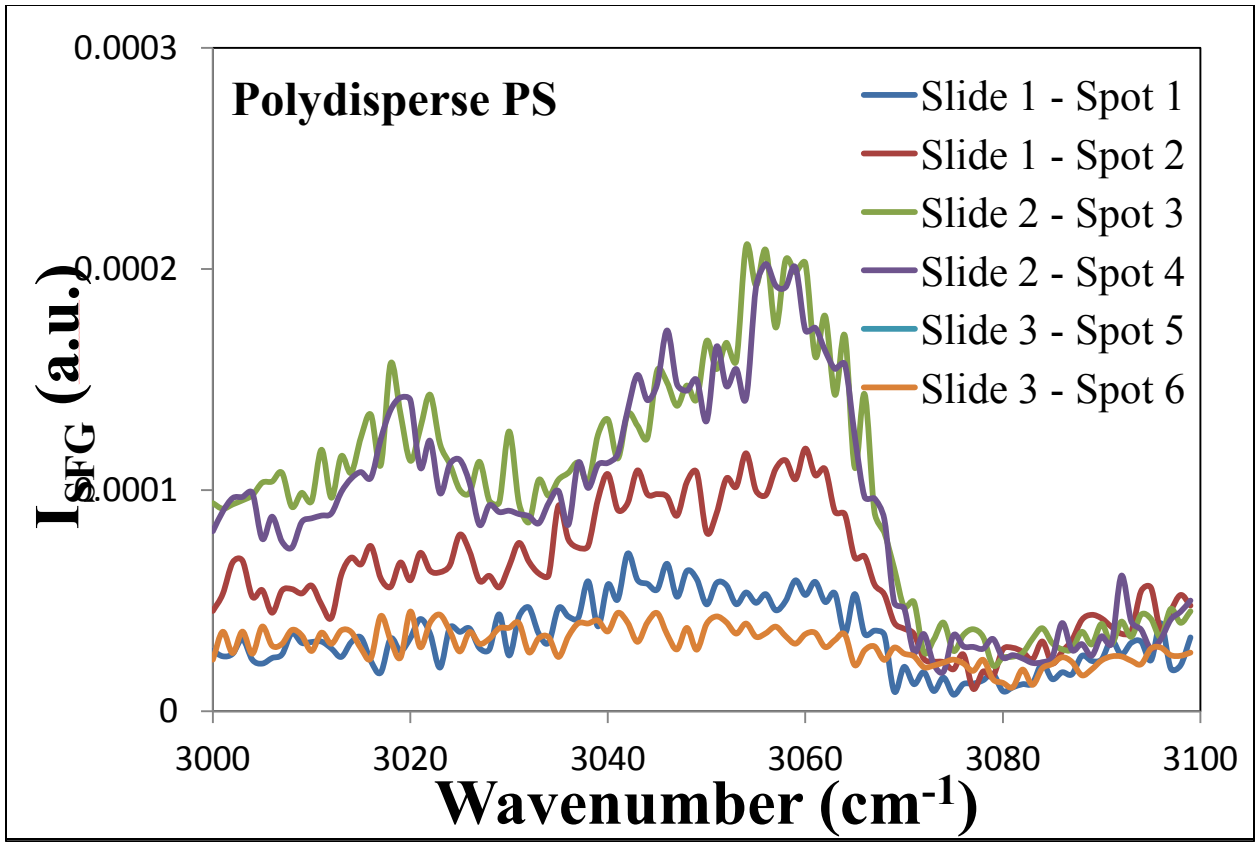

Figure 3.2: Spectra of polydispersePS/air interfaces formed by the dip method.

This method was also applied to monodisperse PS samples resulting in similar lack of repeatability. Figure 3.3 shows spectra for PS/air interfaces from films of monodisperse PS solutions with 4 different molecular weights formed by dipping.

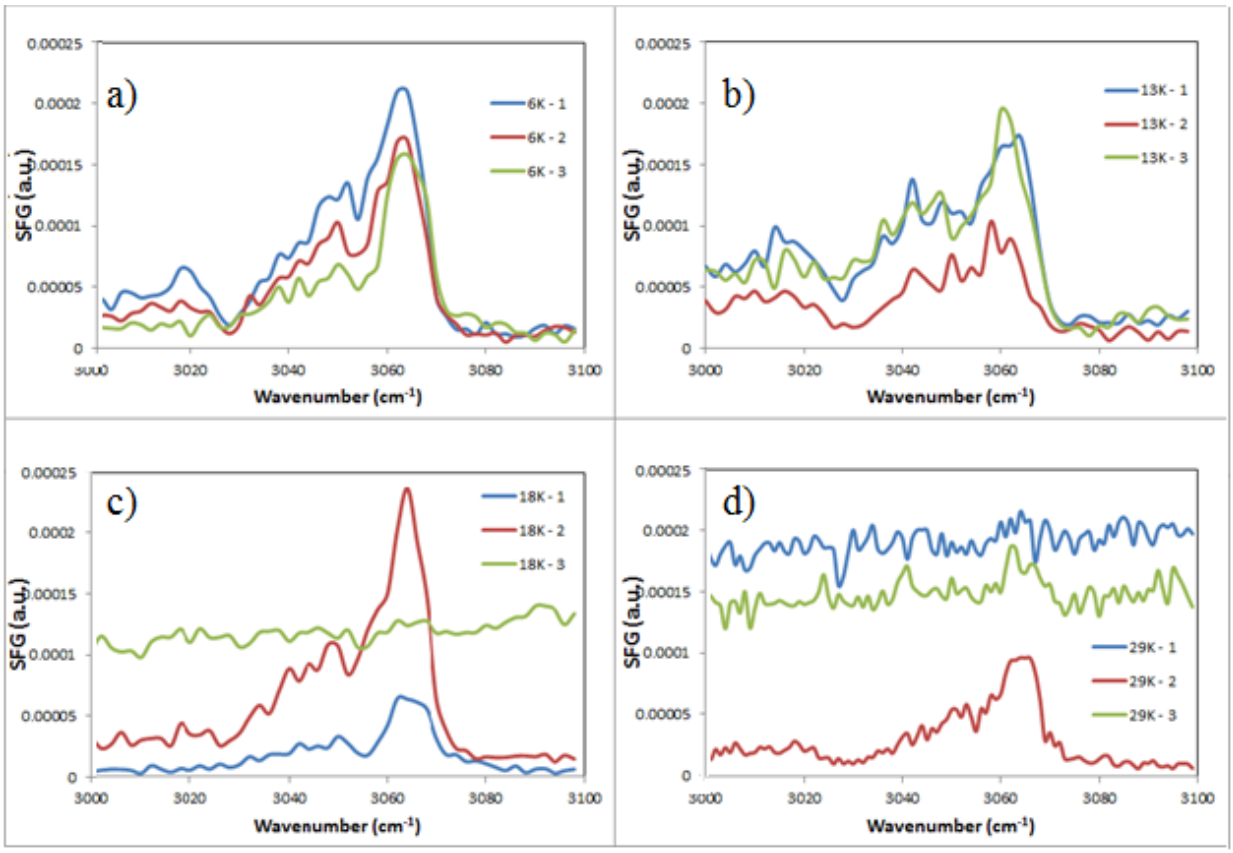

Figure 3.3: Spectra for PS/air interfaces from monodisperse PS films formed by dipping: a) 6K, b) 13K, c) 18K and d) 29K

These results confirmed that the lack of repeatability is due to the film casting method, and is not due to the polydispersity of the polymer. As a result, in order to collect reliable SFG spectra, the spin coating method of film casting was used for all later experiments. This procedure ensures that the polymer film is homogeneous, and that thickness will not be a factor that might affect the results.

3.2.2 Substrate contamination

The lack of repeatability in SFG surprisingly persisted, even with the spin coating method. Figure 3.4 shows SFG spectra for different specimens of the same polymer. These spectra look significantly different.

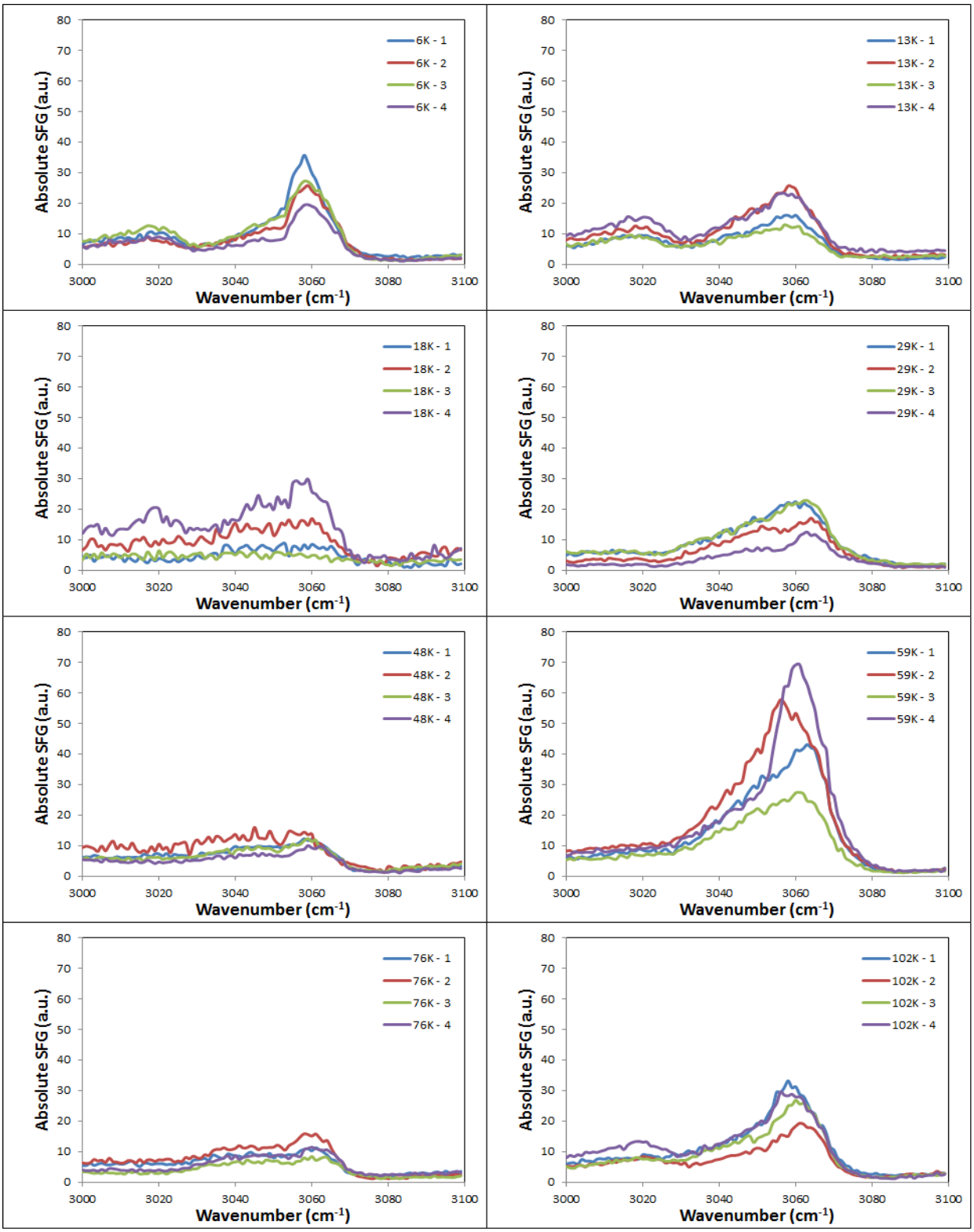

Figure 3.4: Absolute SFG spectra for different specimens of the same polymer for all MWs. Samples prepared by spin coating on glass substrates cleaned with acetone.

Upon investigation, it was found that the substrate was being contaminated with environmental adsorbents, in addition to contaminants in the acetone that was being used for cleaning. This manifested itself in variation in background signal from the substrate. This problem was later avoided by only using fresh, brand new packs of glass substrates, and spin coating the films immediately after opening the pack in the clean room without any cleaning. This reduced the contamination significantly and allowed us to get slightly better spectra from multiple specimens of the same polymer with less noise, as shown in Figure 3.5.

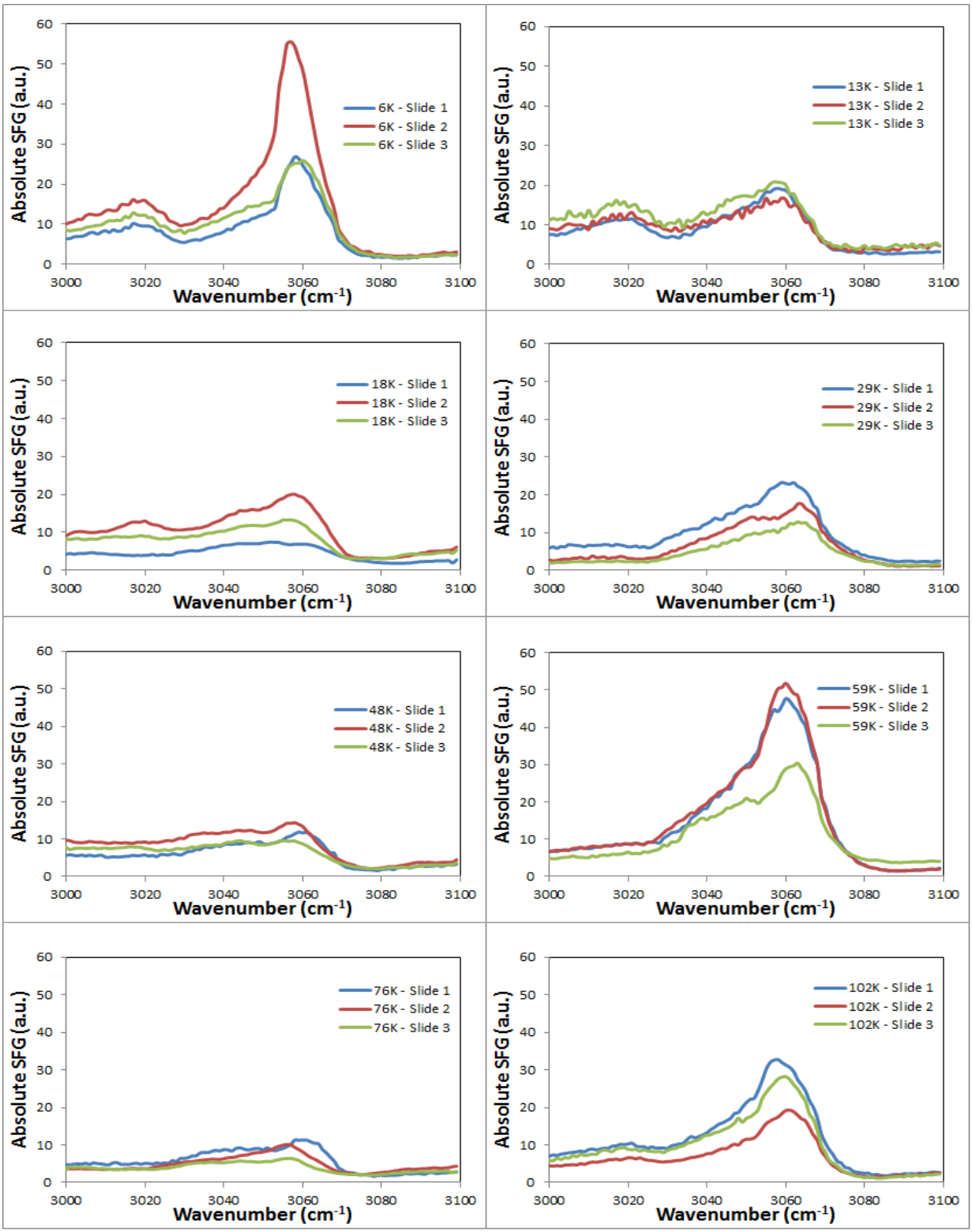

Figure 3.5: Absolute SFG spectra from PS/air interfaces of films formed by spin coating of fresh brand new slides without any cleaning.

3.2.3 Spectrometer system related factors

Despite the fact that the SFG spectra improved upon using spin coating on fresh glass substrates, we believed that we could improve the quality of our spectra further, and get higher degrees of repeatability. This required further study of controllable factors that can affect the SFG spectra, such as:

1. When SFG experiments are performed on different days, the visible and IR pump energies are not exactly the same. This definitely affects the intensity of the SFG signal.
2. The non-resonant background signal is not constant and unique for all samples likely due to minimal contamination that occurred despite our best efforts.
3. When the IR-visible delay is changed, the SFG energy changes accordingly.
4. When the angle or stage height is changed, the beam divergence changes. This will change the IR-visible overlap and the count of sum frequency generated photons.
5. The pulse duration is on the order of picosecond. A slight change in this duration might significantly affect the SFG energy.

We decided that we have to minimize the effect of these factors by incorporating the following five experimental conditions:

1. We must run full sets of experiments on the same day.
2. We must keep the IR and VIS pump energies as uniform as possible by not turning the system off for the whole day.
3. We must perform the experiments at exactly the same spot of every slide, assuming films are similar.

4. We must keep the height of the sample stage as constant as possible (preferably no change).
5. We must keep the two angles of incidence as constant as possible (preferably no change).

The first condition is important because it will allow us to have comparable data with minimal variations due to slight changes in alignment, IR and visible pump energy changes, and variations in atmospheric conditions (i.e. temperature and humidity). In fact, we were able to run three experiments for every molecular weight every day, which gave us more confidence in our results. The second condition is critical because it assures that there are only little variations in pump energy. The third, fourth and fifth conditions help us perform the experiments with little film thickness variation and geometry changes. This is true if we assume that the films are similar. However, according to the AFM results (shown in Figure 3.1), there is about 15% variation. This is acceptable for our experiments because according to Richter et al.[11] the Fresnel weight – hence the SFG intensity – does not change significantly with film thickness variation in the range we are studying (130 ± 20 nm).

We performed new SFG experiments applying these five conditions and the quality of the spectra and their repeatability improved further as shown in Figure 3.6. Afterwards, we decided to collect PPP spectra for all molecular weights. We did not face any of the problems discussed above because we applied all the conditions from the start of the experiments.

So far we have been interested in absolute spectra from different polystyrene/air interfaces. In order to improve our spectra and reduce further any effect of IR and visible energy variations, we normalized the spectra with respect to $I_{IR}*I_{VIS}$. The results will be shown and discuss in the next section.

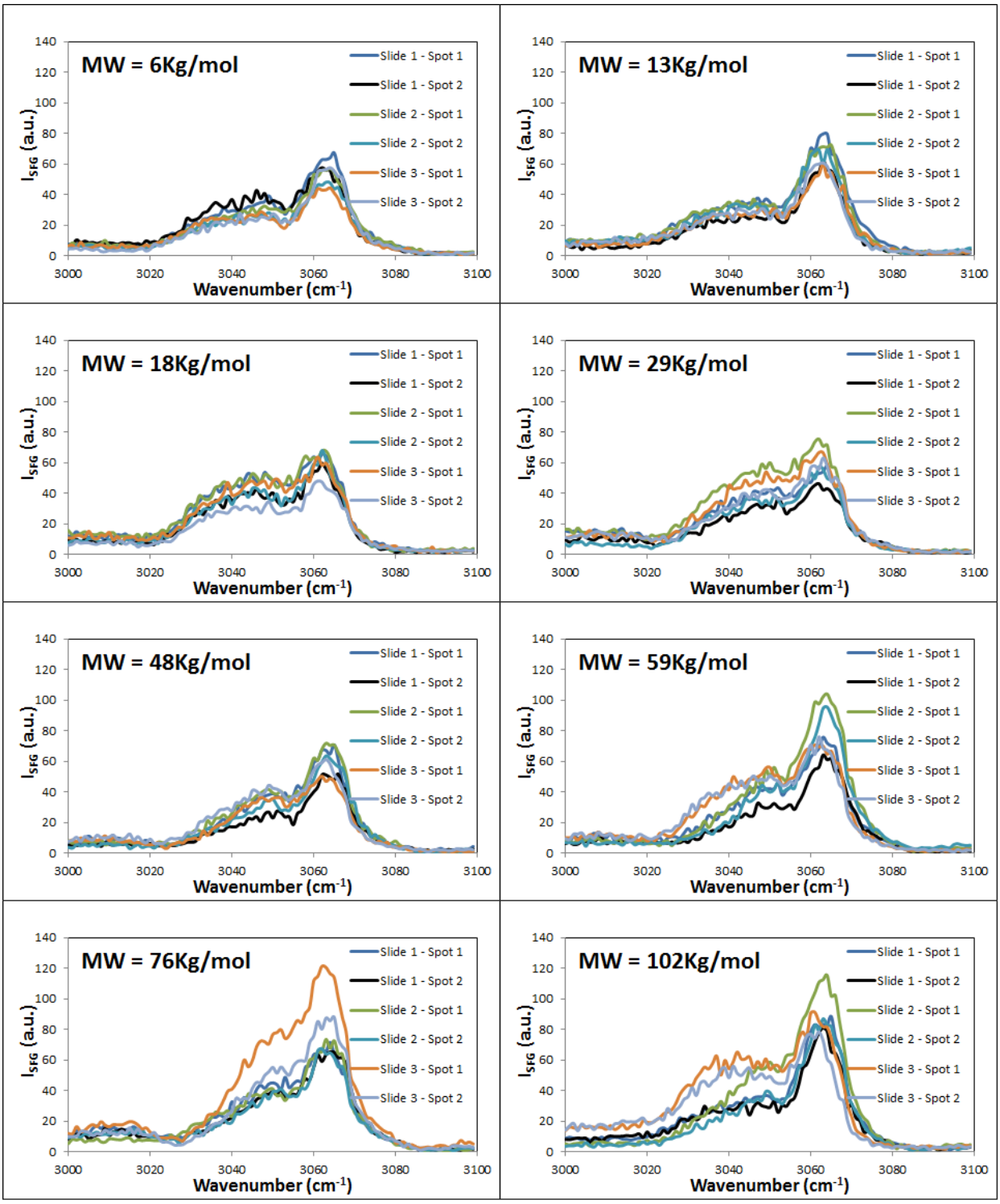

Figure 3.6: Absolute SFG spectra for PS/air interfaces from films of all molecular weights spin coated on fresh brand new glass substrates with no cleaning and accounting for the 5 conditions.

Chapter 4

4.1 Results of monodisperse polymers

In order to take any IR and visible energy fluctuations into consideration, it is appropriate to normalize our spectra with respect to $I_{IR}*I_{VIS}$. Figure 4.1 shows SSP polarized SFG spectra from various spots of PS/air interface on different specimens for all different molecular weights normalized with respect to $I_{IR}*I_{VIS}$. Considering all controllable factors that can affect SFG intensity, the limitations of our system and the very high sensitivity of SSP polarization to contaminants, the quality, reliability and repeatability of these spectra is considered high.

In most spectra presented in Figure 4.1, the peak of vibration mode ν_{20b} at around 3027 cm^{-1} and the dip of mode ν_{7a} at around 3038 cm^{-1} were merged together. This is believed to be because the orientation plane of the ν_{7a} mode was out of phase with the incident plane of IR (P polarized plane) which resulted in weak excitation of this vibration.

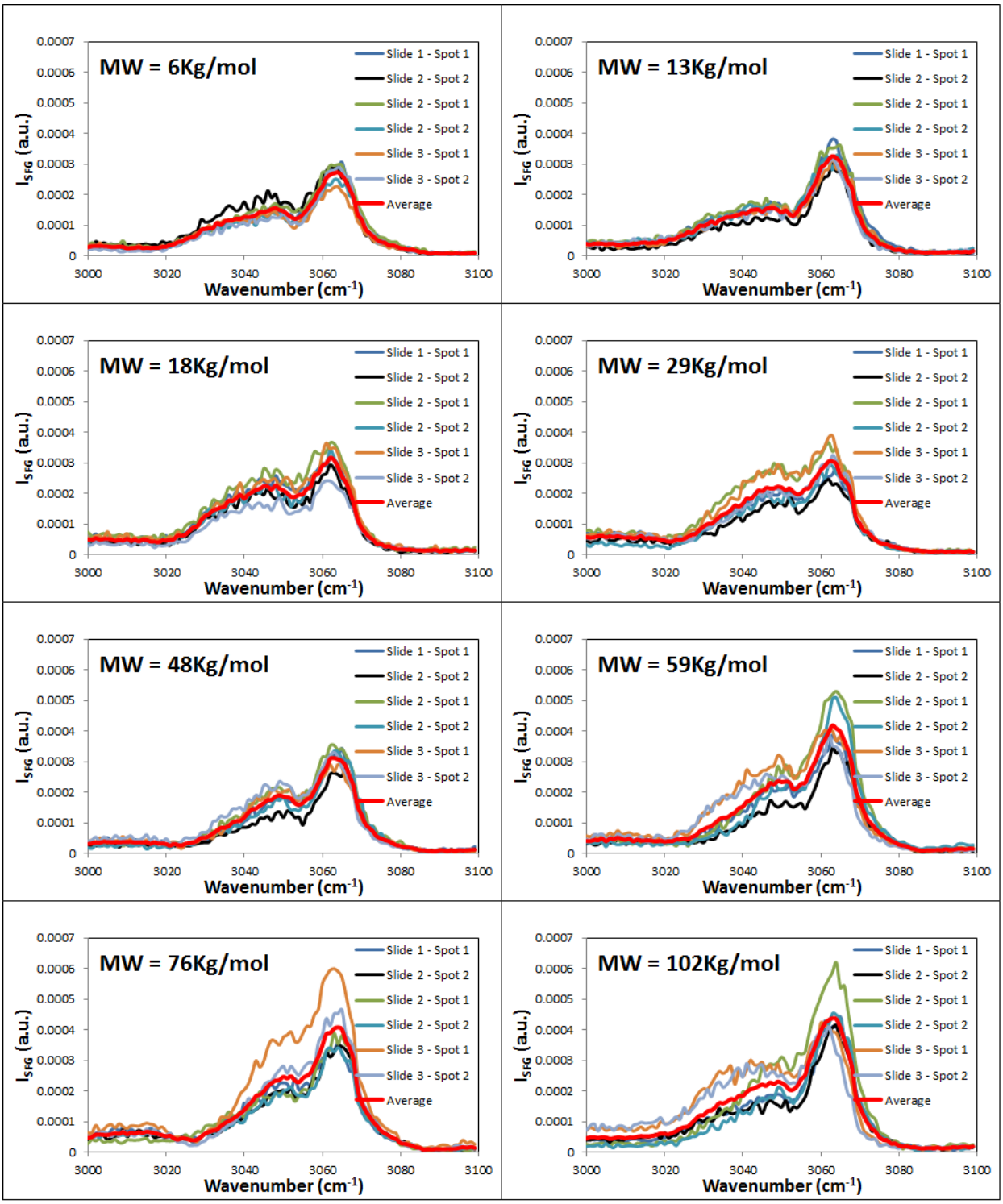

Figure 4.1: SSP polarized SFG spectra from various spots of PS/air interface on different specimens for all different molecular weights normalized with respect to $I_{IR}*I_{VIS}$.

Upon comparing the SSP polarized spectra from PS/air interface of all molecular weights shown in Figure 4.2 (normalized w.r.t. $I_{IR}*I_{VIS}$), there seems to be some variation with molecular weight. The variation does not appear to follow a trend. However, when comparing the highest intensities of the modes ν_2 and ν_{7b} for the SFG spectra normalized w.r.t. $I_{IR}*I_{VIS}$ versus the molecular weight, we can see that the SFG intensity increases with molecular weight for both modes. This comparison was performed only for resolved peaks. The detailed analysis is presented in the following section.

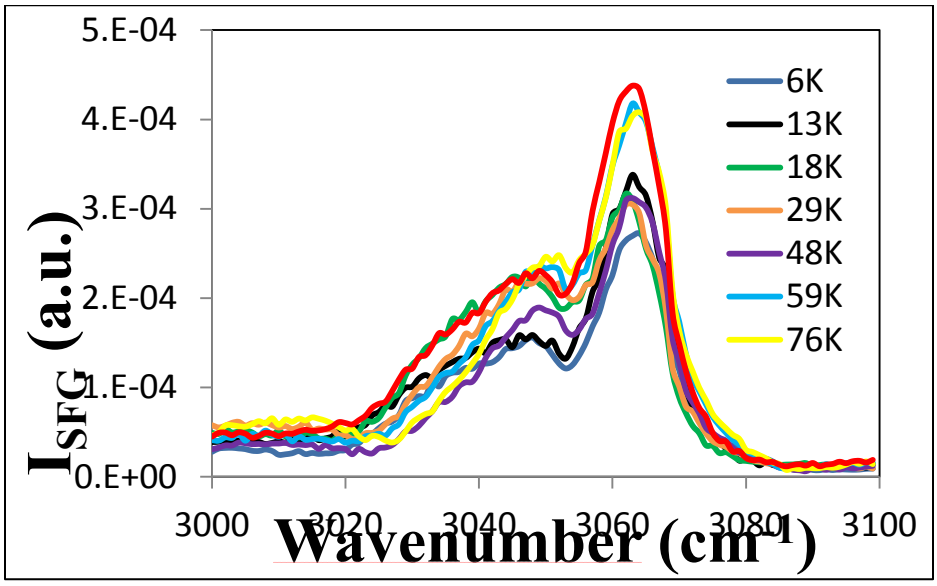

Figure 4.2: Average SFG Spectra from PS/air interface of films of 8 molecular weights normalized w.r.t. $I_{IR}*I_{VIS}$.

To further our study, we collected new SFG spectra with different polarization: PPP. Figure 4.3 shows PPP polarized SFG spectra normalized w.r.t. $I_{IR}*I_{VIS}$ from PS/air interfaces of different specimens for all different molecular weights. We show only 3 spectra for every molecular weight because the repeatability is high after we applied all experimental conditions. The SFG spectra of the same molecular weight showed minimal-to-no differences.

Upon visually comparing the PPP polarized SFG spectra from PS/air interface of different molecular weights normalized w.r.t. $I_{IR}*I_{VIS}$, it seems that the spectra are all similar to each other as shown in Figure 4.4. But when we did the quantitative comparison between maximum SFG intensities for the resolved modes ν_2 and ν_{20b} in these spectra, trends similar to those obtained from the SSP polarized SFG spectra were obtained. The maximum intensities for both modes $\nu_2$and ν_{20b} increase with molecular weight. The detailed analysis is shown in the following section.

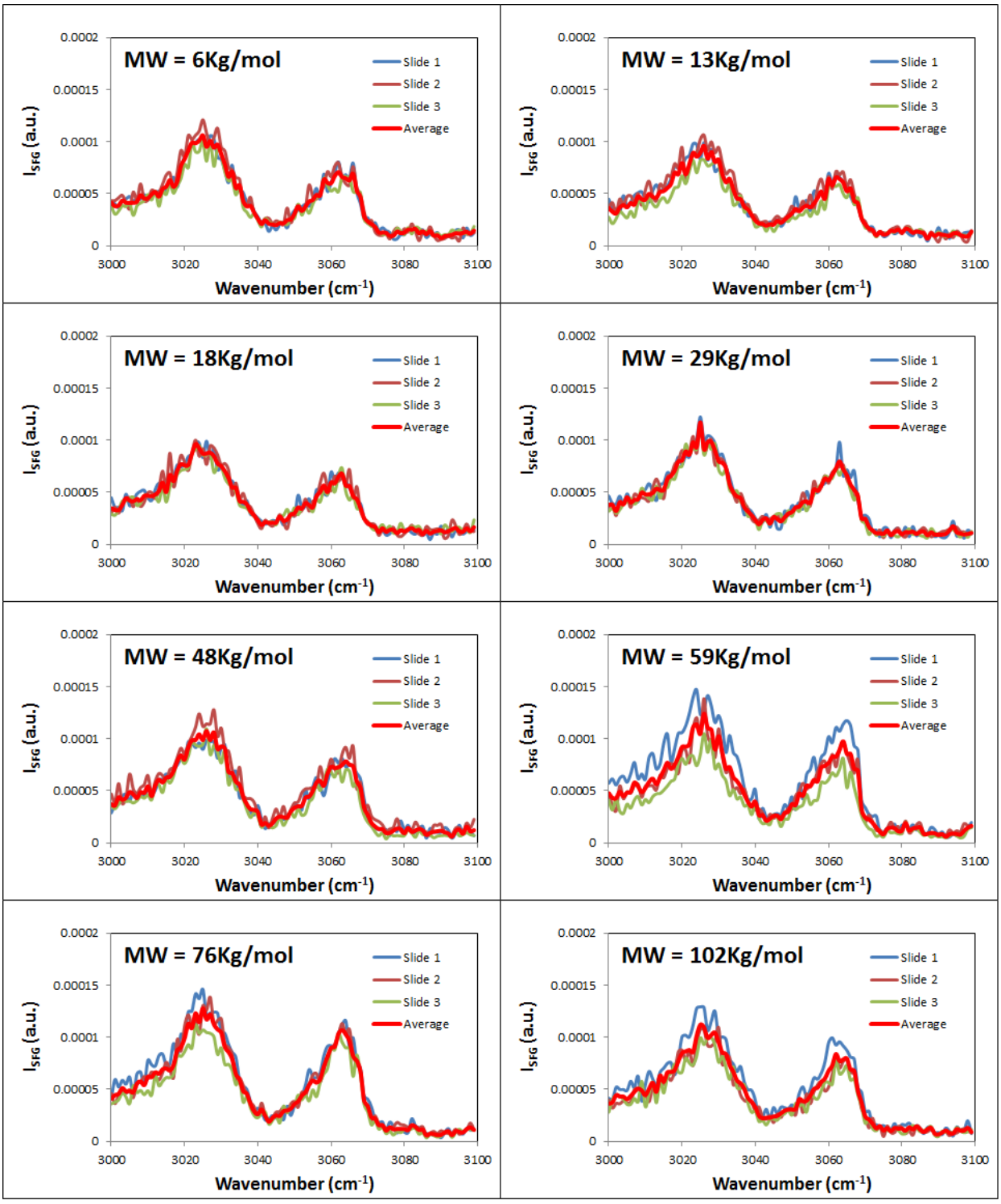

Figure 4.3: PPP polarized SFG spectra from PS/air interfaces of different specimens for the same molecular weight normalized w.r.t. $I_{IR}*I_{VIS}$.

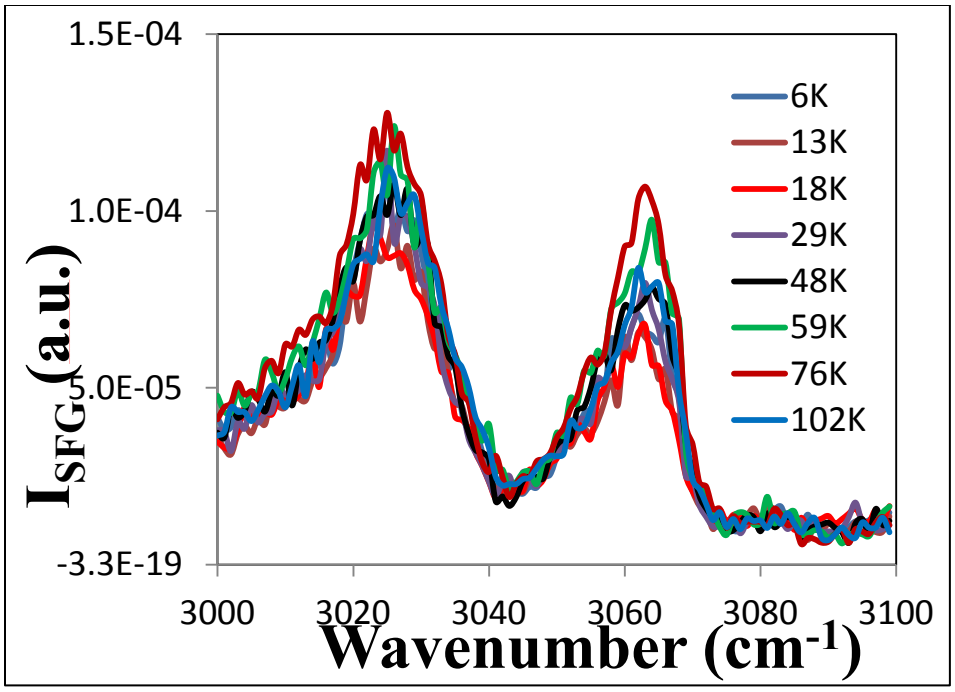

Figure 4.4: Average PPP polarized SFG spectra from PS/air interface of different molecular weights normalized w.r.t. $I_{IR}*I_{VIS}$.

4.2 Statistical Analysis of SFG Spectra from PS/air Interfaces From Pure components

In order to understand if there is any effect of molecular weight on SFG spectra of PS/air interfaces, statistical analysis is performed. As shown in Figures 4.5 and 4.6, the maximum intensities of the studied modes in the average spectra from all PS solutions with different molecular weights seem to increase with molecular weight for both SSP and PPP polarizations respectively. The following analysis is done in order to confirm and quantify this increase. A fit straight line is introduced through the data points using least squares method. There is not any assumption that the variation is linear. However, this trend-line is used to help us determine the significance of the increase.

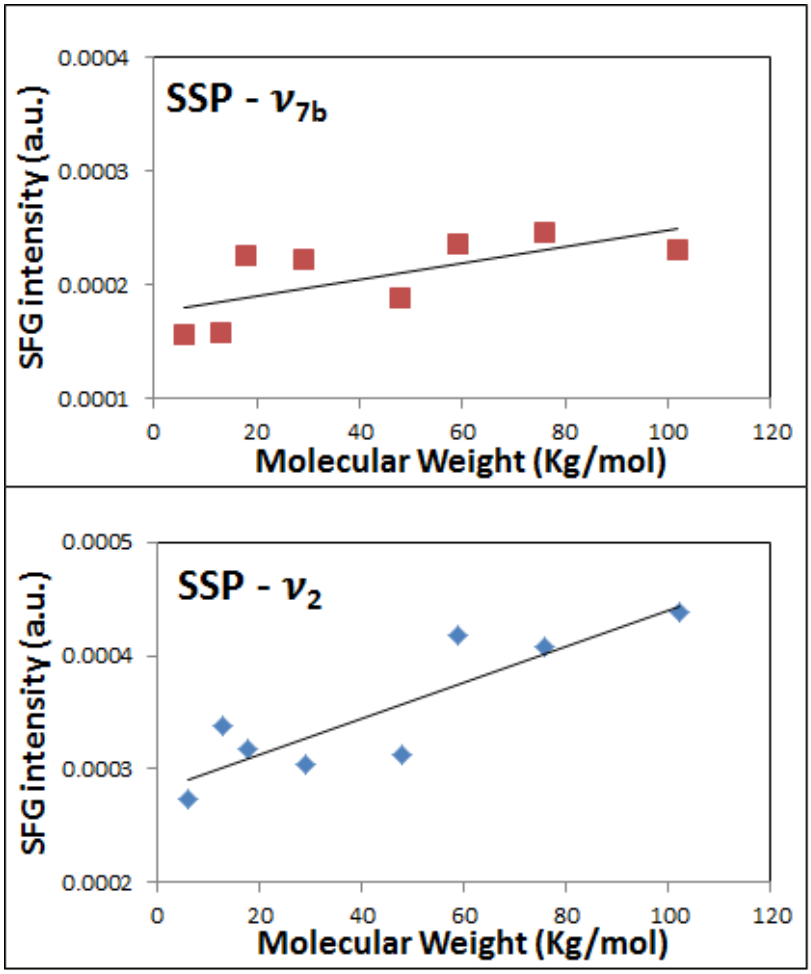

Figure 4.5: Variation of SSP peak intensities of modes $\nu_{7b}$and ν_2 versus molecular weight.

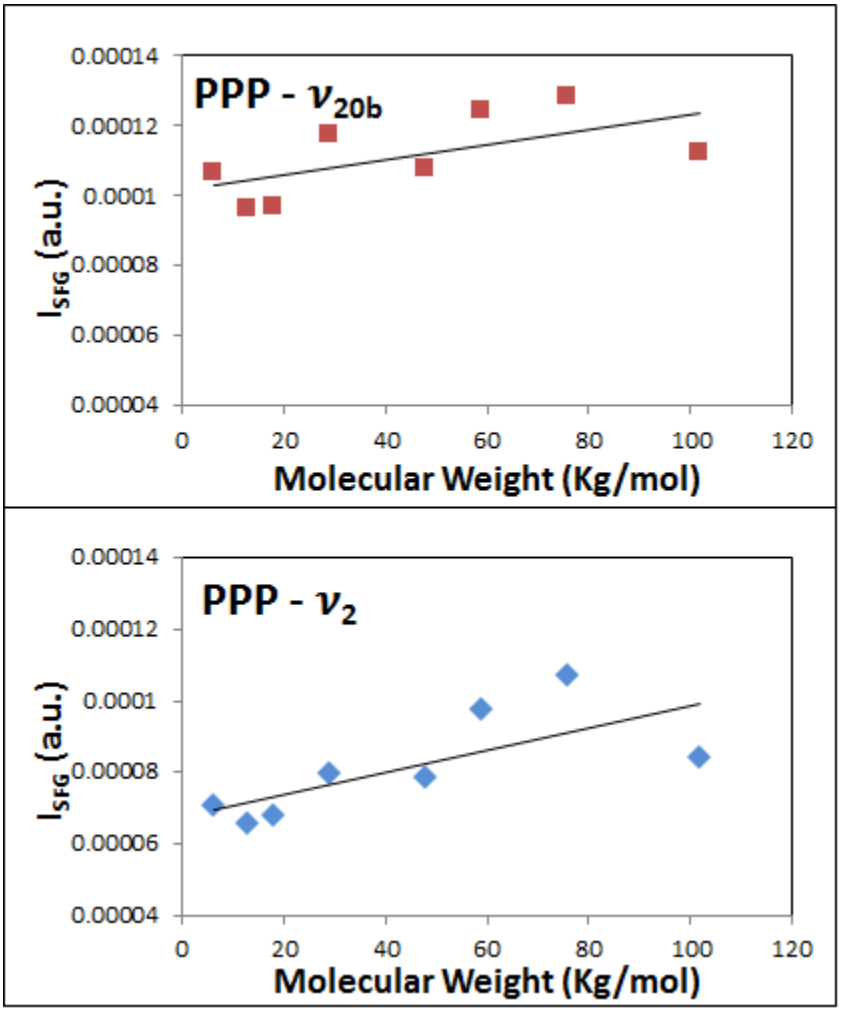

Figure 4.6: Variation of PPP peak intensities of modes $\nu_{20b}$and ν_2 versus molecular weight for monodisperse polymers.

In order to determine whether this increase is real and due to the molecular weight variation, a hypothesis testing using the f-distribution is performed. The f-test determines whether the slope of the fit-line is real or random[29]. Upon determining the degrees of freedom (ν_1 = 1 and ν_2 = 6), the critical values of F ($F_{critical(1,6)}$) are determined from the F-distribution tables[29] with various values of the probability (α), and are listed in Table 4.1. The value of α is the probability that the observed variation happened by chance. The experimental values of F ($F_{exp(1,6)}$) for our data are calculated and shown in Table 4.2. In order to decide what is the best

value of α, $F_{exp(1,6)}$ must be as close to $F_{critical(1,6)}$ as possible[29]. What we are actually choosing is the maximum probability that this variation is due to random factors and happened by chance. In other words, if the maximum value of this probability α is significantly low, we can say that the increase is most probably not random. Since we are able to eliminate all effective factors other than molecular weight variation, we can deduce that the observed increase is a result of molecular weight increase. We use software[30] to calculate the exact value of α for every set of data, which we present in Table 4.3.

Table 4.1: Values of $F_{critical(1,6)}$ for various values of α.

α	$F_{critical(1,6)}$
0.001	35.51
0.01	13.75
0.05	5.99
0.1	3.78
0.15	2.72

Table 4.2: Values of $F_{exp(1,6)}$ for different modes in SSP and PPP polarizations.

Polarization	Mode	$F_{exp(1,6)}$
SSP	ν_{7b}	5.32
	ν_2	19.69
PPP	ν_{20b}	3.77
	ν_2	6.45

Table 4.3 shows the statistical results for the studied peaks in the SSP and PPP polarized SFG spectra. The low values of α indicate that there is low probability that this observed increase happened by chance. For example, the increase in the intensity of the ν_{7b} mode in the SSP polarized SFG spectra has only 6% probability to be by chance. An indicator of how well the data points fit the line is the coefficient of determination (R^2). If the increase in the data points was perfectly linear, the value of R^2 would have been 1. However, we are not much concerned about this value because we are not assuming that the increase in intensities that we determined is linear. In fact, the values of R^2 obtained suggest that the relation between these intensities and the molecular weight is complicated and not linear, and the determination of any functional relationship is beyond the scope of this work.

Table 4.3: Results of statistical analysis for SSP and PPP polarized SFG spectra.

Polarization	Mode	Slope	Error on Slope	y-intercept	Error on y-intercept	R^2	α
SSP	ν_{7b}	$7.2*10^{-7}$	$3.1*10^{-7}$	0.00018	$1.7*10^{-5}$	0.47	0.06
	ν_2	$1.6*10^{-6}$	$3.6*10^{-7}$	0.00028	$1.9*10^{-5}$	0.77	0.004
PPP	ν_{20b}	$2.2*10^{-7}$	$1.1*10^{-7}$	0.0001	$6*10^{-6}$	0.39	0.1
	ν_2	$3.1*10^{-7}$	$1.2*10^{-7}$	$6.8*10^{-5}$	$6.6*10^{-6}$	0.52	0.04

Before confirming these results, understanding the effect of non-resonant background signal on the SFG spectra is critical. As a result, another analysis was performed to make sure that such increase in intensity was only due to the increase in molecular weight, and not due to background signal variation. The results of the analysis are shown in Table 4.4.

Table 4.4: Results of statistical analysis for background signal in SSP and PPP spectra.

Polarization	ω_2 (cm^{-1})	Slope	Error on Slope	y-intercept	Error on y-intercept	R^2	α
SSP	3000	$5.8*10^{-8}$	$1.2*10^{-7}$	$4*10^{-5}$	$6.2*10^{-6}$	0.04	0.63
PPP	3000	$1.9*10^{-8}$	$5*10^{-8}$	$3.8*10^{-5}$	$2.7*10^{-6}$	0.02	0.71

The results in Table 4.4 show that an increase in background signal is taking place with the increase of molecular weight, represented by slope value and the shape of the trend-lines in Figure 4.7. However, the analysis shows that this increase has a probability of 63% to be happening by chance for SSP spectra and 71% for PPP spectra. In other words, this increase is most probably not real, and the change in background signal has no direct effect on the increasing trend of peak intensities of the modes studied above.

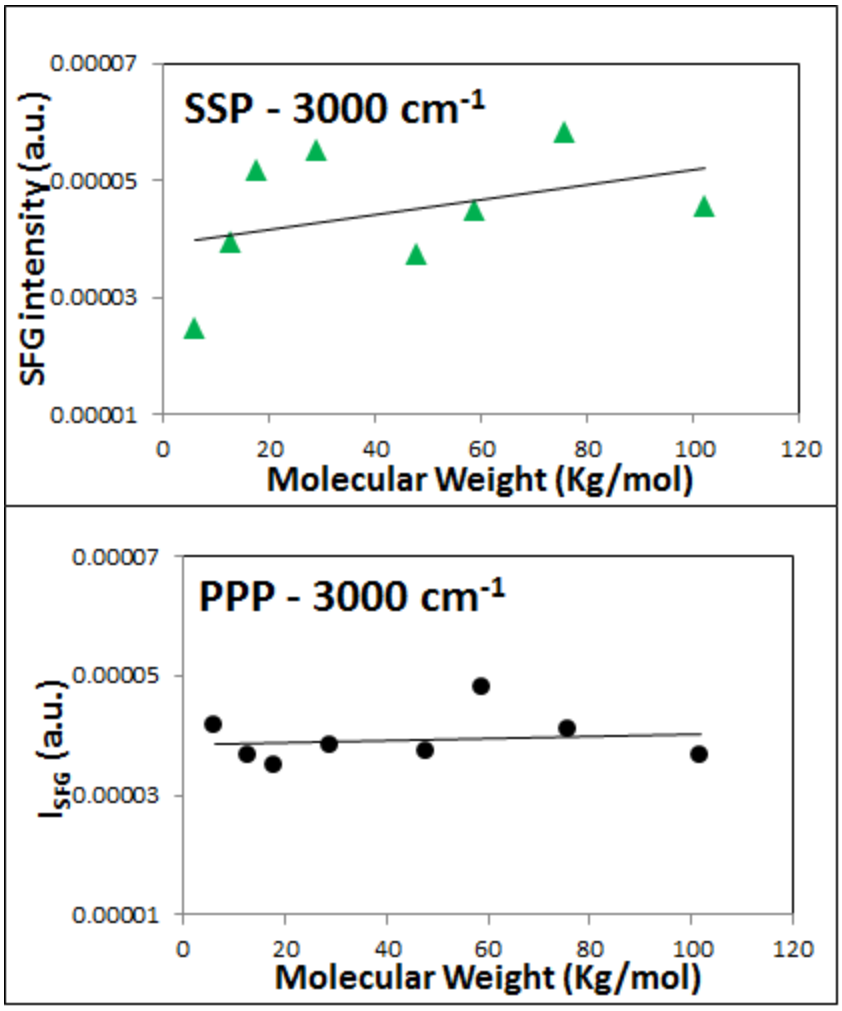

Figure 4.7: Variation of SSP and PPP background signal versus molecular weight.

4.3Results of Mixtures

The last group of experiments was performed using mixtures of polystyrene solutions composed of different components. Table 4.5 shows the weight percentages that were used.

Table 4.5: Weight percentages of mixtures

Mixture number	Weight percentages
1	50/50 - 6K/13K
2	50/50- 6K/48K
3	50/50 - 6K/59K
4	50/50 - 6K/102K
5	25/75 - 13K/76K
6	50/50 - 13K/76K
7	75/25 - 13K/76K
8	25/75 - 29K/102K
9	50/50 - 29K/102K
10	75/50 - 29K/102K
11	50/50 - 59K/102K
12	50/50 - 76K/102K

Both SSP and PPP polarized SFG spectra were collected for PS/air interfaces from films prepared by spin coating. These experiments were done to see how spectra from mixtures compare to spectra from monodisperse polymers and how they compare to each other.

Figures 4.8-a and 4.8-b show SSP polarized SFG spectra from PS/air interfaces from films of the mixtures. As with monodisperse polymers, little variation within the same composition was observed. However, a new peak at around 3010 cm-1 appeared in some of the mixtures. According to the table of IR absorption, this peak possibly represents a C-H stretch of an aliphatic alkene group. We are not sure how to interpret this peak, but we believe it could be due to contamination.

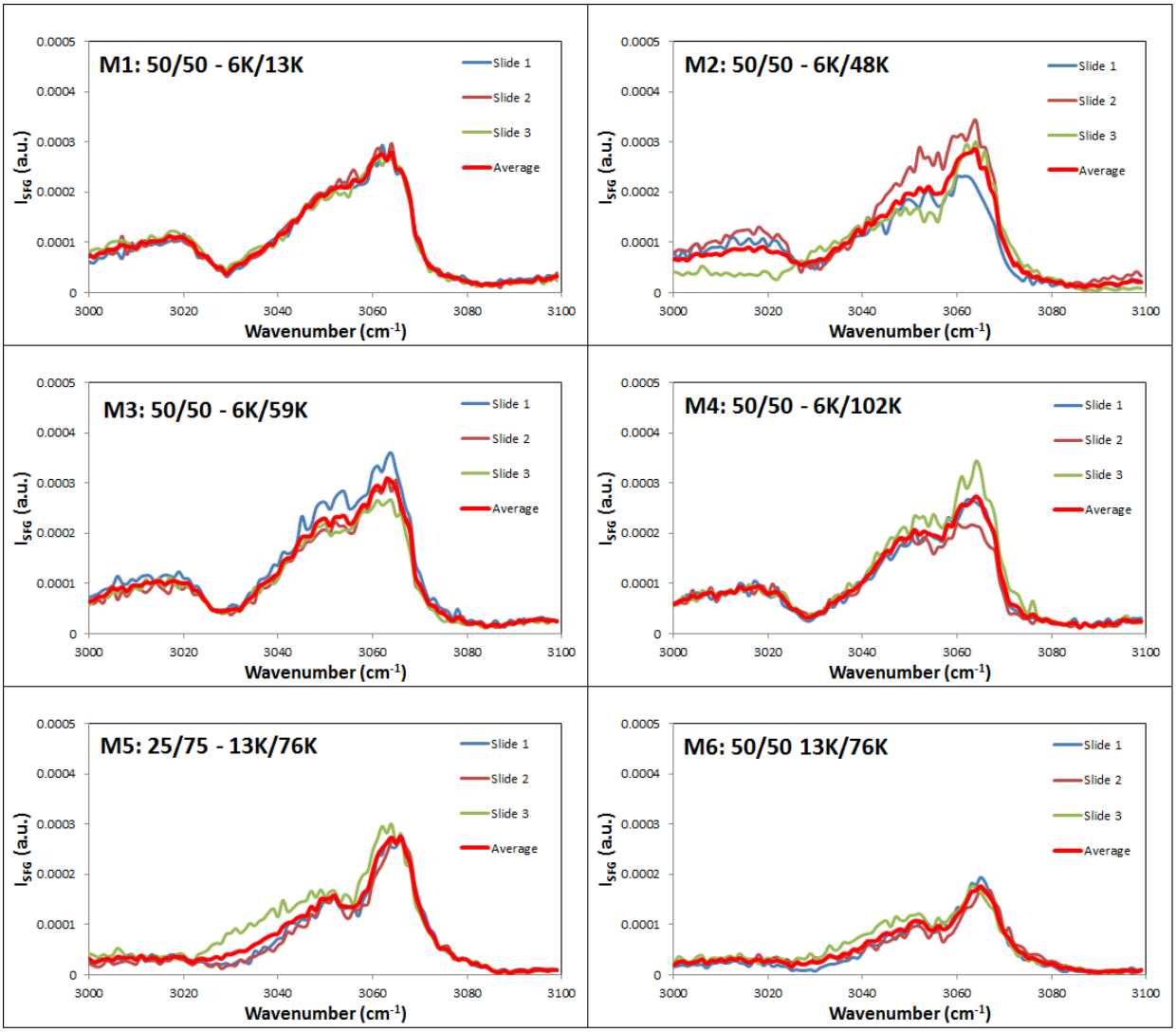

Figure 4.8-a: SSP polarized SFG spectra from PS/air interfaces from films of mixtures 1 to 6 normalized w.r.t. $I_{IR}*I_{VIS}$.

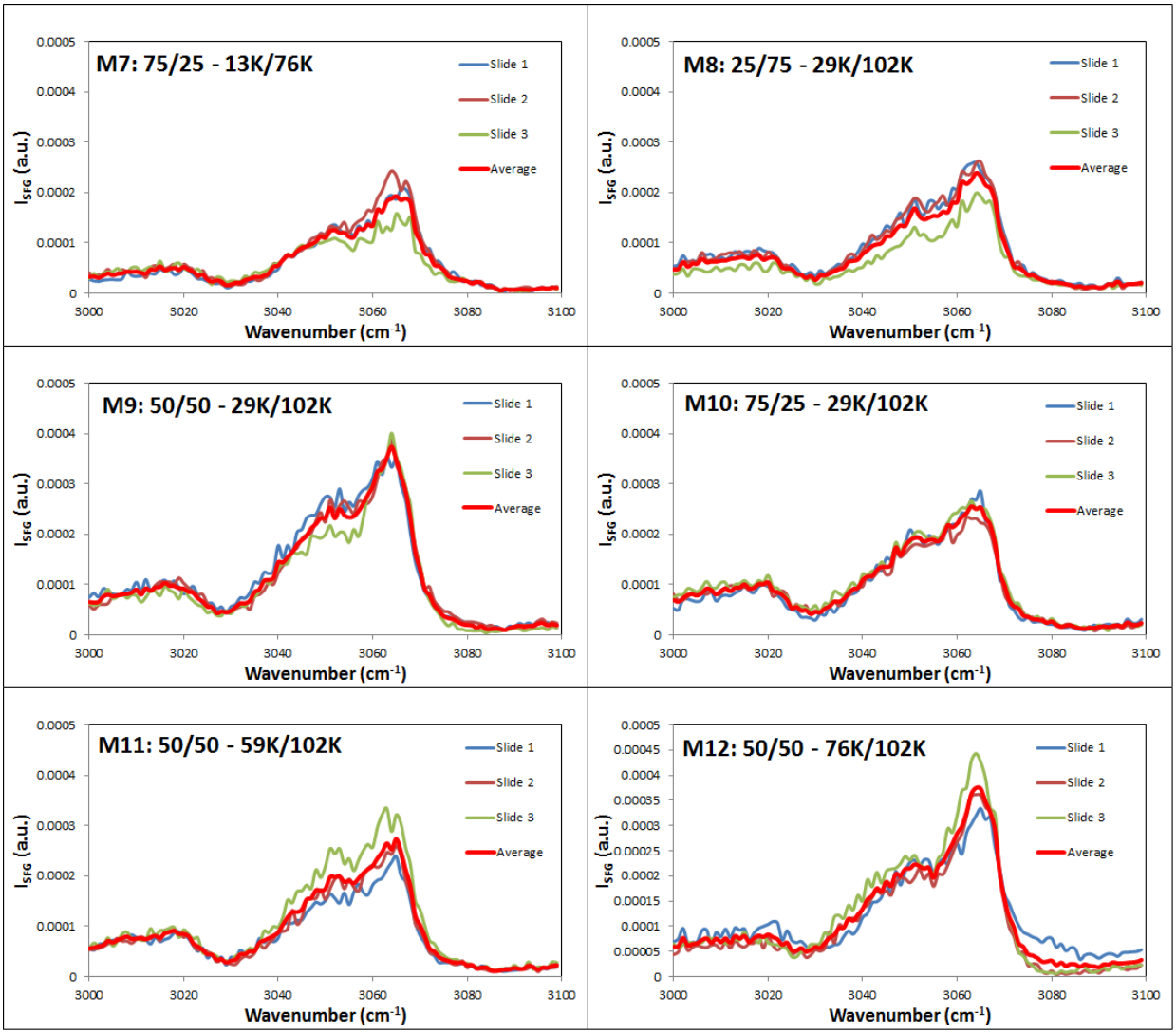

Figure 4.8-b: SSP polarized SFG spectra from PS/air interfaces from films of mixtures 7 to 12 normalized w.r.t. $I_{IR}*I_{VIS}$.

When comparing the spectra of the mixtures to those of the monodisperse polymers, they seemed to be different and not similar to either of them. The SSP polarized SFG spectra from PS/air interfaces from films of mixtures 1 to 12 normalized w.r.t. $I_{IR}*I_{VIS}$ are shown in Figures 4.9-a and 4.9-b.

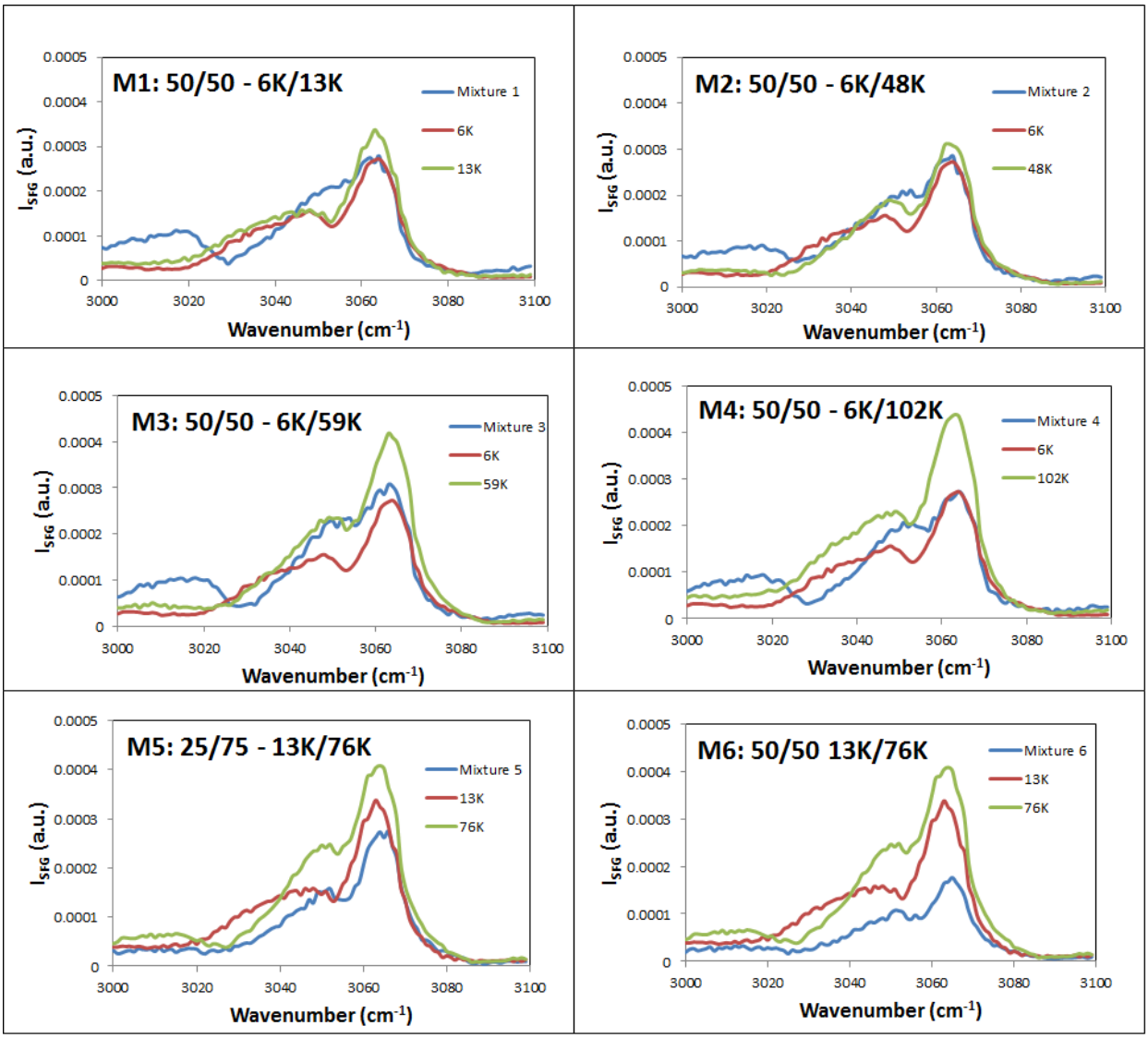

Figure 4.9-a: SSP polarized SFG spectra from PS/air interfaces from films of mixtures 1 to 6 normalized w.r.t. $I_{IR}*I_{VIS}$ compared to monodisperse polymers.

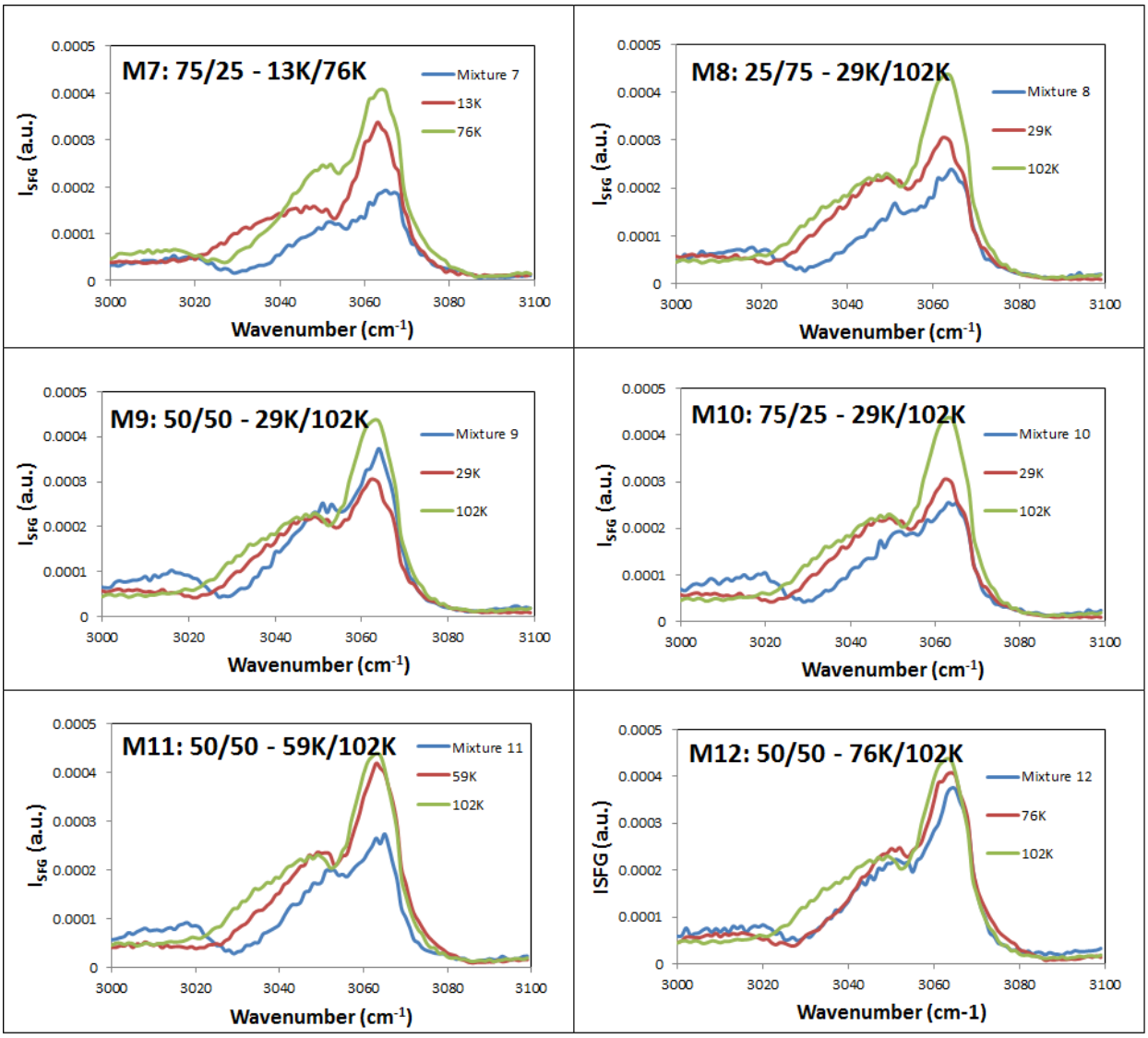

Figure 4.9-b: SSP polarized SFG spectra from PS/air interfaces from films of mixtures 7 to 12 normalized w.r.t. $I_{IR}*I_{VIS}$.

Figure 4.10 shows SSP polarized SFG spectra from PS/air interfaces from films of the mixtures normalized with respect to $I_{IR}*I_{VIS}$. There seems to be no trend of variation with increasing the molecular weight. However, this is not surprising since the molecular weights of the mixtures do not follow a trend. Detailed analysis of the variation of SFG spectra of the mixture as a function of molecular weight is presented in the following section.

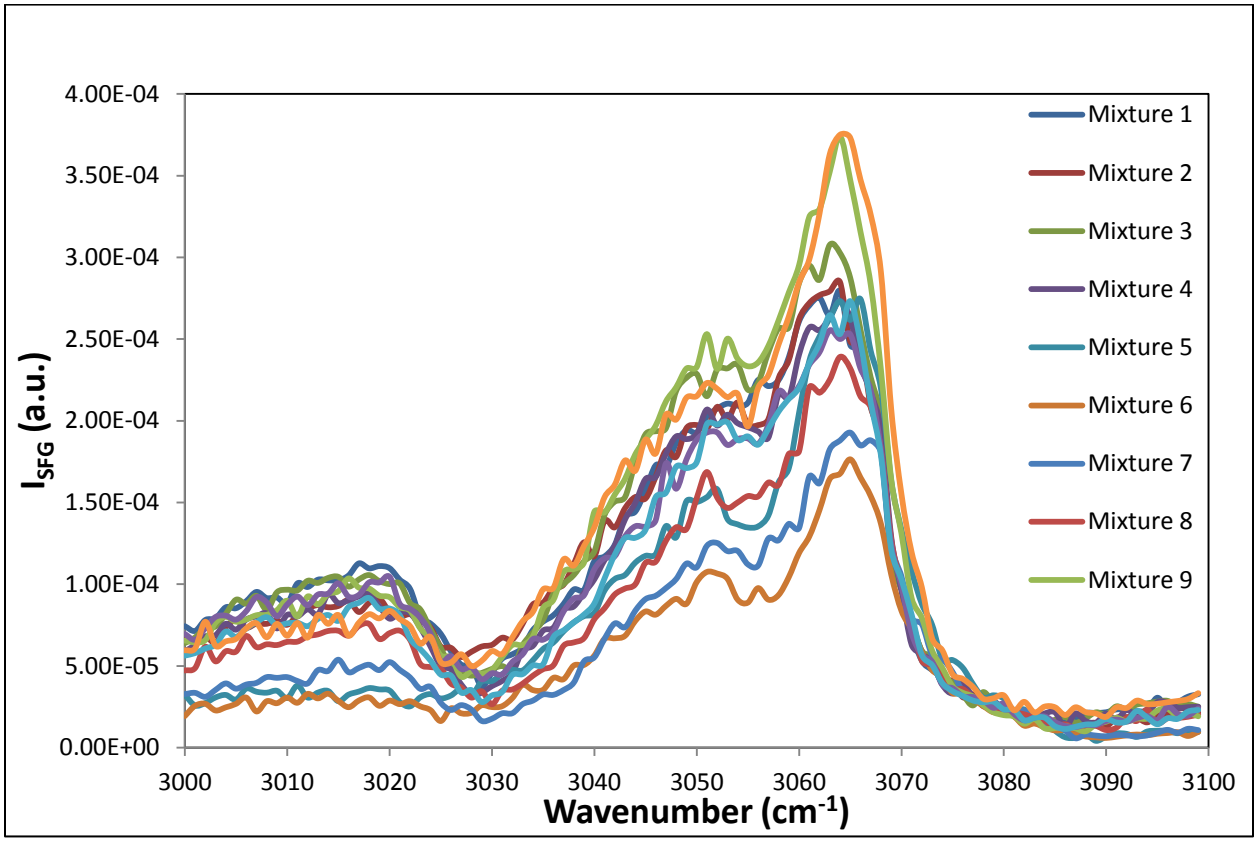

Figures 4.10: SSP polarized SFG spectra from PS/air interfaces from films of the mixtures normalized with respect to $I_{IR}*I_{VIS}$.

The same set of experiments was repeated with PPP polarization combination. The spectra were repeatable. Unlike the SSP spectra, all spectra of mixtures looked very close to each other and very close to those of monodisperse polymers. Figure 4.11 shows PPP polarized SFG spectra from PS/air interfaces from films of the mixtures normalized with respect to $I_{IR}*I_{VIS}$. Figure 4.12 shows PPP polarized average SFG spectra from of the mixtures normalized with respect to $I_{IR}*I_{VIS}$ compared to spectra of monodisperse polymers.

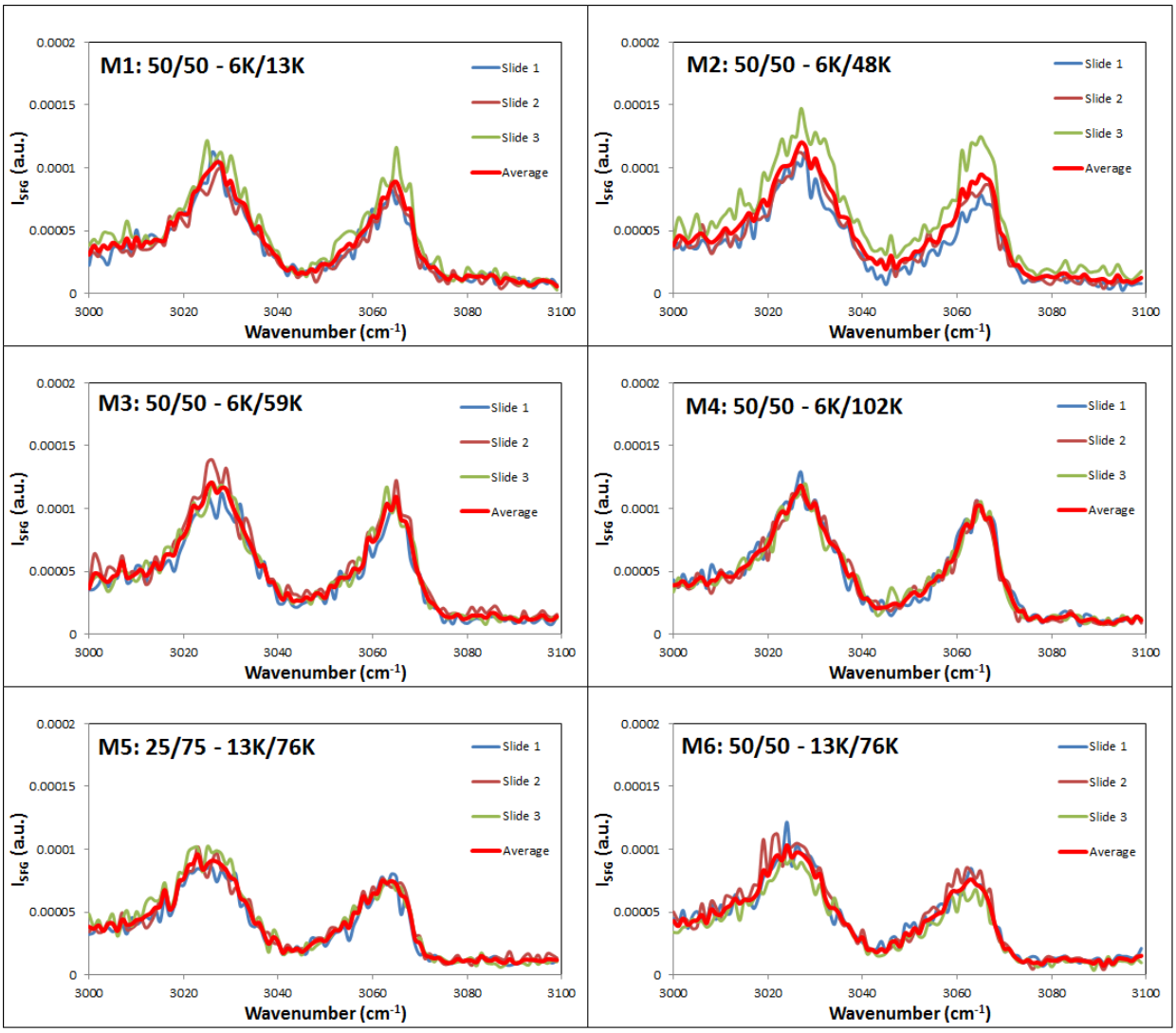

Figure 4.11 - a: PPP polarized SFG spectra from PS/air interfaces from films of mixtures 1 to 6 normalized with respect to $I_{IR}*I_{VIS}$.

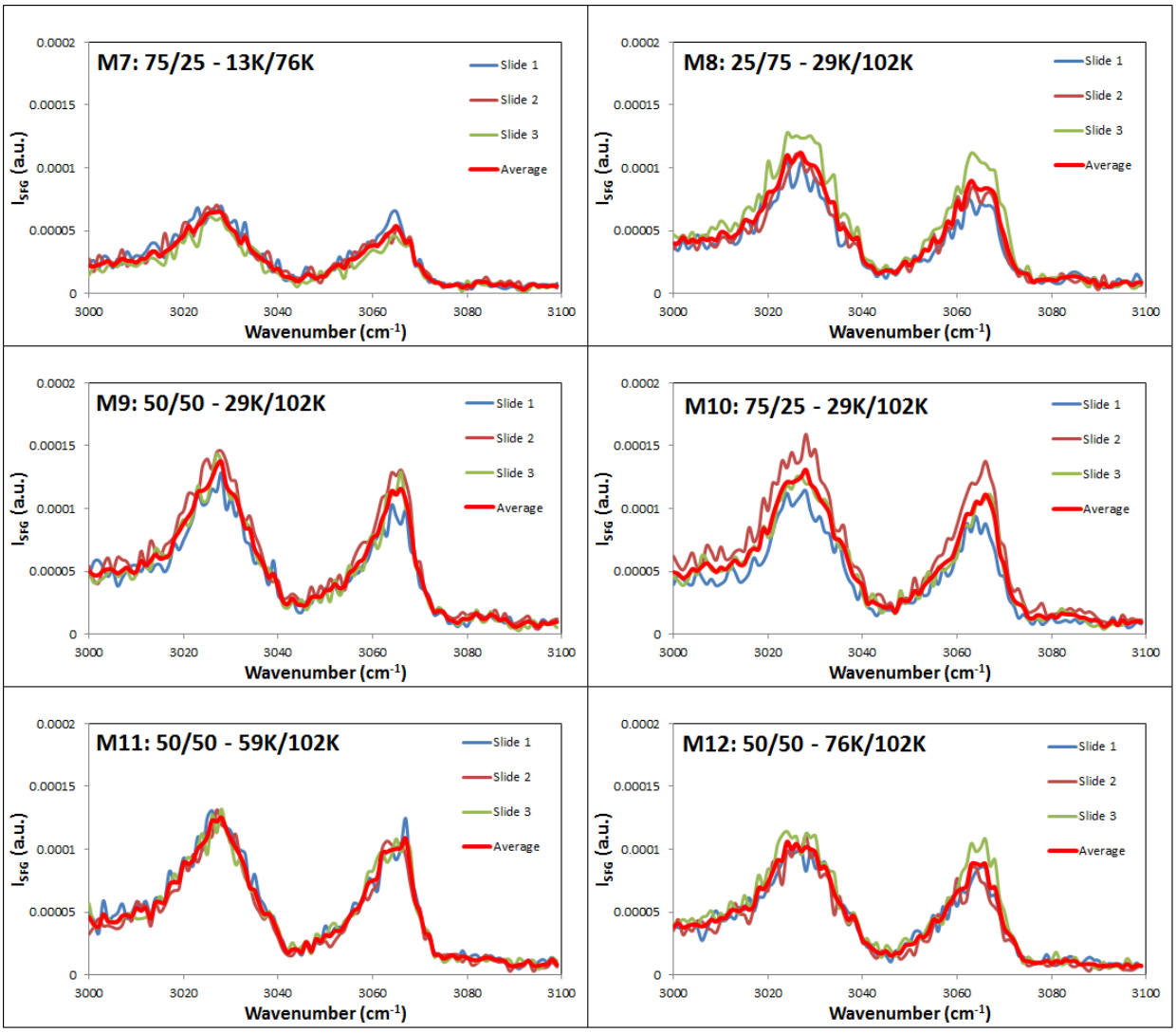

Figure 4.11– b: PPP polarized SFG spectra from PS/air interfaces from films of mixtures 7 to 12 normalized with respect to $I_{IR}*I_{VIS}$.

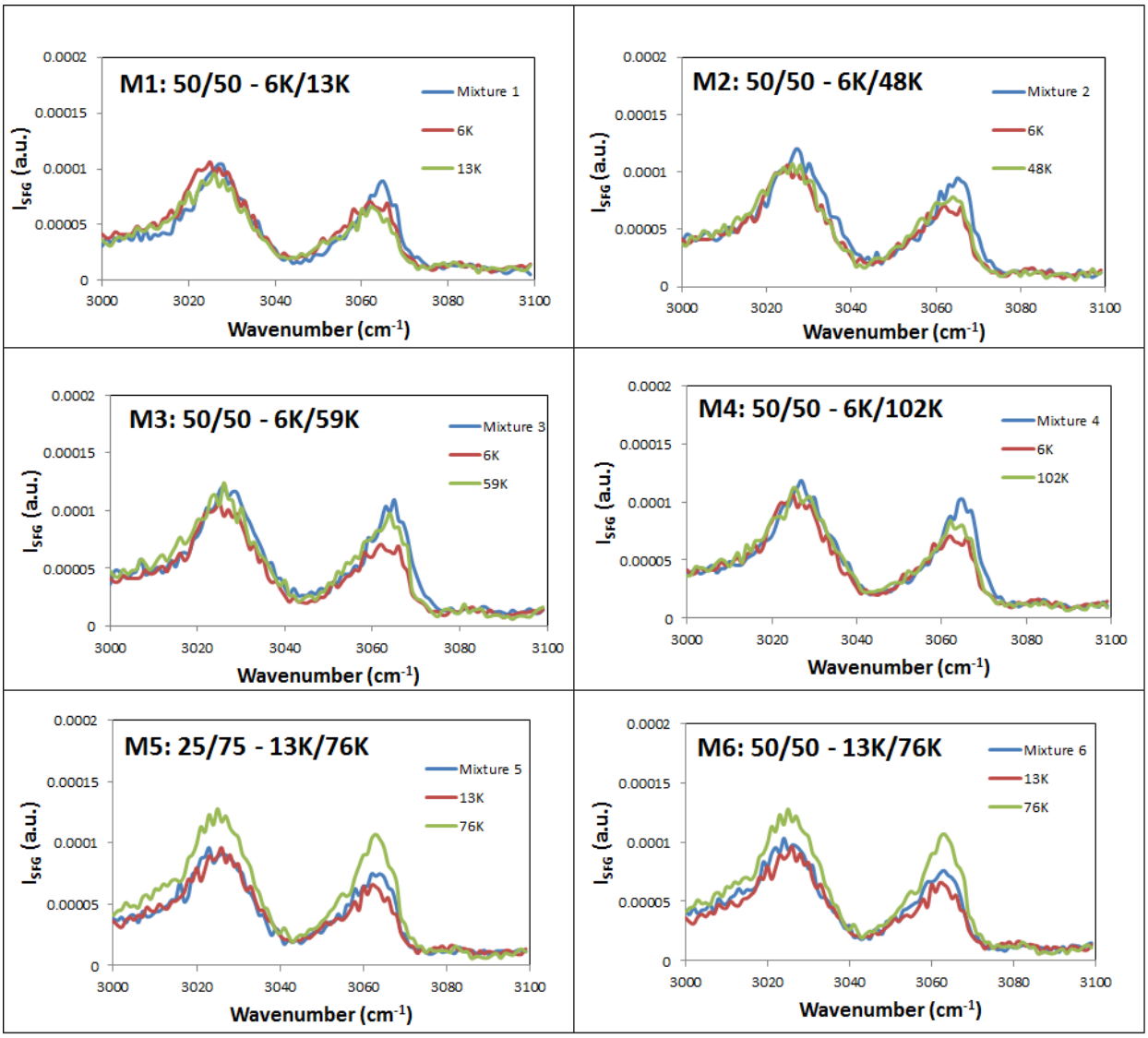

Figure 4.12 – a: PPP polarized average SFG spectra from PS/air interfaces from films of mixtures 1 to 6 normalized with respect to $I_{IR}*I_{VIS}$ compared to spectra of monodisperse polymers.

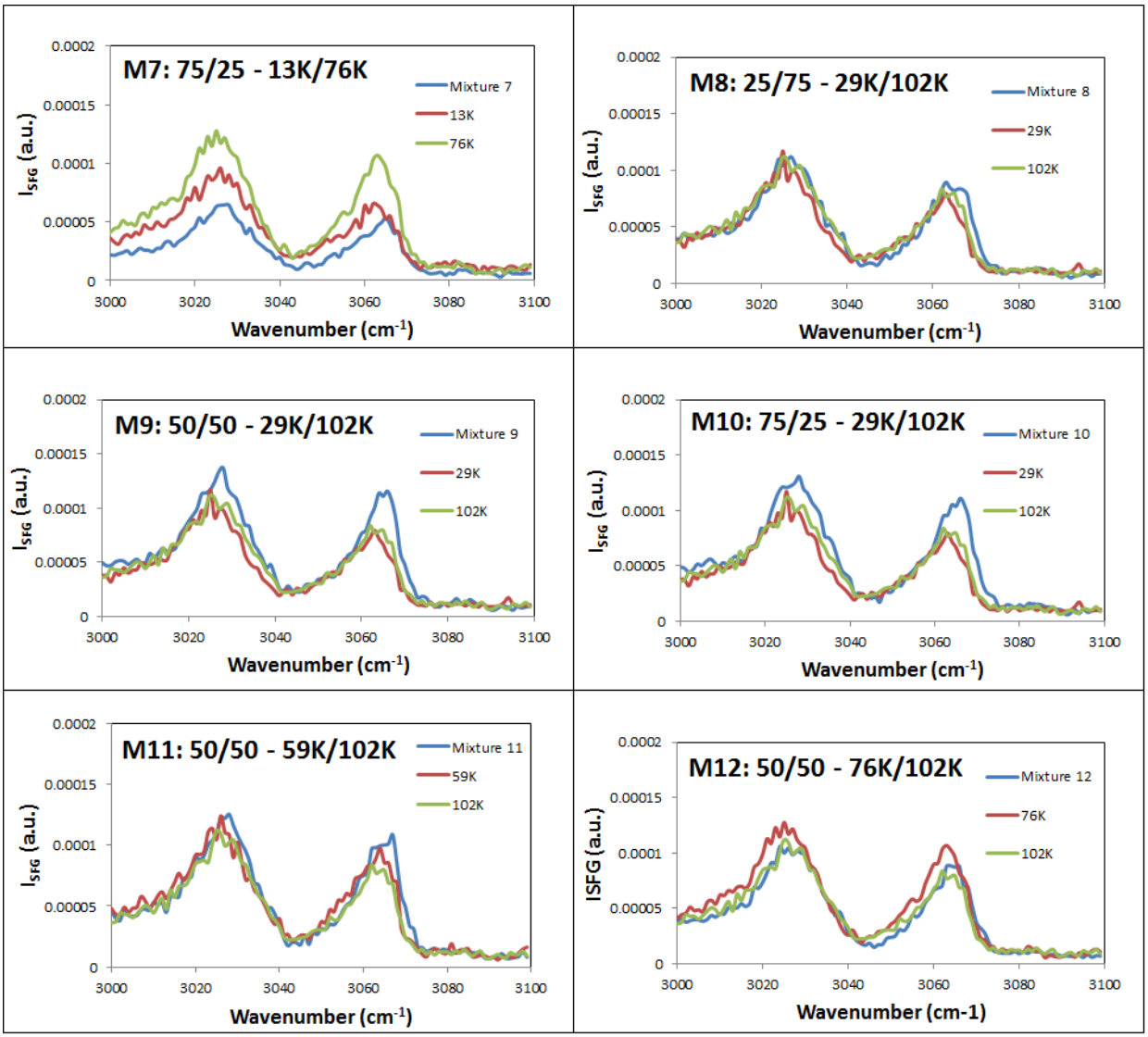

Figure 4.12 – b: PPP polarized average SFG spectra from PS/air interfaces from films of mixtures 7 to 12 normalized with respect to $I_{IR}*I_{VIS}$ compared to spectra of monodisperse polymers.

4.4 Statistical Analysis of SFG Spectra from PS/air Interfaces from Mixtures

In order to determine if there is any consistent variation of SFG intensity of modes ν_{7b} and ν_2 in SSP polarized SFG spectra and modes ν_{20b} and ν_2 in PPP polarized SFG spectra from PS/air interfaces of mixtures, 4 different statistical analyses are performed.

The first analysis is to check if there is any consistent variation of SFG intensity of the modes as a function of weight average molecular weight. The weight average molecular weight is calculated based on the compositions of components. Table 4.6 shows the average molecular weights of all mixtures placed in an increasing order. Figures 4.13 and 4.14 show the variation of SFG intensities of modes ν_{7b} and ν_2 in SSP polarized SFG spectra and modes ν_{20b} and ν_2 in PPP polarized SFG spectra from PS/air interfaces of mixtures after normalization w.r.t. $I_{IR}*I_{VIS}$ respectively as a function of Average M_W.

Table 4.6: Average molecular weights of all mixtures placed in an increasing order.

Mixture	**Average M_W (Kg/mol)**
1	9.5
2	27
7	28.75
3	32.5
6	44.5
10	47.25
4	54
5	60.25
9	65.5
11	80.5
8	83.75
12	89

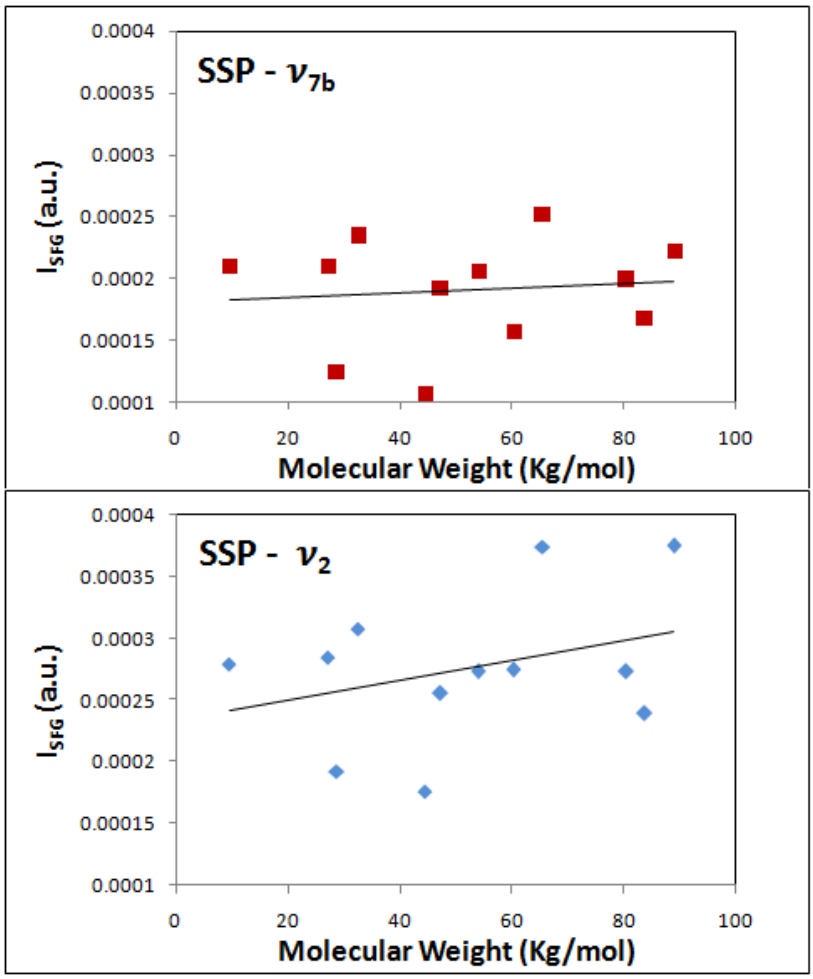

Figure 4.13: Variation of SSP peak intensities of modes ν_{20b} and ν_2 versus weight average molecular weights for mixtures.

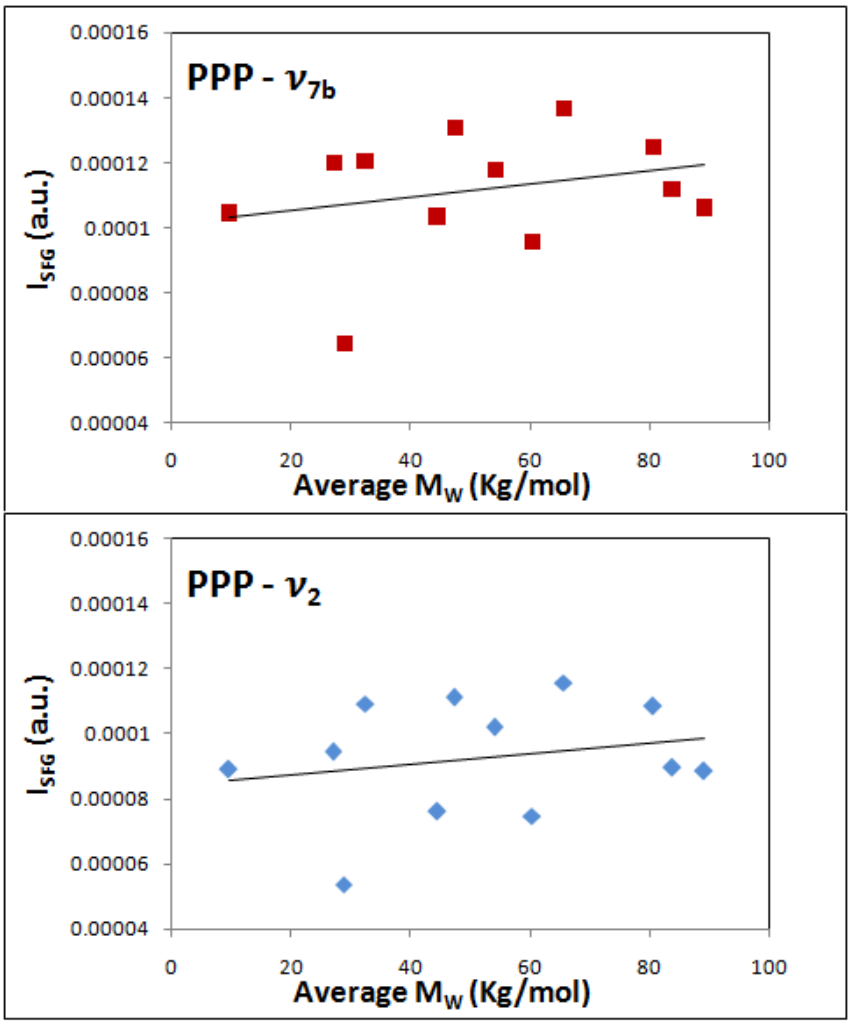

Figure 4.14: Variation of PPP peak intensities of modes ν_{20b} and ν_2 versus weight average molecular weights for mixtures.

The data plotted in the graphs of Figures 4.13 and 4.14 show that there seems to be an increasing trend of SFG intensities of the modes with average molecular weight. The same statistical analysis explained in section 4.2 is used in this section in order to determine credibility of this observation. The results of this analysis are shown in Table 4.7. Unlike with monodisperse polymers, the probabilities that these increases are happening by chance are pretty high. In other words, the variation of intensities of these modes is not consistent with that of the average molecular weights.

Table 4.7: Results of statistical analysis for SSP and PPP polarized SFG spectra for mixtures as a function of weight average molecular weight.

Polarization	Mode	Slope	Error on Slope	y-intercept	Error on y-intercept	R^2	α
SSP	ν_{7b}	$1.9*10^{-7}$	$5.5*10^{-7}$	0.0002	$3.1*10^{-5}$	0.01	0.74
	ν_2	$8.0*10^{-7}$	$7.1*10^{-7}$	0.0002	$4.1*10^{-5}$	0.11	0.28
PPP	ν_{20b}	$2.0*10^{-7}$	$2.3*10^{-7}$	0.0001	$1.3*10^{-5}$	0.07	0.41
	ν_2	$1.6*10^{-7}$	$2.3*10^{-7}$	$8.4*10^{-5}$	$1.3*10^{-5}$	0.05	0.50

The second analysis is to check if there is any consistent variation of SFG intensity of the modes as a function of number average molecular weight. The number average molecular weight is calculated using the mole fraction of the components in the mixtures: $M_N = M_1 \frac{n_1}{n_1+n_2} + M_2 \frac{n_2}{n_1+n_2}$ where n_1 is the number of moles of the lower molecular weight component and n_2 is the number of moles of the higher molecular weight component. Table 4.8 shows the number average molecular weights of all mixtures placed in an increasing order. Figures 4.15 and 4.16 show the variation of SFG intensities of modes ν_{7b} and ν_2 in SSP polarized SFG spectra and modes ν_{20b} and ν_2 in PPP polarized SFG spectra from PS/air interfaces of mixtures after normalization w.r.t. $I_{IR}*I_{VIS}$ respectively as a function of M_N.

Table 4.8 Number average molecular weights of all mixtures placed in an increasing order.

Mixture	**M_N (Kg/mol)**
1	8.2
2	10.7
3	10.9
4	11.3
7	16.4
6	22.2
5	34.4
10	35.3
9	45.2
8	62.6
11	74.8
12	87.1

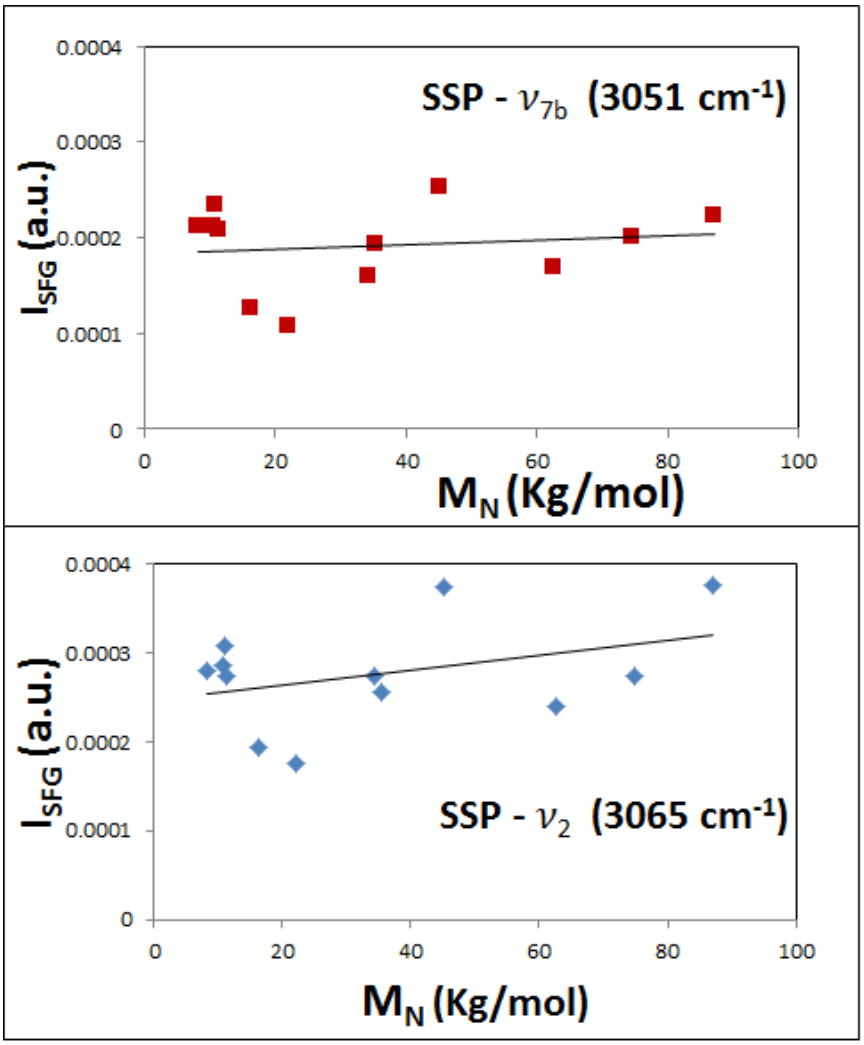

Figure 4.15: Variation of SSP peak intensities of modes ν_{7b} and ν_2 versus number average molecular weights for mixtures.

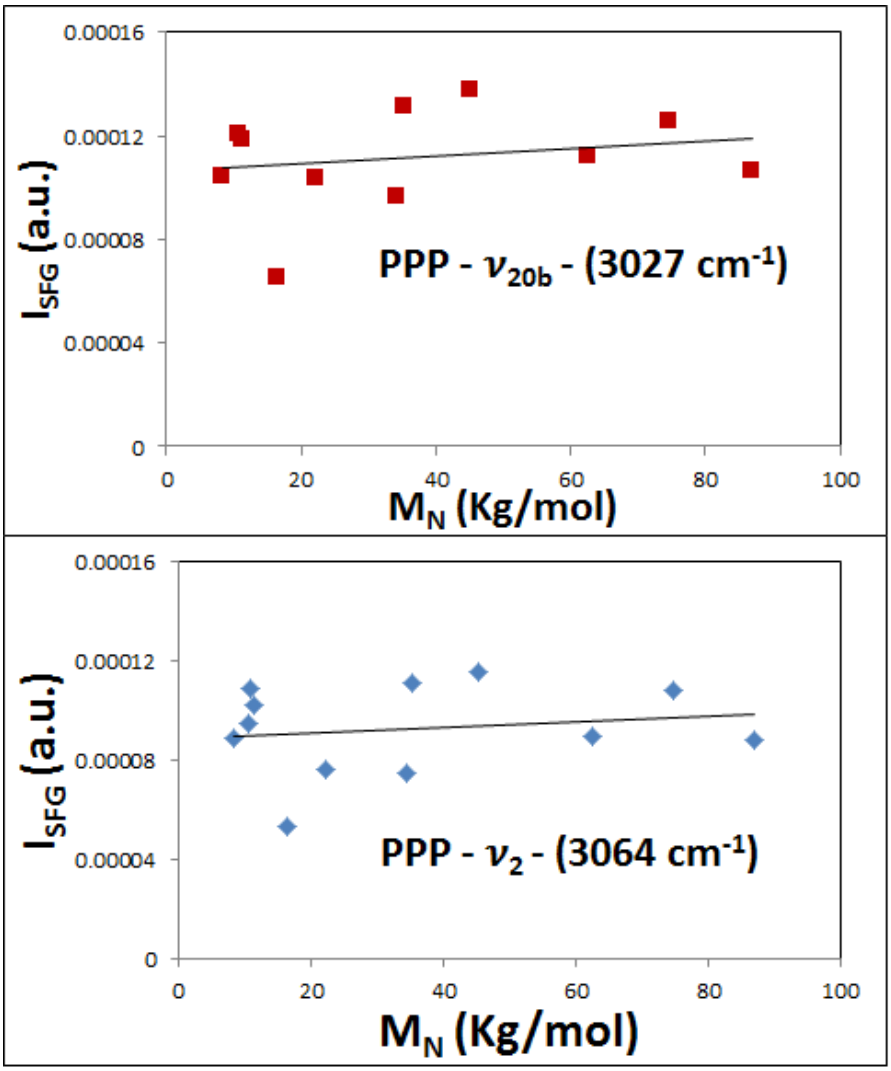

Figure 4.16: Variation of PPP peak intensities of modes ν_{20b} and ν_2 versus number average molecular weights for mixtures.

Upon performing the f-test analysis, we deduce that there is no consistency in the variation. The high values of α shown in Table 4.9 confirm that if a trend of variation of intensities as a function of MN exists, it most probably occurred by chance.

Table 4.9: Results of statistical analysis for SSP and PPP polarized SFG spectra for mixtures as a function of number average molecular weight.

Polarization	Mode	Slope	Error on Slope	y-intercept	Error on y-intercept	R^2	α
SSP	ν_{7b}	$2.3*10^{-7}$	$5*10^{-7}$	0.00014	$2.18*10^{-5}$	0.02	0.65
	ν_2	$8.4*10^{-7}$	$6.4*10^{-7}$	0.00025	$2.8*10^{-5}$	0.14	0.22
PPP	ν_{20b}	$1.4*10^{-7}$	$2.2*10^{-7}$	0.00011	$9.5*10^{-6}$	0.03	0.54
	ν_2	$1.2*10^{-7}$	$2.1*10^{-7}$	$8.9*10^{-5}$	$9.1*10^{-6}$	0.03	0.59

The third statistical analysis is to check if there is any consistent variation of SFG intensity of the modes as a function of higher molecular weights in the mixtures. Figures 4.17 and 4.18 show the variation of SFG intensities of modes ν_{7b} and ν_2 in SSP polarized SFG spectra and modes ν_{20b} and ν_2 in PPP polarized SFG spectra from PS/air interfaces of mixtures after normalization w.r.t. $I_{IR}*I_{VIS}$ respectively as a function of high M_W.

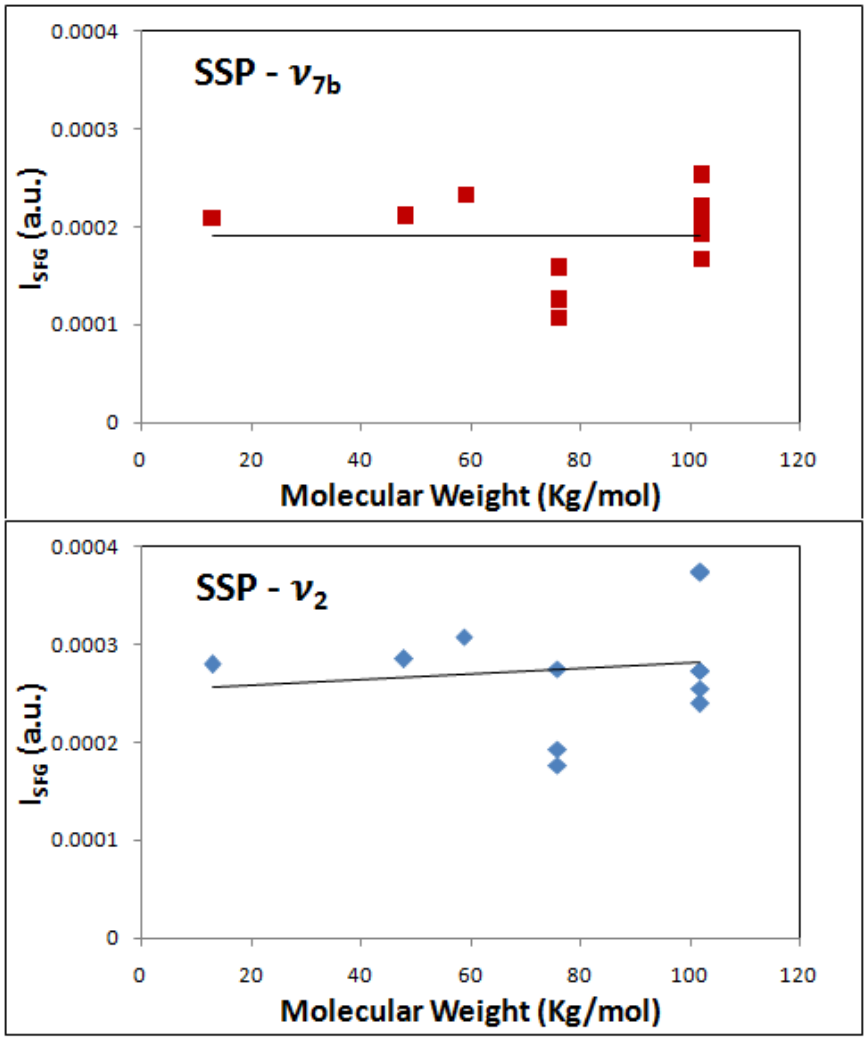

Figure 4.17: Variation of SSP peak intensities of modes ν_{7b} and ν_2 versus high molecular weights for mixtures.

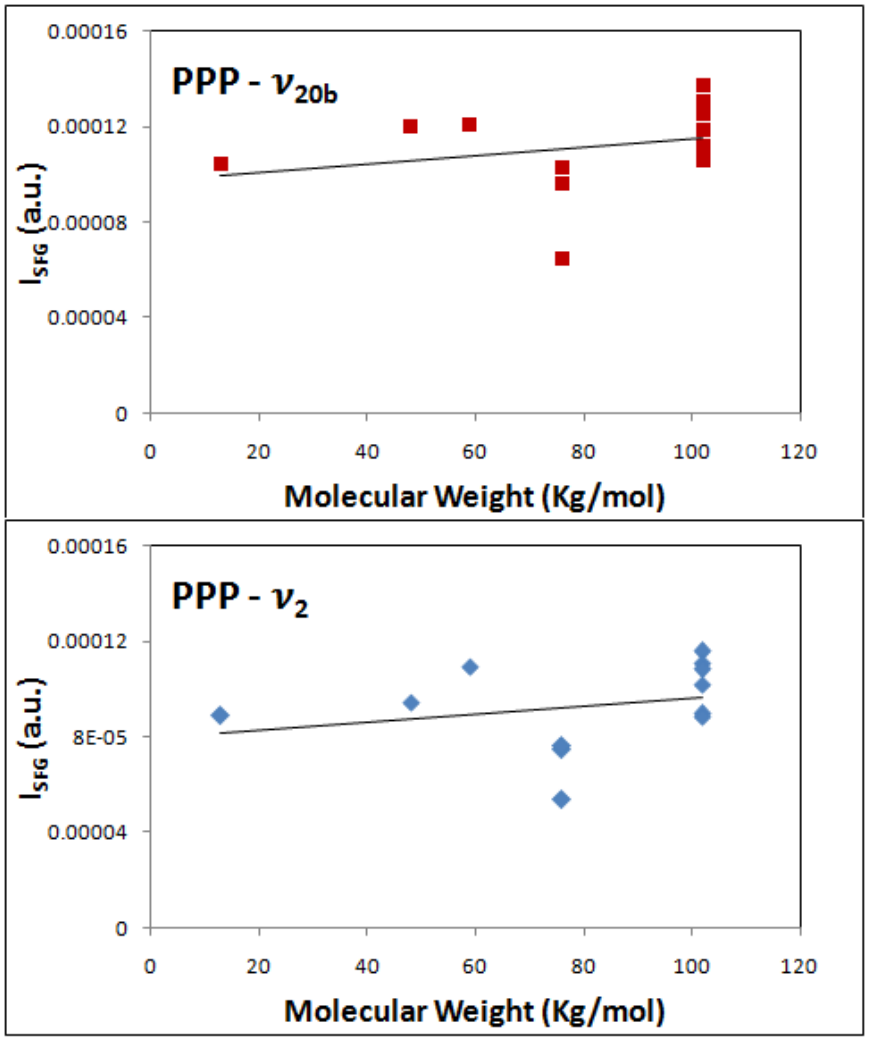

Figure 4.18: Variation of PPP peak intensities of modes ν_{20b} and ν_2 versus high molecular weights for mixtures.

Upon performing the f-test analysis, we deduce that there is no consistency in the variation. The high values of α shown in Table 4.10 confirm that if a trend of variation of intensities as a function of high M_W exists, it most probably occurred by chance.

Table 4.10: Results of statistical analysis for SSP and PPP polarized SFG spectra for mixtures as a function of the high molecular weight.

Polarization	Mode	Slope	Error on Slope	y-intercept	Error on y-intercept	R^2	α
SSP	ν_{7b}	$2.4*10^{-9}$	$4.8*10^{-7}$	$1.9*10^{-4}$	$4.1*10^{-5}$	$2.6*10^{-6}$	0.99
	ν_2	$2.8*10^{-7}$	$6.6*10^{-7}$	$2.5*10^{-4}$	$9.4*10^{-5}$	0.02	0.68
PPP	ν_{20b}	$1.8*10^{-7}$	$2.0*10^{-7}$	$9.7*10^{-5}$	$1.7*10^{-5}$	0.007	0.4
	ν_2	$1.6*10^{-7}$	$2.0*10^{-7}$	$8.0*10^{-5}$	$1.7*10^{-5}$	0.06	0.43

The fourth statistical analysis is to check if there is any consistent variation of SFG intensity of the modes as a function of lower molecular weights in the mixtures. Figures 4.19 and 4.20 show the variation of SFG intensities of modes ν_{7b} and ν_2 in SSP polarized SFG spectra and modes ν_{20b} and ν_2 in PPP polarized SFG spectra from PS/air interfaces of mixtures after normalization w.r.t. $I_{IR}*I_{VIS}$ respectively as a function of low M_W.

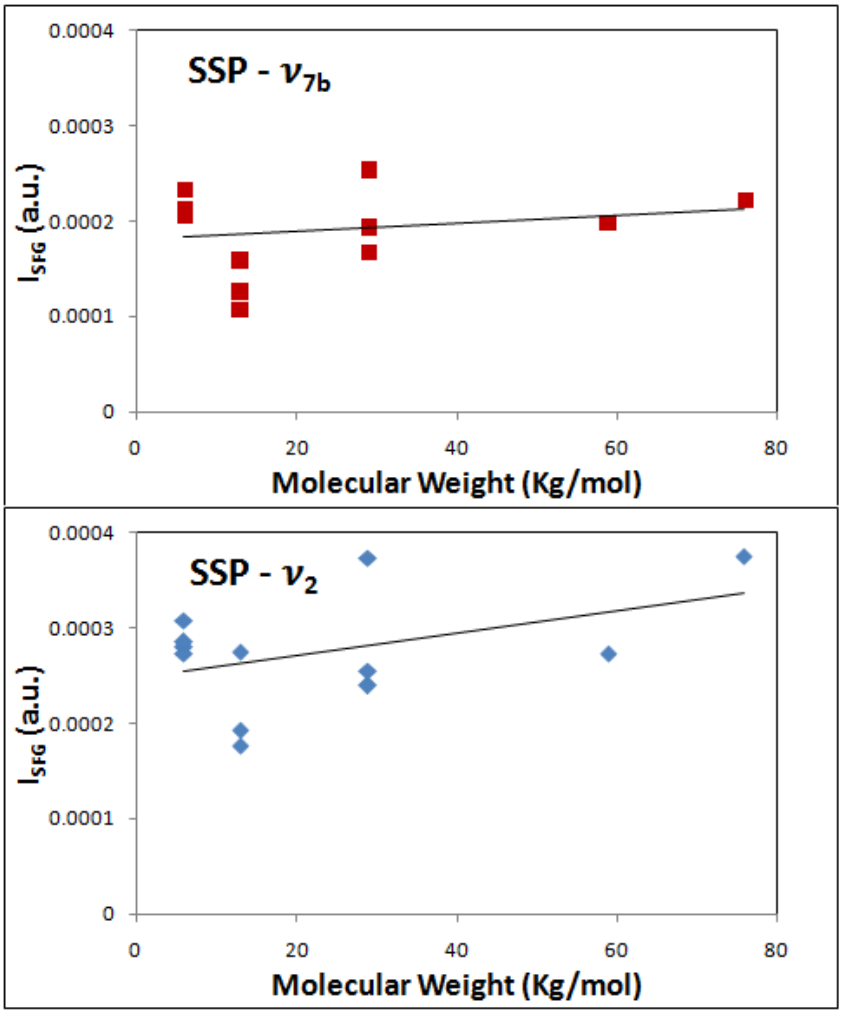

Figure 4.19: Variation of SSP peak intensities of modes ν_{7b} and ν_2 versus low molecular weights for mixtures.

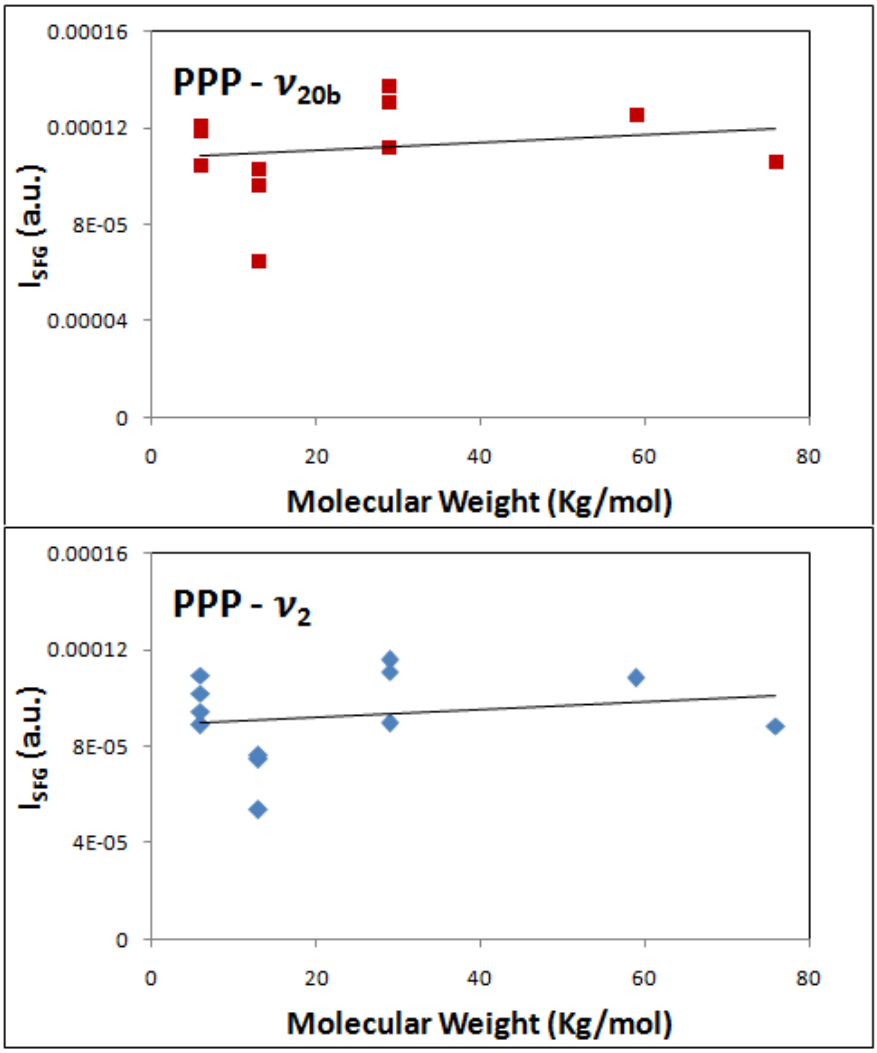

Figure 4.20: Variation of PPP peak intensities of modes ν_{20b} and ν_2 versus low molecular weights for mixtures.

Upon performing the f-test analysis, we deduce that there is no consistency in the variation. The high values of α shown in Table 4.11 confirm that if a trend of variation of intensities as a function of low M_W exists, it most probably occurred by chance.

Table 4.11: Results of statistical analysis for SSP and PPP polarized SFG spectra for mixtures as a function of the low molecular weight.

Polarization	Mode	Slope	Error on Slope	y-intercept	Error on y-intercept	R^2	α
SSP	ν_{7b}	$4.2*10^{-7}$	$5.9*10^{-7}$	$1.8*10^{-4}$	$1.9*10^{-5}$	0.05	0.5
	ν_2	$1.2*10^{-6}$	$7.5*10^{-7}$	$2.5*10^{-4}$	$2.4*10^{-5}$	0.2	0.15
PPP	ν_{20b}	$1.6*10^{-7}$	$2.6*10^{-7}$	$1.1*10^{-4}$	$8.4*10^{-6}$	0.03	0.57
	ν_2	$1.6*10^{-7}$	$2.0*10^{-7}$	$9*10^{-5}$	$8.0*10^{-6}$	0.04	0.54

4.5 Nonlinear fitting of data

In order to perform a quantitative analysis on the SFG spectra that were collected, it is important to perform nonlinear curve fitting. The spectra are fit using a custom-written Igor Pro software procedure[31] that convolutes Lorentzians in accordance with the following equations[31]:

$$I_{SFG} \propto \left|\chi^{(2)}\right|^2 I_{VIS} I_{IR} \qquad [4.5.1]$$

and

$$\chi_{RV}^{(2)} \propto N_{ads} \langle \frac{A_{v,ij} M_{v,k}}{\omega_{IR} - \omega_v + i\Gamma_v} \rangle \qquad [4.5.2]$$

where N_{ads} is the number of molecules at the interface and $M_{v,k}$ is the infrared transition dipole moment. The procedure[31] which is included in Appendix A includes a term to account for a nonresonant contribution. Each vibrational mode (i.e. Lorentzian term) and the nonresonant contribution has an associated phase factor. Since we are able to observe 3 resolved peaks in all our SSP spectra, we fit our data with 3 Lorenzian peaks. In addition, Igor Pro calculates the standard deviations for the parameters[32]. Numerous trials with various initial guesses were performed until the standard deviation was minimized and qualitative parameters were generated. Table 4.12 shows all parameters obtained from fitting for all molecular weights from the SSP polarized SFG spectra and Table 4.13 shows those from PPP polarized SFG spectra. Figures 4.21 and 4.22 show graphs of how the parameters collected from nonlinear fitting are changing with MW for both SSP and PPP polarized SFG spectra respectively.

To determine the significance of any trend that might appear on the fitting parameters, we performed the statistical analysis that we explained earlier. Except for the mode ν_2 in the SSP polarized SFG spectra, the results shown in Table 4.14 suggest that if any trends exist, it most probably happened by chance. This is represented by the high values of α. As for the mode ν_2 in SSP polarized spectra, it seems to have a real significant increasing trend for both its amplitude and width.

Table 4.12: Parameters obtained from fittings from the SSP polarized SFG spectra

	6K	13K	18K	29K	48K	59K	76K	102K
ω_{20b}	3027.5 ± 0.0	3027.5 ± 0.0	3027.5 ± 0.0	3027.5 ± 0.0	3027.5 ± 0.0	3027.5 ± 0.0	3027.5 ± 0.0	3027.5 ± 0.0
A_{20b}	0.032 ± 0.002	0.033 ± 0.003	0.051 ± 0.003	0.035 ± 0.004	0.034 ± 0.004	0.036 ± 0.005	0.026 ± 0.004	0.049 ± 0.004
Γ_{20b}	9.0 ± 0.5	10.5 ± 0.9	10.2 ± 0.5	9.3 ± 0.9	10.1 ± 1.0	10.8 ± 1.2	7.7 ± 1.1	12.1 ± 0.8
ω_{7b}	3050.9 ± 0.0	3050.9 ± 0.0	3050.9 ± 0.0	3050.9 ± 0.0	3050.9 ± 0.0	3050.9 ± 0.0	3050.9 ± 0.0	3050.9 ± 0.0
A_{7b}	0.017 ± 0.001	0.018 ± 0.002	0.021 ± 0.002	0.033 ± 0.004	0.028 ± 0.002	0.028 ± 0.003	0.036 ± 0.005	0.015 ± 0.002
Γ_{7b}	4.7 ± 0.3	5.3 ± 0.4	5.3 ± 0.4	7.0 ± 0.6	5.8 ± 0.4	5.9 ± 0.4	6.7 ± 0.6	4.4 ± 0.4
ω_2	3064.7 ± 0.0	3064.7 ± 0.0	3064.7 ± 0.0	3064.7 ± 0.0	3064.7 ± 0.0	3064.7 ± 0.0	3064.7 ± 0.0	3064.7 ± 0.0
A_2	0.093 ± 0.003	0.002 ± 0.002	0.104 ± 0.002	0.098 ± 0.004	0.094 ± 0.002	0.113 ± 0.003	0.108 ± 0.004	0.118 ± 0.002
Γ_2	6.8 ± 0.1	6.6 ± 0.1	7.1 ± 0.1	6.9 ± 0.2	6.3 ± 0.1	6.5 ± 0.1	6.5 ± 0.2	6.6 ± 0.1

Table 4.13: Parameters obtained from fittings from the PPP polarized SFG spectra

	6K	13K	18K	29K	48K	59K	76K	102K
ω20b	3028.5 ± 0.0	3028.5 ± 0.0	3028.5 ± 0.0	3028.5 ± 0.0	3028.5 ± 0.0	3028.5 ± 0.0	3028.5 ± 0.0	3028.5 ± 0.0
A20b	0.063 ± 0.005	0.066 ± 0.007	0.072 ± 0.007	0.064 ± 0.006	0.069 ± 0.005	0.068 ± 0.007	0.080 ± 0.007	0.065 ± 0.006
Γ20b	9.1 ± 0.5	10.0 ± 0.6	10.4 ± 0.5	9.0 ± 0.5	9.5 ± 0.4	9.5 ± 0.5	9.6 ± 0.5	9.5 ± 0.5
ω7b	3055.8 ± 0.0	3055.8 ± 0.0	3055.8 ± 0.0	3055.8 ± 0.0	3055.8 ± 0.0	3055.8 ± 0.0	3055.8 ± 0.0	3055.8 ± 0.0
A7b	0.035 ± 0.010	0.051 ± 0.018	0.075 ± 0.022	0.061 ± 0.019	0.044 ± 0.009	0.036 ± 0.011	0.069 ± 0.021	0.034 ± 0.014
Γ7b	8.9 ± 1.7	12.4 ± 3.0	15.0 ± 2.7	14.2 ± 3.2	9.6 ± 1.3	8.9 ± 1.7	12.8 ± 2.7	10.0 ± 2.8
ω2	3067.0 ± 0.0	3067.0 ± 0.0	3067.0 ± 0.0	3067.0 ± 0.0	3067.0 ± 0.0	3067.0 ± 0.0	3067.0 ± 0.0	3067.0 ± 0.0
A2	0.050 ± 0.007	0.012 ± 0.012	0.068 ± 0.012	0.063 ± 0.010	0.052 ± 0.005	0.052 ± 0.006	0.075 ± 0.011	0.060 ± 0.010
Γ2	4.2 ± 0.6	4.8 ± 0.9	5.4 ± 0.8	5.1 ± 0.7	4.1 ± 0.4	4.0 ± 0.4	5.3 ± 0.6	4.9 ± 0.6

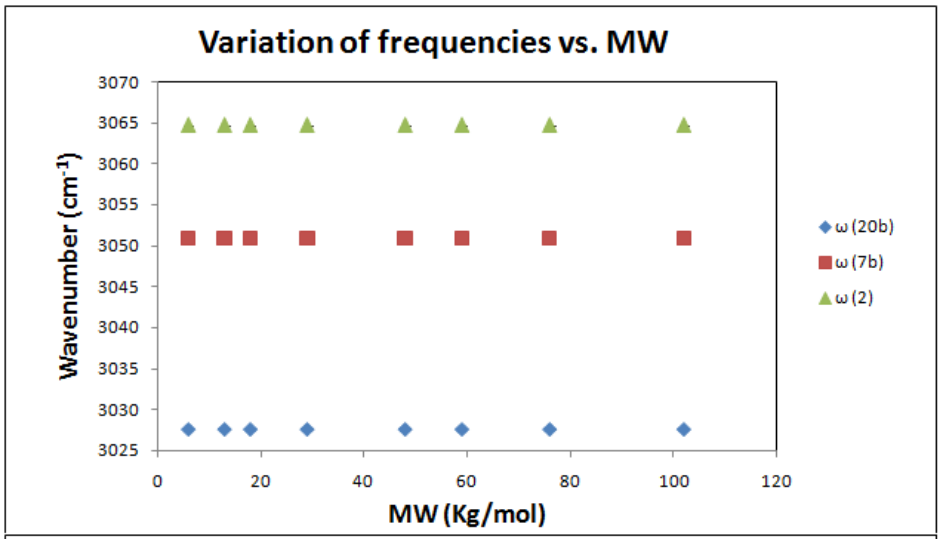

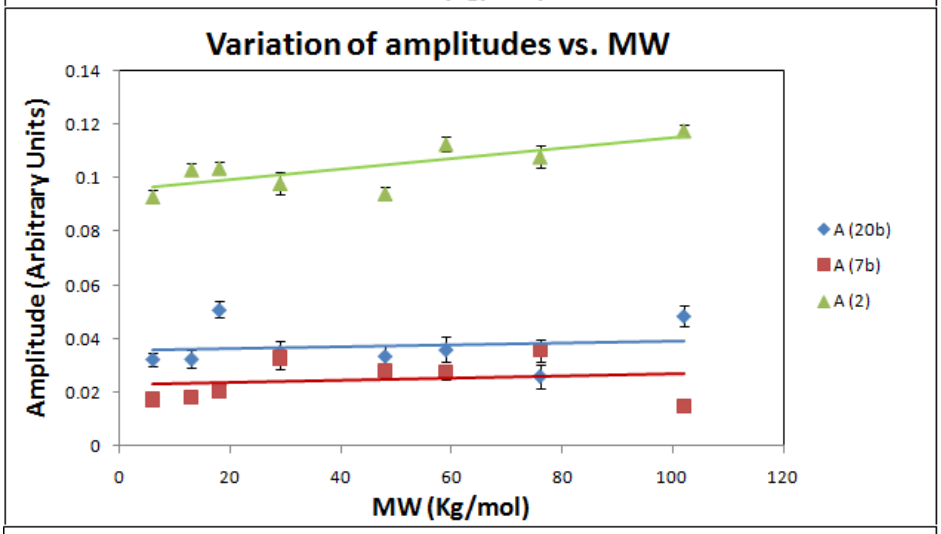

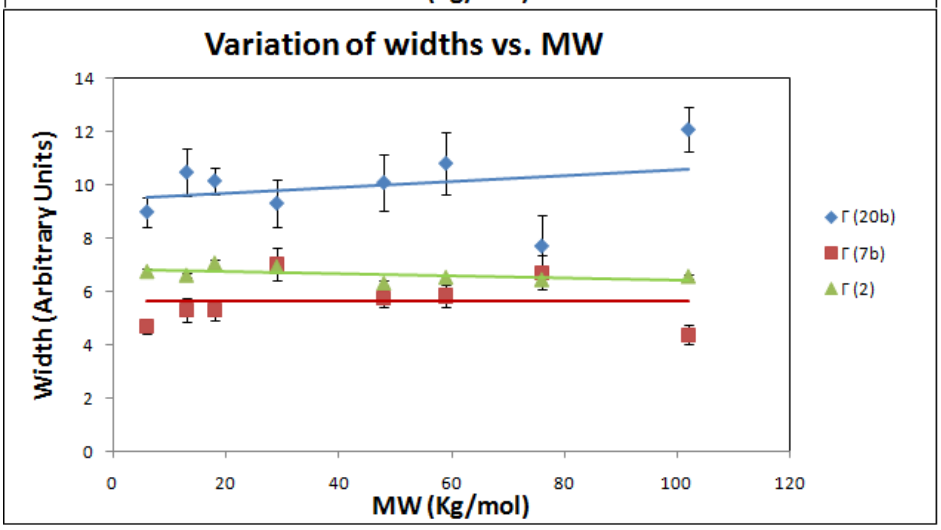

Figures 4.21: Variation of parameters with M_W for SSP polarized SFG spectra.

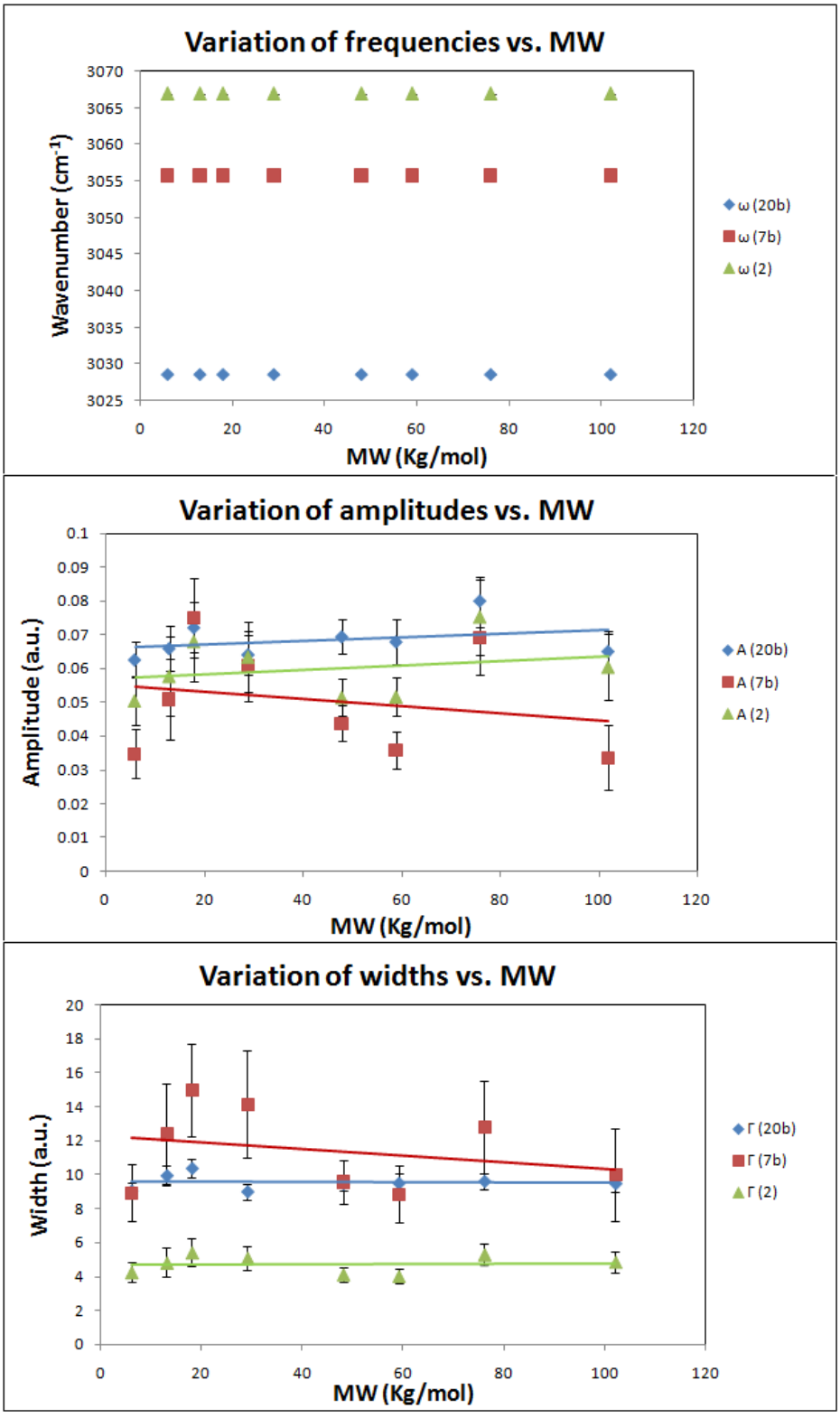

Figures 4.22: Variation of parameters with M_W for PPP polarized SFG spectra.

Table 4.14: Results of statistical analysis for fitting parameters of monodisperse polymers.

Polarization	Mode	Slope	Error on Slope	y-intercept	Error on y-intercept	R^2	α
SSP	A_{20b}	$3.5*10^{-5}$	0.0001	0.04	0.006	0.02	0.75
	Γ_{20b}	0.01	0.02	9.5	0.81	0.08	0.49
	A_{7b}	$3.9*10^{-5}$	$9.1*10^{-5}$	0.02	0.005	0.03	0.68
	Γ_{7b}	-0.0002	0.01	5.7	0.6	$7.2*10^{-5}$	0.98
	A_2	0.0002	$6.9*10^{-5}$	0.1	0.004	0.57	0.03
	Γ_2	-0.004	0.003	6.8	0.14	0.29	0.17
PPP	A_{20b}	$5.5*10^{-5}$	$6.3*10^{-5}$	0.07	0.0034	0.11	0.42
	Γ_{20b}	-0.001	0.005	9.6	0.3	0.0082	0.83
	A_{7b}	-0.0001	0.0002	0.055	0.01	0.05	0.6
	Γ_{7b}	-0.02	0.03	12.3	1.5	0.07	0.5
	A_2	$6.7*10^{-5}$	0.0001	0.057	0.0056	0.065	0.5
	Γ_2	0.0007	0.007	4.7	0.36	0.0018	0.92

The random variations that the fitting parameters seem to have can be explained by the complexity of the relationship that combines them together. In other words, the variations of the frequencies, amplitudes and widths of the three resolved modes that we take into consideration are interacting all together based on Equation 1.3.6.

$$I(\omega_{SF}) \propto \left|\chi^{(2)}\right|^2 = \left|\chi_{eff,NR} + \sum_q \frac{A_q}{\omega_2 - \omega_q - i\Gamma_q}\right|^2 \qquad [1.3.6]^{9, 10, 11, 23, 24, 26}$$

As Equation 1.3.6 shows, the SFG intensity includes the square of the summation of resonant and nonresonant susceptabilities. The resonant part is in turn a nonlinear function of amplitudes, frequencies and widths of all fitted vibration modes. As a result, the variation of fitting parameters do not necessary have to follow the same pattern which the corresponding SFG intensity does. We are not claiming that the variations of the parameters are necessarily random. What we are suggesting is that these parameters can be varying consistently according to a complicated functional relationship. Determining this function is beyond the scope of this work.

4.6 Tilt angle determination

First, it is important to mention that there are two angles that govern the orientation of the phenyl rings, the tilt angle which varies in the x-z plane, and the twist angle which moves in the y-z plane. In this work, we assume that only the tilt angle is responsible for any SFG variation, and we do not study the effects of the twist angle variation. In order to determine the tilt of the phenyl groups of the polystyrene molecules on the PS/air interface, the sets of parameters collected from the nonlinear fitting were used. In fact, the amplitudes of the peaks of the vibrational modes are the parameters that allow us to estimate the tilt angle of the phenyl groups of the PS molecules.

It is also important to note that there are different types of vibrations within the molecule, based on the values of the nonzero elements of the hyperpolarizability tensor (β). The hyperpolarizability is a tensor that includes theoretical nonlinear properties of a single molecule. The elements that represent the bulk with inversion symmetry will vanish, while those that represent the interface with broken inversion symmetry will not. For SFG, it is a third rank tensor with 27 elements. The β tensor is shown below:

$$\beta = \begin{vmatrix} \beta aaa & \beta aab & \beta aac \\ \beta aba & \beta abb & \beta abc \\ \beta aca & \beta acb & \beta acc \\ \beta baa & \beta bab & \beta bac \\ \beta bba & \beta bbb & \beta bbc \\ \beta bca & \beta bcb & \beta bcc \\ \beta baa & \beta cab & \beta cac \\ \beta cba & \beta cbb & \beta cbc \\ \beta cca & \beta ccb & \beta ccc \end{vmatrix}$$

The coordinates that are used in the β tensor above are molecular coordinates, and are transformed from the surface coordinates. As shown in Figure 4.23, the "c" axis is that which passes through the C_2 rotation axis across the phenyl group and through the C-C bond between the aliphatic hydrocarbon chain and the aromatic phenyl ring. The other two axes "a" and "b" are orthogonal to "c".

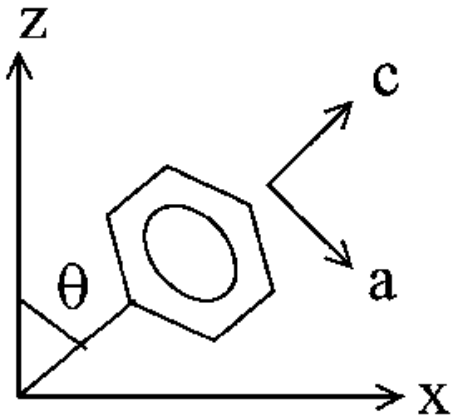

Figure 4.23: Illustration of molecular coordinates versus surface coordinates.

The five different vibrations of the C-H bonds in the phenyl group of the PS molecules can be categorized into two types, type I and type II, based on the symmetry of the vibration[10]. In other words, if the C-H bonds are vibrating symmetrically with respect to the c-axis, the vibrations are considered type I, and if they are vibrating anti-symmetrically with respect to the c-axis, then the vibrations are considered type II. Modes ν_2, ν_{7a}, and ν_{20a} belong to type I vibrations, while modes ν_{7b} and ν_{20b} belong to type II vibrations. For type I vibrations, there are only two nonzero elements in β: β_{aac} and β_{ccc}. For type II, there are only two nonzero elements in β: $\beta_{caa} = \beta_{aca}$. This categorization is critical for the determination of the tilt angle, and will be explained later.

An estimate of the tilt angle of the phenyl groups of the PS molecules can be determined using the following equation:

$$R = \left|\frac{A_{q,II}}{A_{q,I}}\right| = \left|\left(\frac{\beta_{caa,II}}{\beta_{aac,I}}\right)\left(\frac{2(\langle cos3\theta\rangle - \langle cos\theta\rangle)}{(7+2r)\langle cos\theta\rangle + (1-2r)\langle cos3\theta\rangle}\right)\right| \quad [4.2.1][10]$$

R is the ratio of two amplitudes for two vibrations from two different types, θ is the tilt angle which we are looking for, and r is is the ratio of two nonzero hyperpolarizability elements of the same type. This ratio has been calculated by Whiffen et al.[33] for benzene rings using the bond polarizability matrix and it is equals to 0.25:

$$r = \frac{\beta_{ccc}}{\beta_{aac}} = 0.25 \quad [4.2.2]$$

Equation 4.2.1 shows how the tilt angle of the phenyl groups of the PS molecules will change as the ratios of amplitudes from different types change. Dhinojwola et al determined the value of $\left(\frac{\beta_{caa,II}}{\beta_{aac,I}}\right)$ for polystyrene using IR and Raman spectra, and it is equal to 2.0.

Now, R is plotted as a function of θ, where θ varies from 0^O to 90^O. The plot is shown in Figure 4.24.

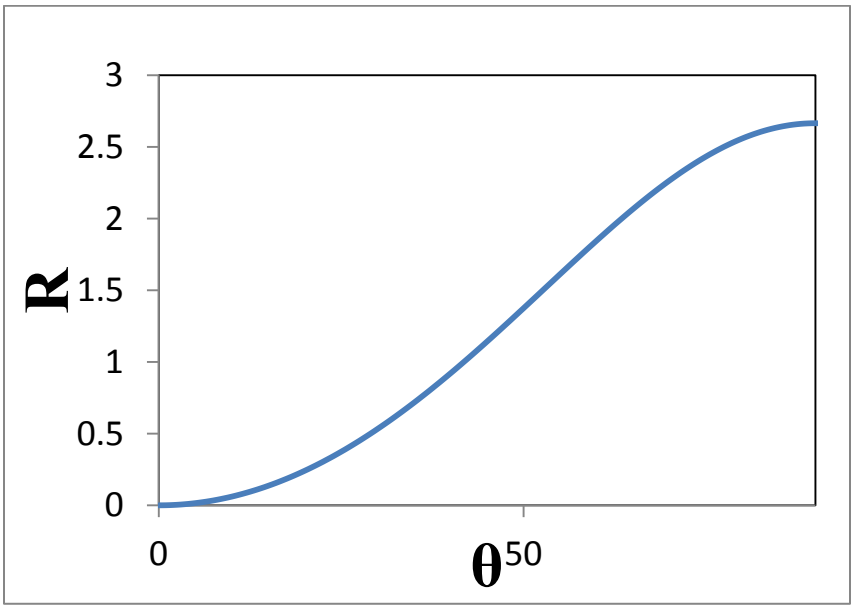

Figure 4.24: Graph showing the change in R as a function of the tilt angle θ.

In our calculations, we use the mode ν_2 for Type I and the mode ν_{20b} for Type II. Using the amplitudes obtained by fitting, we calculate the values of R. The results are shown in Table 4.15, and the orientation angles are plotted versus molecular weight in Figure 4.25.

Table 4.15: Tilt angles for the different molecular weights

	$A_{20b,II}$	$A_{2,I}$	R	Angle (°)
6K	0.032	0.093	0.348	24
13K	0.033	0.103	0.315	23
18K	0.021	0.104	0.199	18.5
29K	0.035	0.098	0.359	24.5
48K	0.034	0.094	0.356	24.5
59K	0.036	0.113	0.319	23.5
76K	0.026	0.108	0.242	20
102K	0.049	0.118	0.413	26

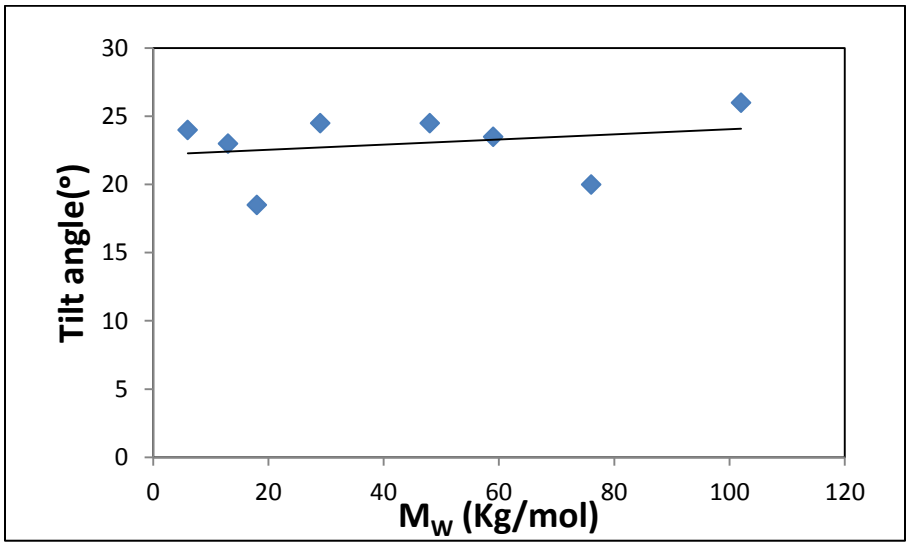

Figure 4.25: Variation of tilt angles of phenyl groups in monodisperse PS molecules as a function of molecular weight.

It is not possible to correlate the tilt angle to the molecular weight using the graph in Figure 4.25. In fact, upon performing the statistical analysis on these results, the probability that this increase happened by chance is 55%. Again, this does not necessarily mean that the orientation angle is not changing in a consistent manner versus molecular weight. It simply means that we are unable yet to determine the functional relationship between the angle and the molecular weight due to the nonlinearity of the fitting, and the correlation of the parameters.

Chapter 5

Discussion

The intensities of the resolved peaks in the SFG spectra of monodisperse polystyrene/air interfaces increase with molecular weight. We believe this is because of slight changes in the orientation angle of phenyl groups of PS chains with the increase of molecular weight. According to Chen[34], when SFG occurs, the molecular hyperpolarizabilty is projected on the lab coordinates that correspond to the vibration. For example, assuming that the vibration is parallel to the y-axis as shown in Figure 5.1-a, the hyperpolarizability will be projected on the y-axis only. If the molecule is tilted and the vibration is forming an angle Θ with y-axis as in Figure 5.1-b, the hyperpolarizabilty will be projected on both x-axis and y-axis. If the molecule is perpendicular to the y-axis as shown in Figure 5.1-c, the hyperpolarizability will be projected on the x-axis only. We consider x and y axes only because the vibrations of the phenyl group are two dimensional. As a result, the value of the projection of the hyperpolarizabilty on y-axis decreases as the tilt angle increase, while the projection of the hyperpolarizabilty on x-axis increases as the tilt angle increase. In other words, the effect of tilt angle depends on the direction of the SFG vector of every vibration.

We suggest that this tilt angle effect is in turn governed by the molecular weight variation of the polymers since all other possible factors have been eliminated. Why does the orientation angle change with molecular weight? This is a big question, and the answer to it cannot be addressed in this thesis.

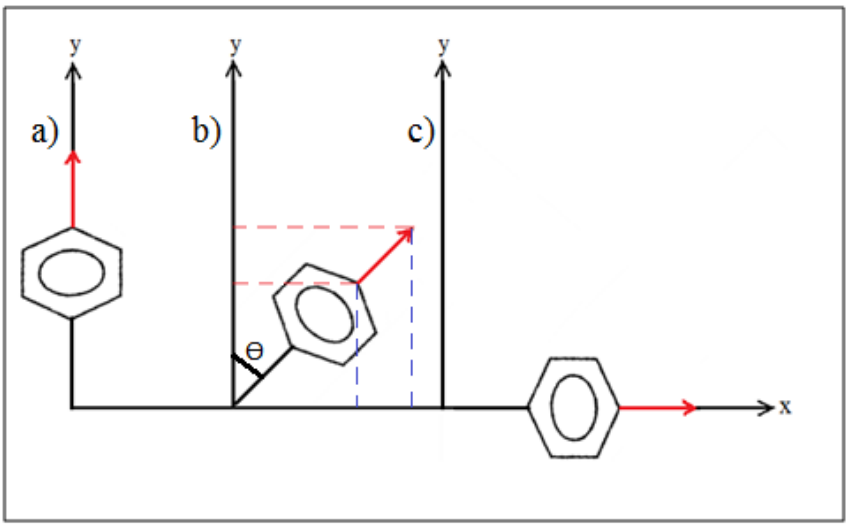

Figure 5.1: Hyperpolarizability projections as tilt angle changes.

The results that were obtained for mixtures, the parameters generated by fitting the data into equation 1.3.6, and orientation angles are different from what was determined above. However, this does not mean that the observed variations must be random.

When two monodisperse polymers are mixed together, different chain lengths exist. This means that according to our explanation, different tilt angles exist. This will lead to further complications of the SFG phenomenon, which might be why we do not see a unique pattern. With the fitting parameters, it is not surprising that these parameters do not follow an obvious pattern because of the complexity and nonlinearity of equation 1.3.6, and the correlation of the parameters. Since we obtain the tilt angle using the fitting parameters, we do not see a consistent pattern for the tilt angle variation either. We suggest, again, that the tilt angle might be affecting peak intensities, but we do not understand the functionality of this effect yet due to the dependence on parameters that are related in a complex manner.

Chapter 6

Conclusions:

The direct effect of molecular weight is on the SFG intensities of the peaks. The intensities of resolved peaks in SFG spectra of monodisperse PS which are normalized w.r.t. $I_{IR}*I_{VIS}$ increase with molecular weight. However, things get complicated when we mix two or more pure monodisperse polymers with various compositions because this conclusion does not seem to hold. In addition, when we perform nonlinear fitting, the parameters (amplitude, frequency and width) do not seem to follow the same trend as the SFG intensities. We explain this by the complexity of equation 1.3.6 that relates them together. The same conclusion was found when determining the tilt angles when we do not study the effect of the twist angle. We do not claim that molecular weight has no direct effect on fitting parameters and tilt angle, but we suggest that they might be affected by molecular weight in a complicated way that we do not understand yet.

References

[1] D. L. Pavia, G. M. Lampman, & G. S. Kriz, 2001. *Introduction to spectroscopy: A guide for students of organic chemistry*. Fort Worth: Harcourt College Publishers.

[2] R. Brown. 1828. *A Brief Account of Microscopical Investigations on the Particles Contained in the Pollen of Plants*,The miscellaneous botanical works of Robert Brown, Volume 1.

[3] J. F. Ogilvie. 1989. *Infrared Spectroscopy of Diatomic Molecules-the First Century*. Chinese Journal of Physics. Vol. 27 No. 4

[4] W. Parson. 2007. *Modern Optical Spectroscopy with Exercises and Examples from Biophysics and Biochemistry*. Springer

[5] L. H. Sperling. 2006. *Introduction to Physical Polymer Science*. 4th ed. Wiley

[6] K. S. Gautam, A. D. Schwab, and A. Dhinojwala. *Molecular Structure of Polystyrene at Air/Polymer and Solid/Polymer Interfaces*, Phys. Rev. Lett, 85, 18, Oct. 30, 2000.

[7] P. R. Dvornic, M.J. Owen (eds.), *Silicone Surface Science*, Advances in Silicon Science 4, Chapter 2. © Springer Science + Business Media Dordrecht 2012

[8] P. A. Franken, A. E. Hill, C. E. Peters, and G. Weinreich. *Generation of Optical Harmonics*, Phys. Rev. Lett. 7, 118–119 (1961).

[9] J. H. Hunt, P. Guyot-Sionnest, Y.R. Shen, *Observation of C-H stretch vibrations of monolayers of molecules optical sum-frequency generation*, Chemical Physics Letters, Vol. 133, Iss. 3, 16 January 1987, Pp. 189-192.

[10] K. S. Gautam, A. D. Schwab, and A. Dhinojwala. *Molecular Structure of Polystyrene at Air/Polymer and Solid/Polymer Interfaces*, Phys. Rev. Lett, 85, 18, Oct. 30, 2000.

[11] K. A. Briggman, J. C. Stephenson, W. E. Wallace, and L. J. Richter, *Absolute Molecular Orientational Distribution of the Polystyrene Surface*, J. Phys. Chem. B 2001, 105, 2785-2791.

[12] C. Y. Liang and S. Krimm; *Infrared Spectra of High Polymers. VI. Polystyrene*; Journal of Polymer Science vol. XXVII, pp. 241-254 (1958)

[13] "Both HF and DFT calculations with the B3LYP functional were performed with the 6-311G(2d,2p) basis set with Gaussian 98."

[14] Wilson, E. B., *FT-IR, FT-Raman and ab-initio studies of 1,3-diphenyl thiourea*, Jr. Phys. Rev., 45,706 (1934).

[15] G. Varsanyi, *Vibrational Spectra of Benzene Derivatives* (Academic Press, New York, 1969).

[16] D. Zhang, S. M. Dougal, and M. S. Yeganeh, *Effects of UV Irradiation and Plasma Treatment on a Polystyrene Surface Studied by IR-Visible Sum Frequency Generation Spectroscopy*, Langmuir 2000, 16, 4528-4532.

[17] A. Opdahl and G. A. Somorjai, *Solvent Vapor Induced Ordering and Disordering of Phenyl Side Branches at the Air/Polystyrene Interface Studied by SFG*, Langmuir 2002, 18, 9409-9412.

[18] C. S.-C. Yang, P. T. Wilson, and L. J. Richter, *Structure of Polystyrene at the Interface with Various Liquids*, Macromolecules 2004, 37, 7742-7746.

[19] M. Flörsheimer, C. Brillert, and H. Fuchs, *Chemical Imaging of Interfaces by Sum Frequency Microscopy*, Langmuir 1999, 15, 5437-5439.

[20] K. Kuhnke, D. M. P. Hoffmann, X. C. Wu, A. M. Bittner, and K. Kern, *Chemical imaging of interfaces by sum-frequency generation microscopy: Application to patterned self-assembled monolayers*, Applied Physics Letters, 83, 18, Nov. 3, 2003.

[21] L. Dreesena, Y. Sartenaera, C. Humberta, A.A. Mania, J.-J. Lemairea, C. Me´thivierb, C.-M. Pradierb, P.A. Thirya, *A. Peremans, Sum-frequency generation spectroscopy applied to model biosensors systems*, Thin Solid Films, 464–465 (2004) 373– 378.

[22] Y. Sartenaer, G. Tourillon, L. Dreesen, D. Lis, A. A. Mani, P. A. Thiry, A. Peremans, *Sum-frequency generation spectroscopy of DNA monolayers*, Biosensors and Bioelectronics 22 (2007) 2179–2183.

[23] Bertrand Busson and Abderrahmane Tadjeddine, *Non-Uniqueness of Parameters Extracted from Resonant Second-Order Nonlinear Optical Spectroscopies*, J. Phys. Chem. C 2009, 113, 21895–21902.

[24] M. Buck and M. Himmelhaus. *Vibrational spectroscopy of interfaces by infrared–visible sum frequency generation*. J. Vac. Sci. Technol. A 19, 2717 (2001)

[25] R. L. P. G. Amaral, N. A. Lemos. *A dipole in a dielectric: Intriguing results and shape dependence of the distant electric field*. Am.J.Phys. 71 (2003) 392-396

[26] M. Bonn, H. Ueba and M. Wolf. *Theory of sum-frequency generation spectroscopy of adsorbed molecules using the density matrix method—broadband vibrational sum-frequency generation and applications*. J. Phys.: Condensed Matter (2005) 17 S201

[27] A. D. Curtis, S. B. Reynolds, A. R. Calchera, and J. E. Patterson. *Understanding the Role of Nonresonant Sum-Frequency Generation from Polystyrene Thin Films*. J. Phys. Chem. Lett. (2010), 1, 2435–2439

[28] EKSPLA. SFG Spectrometer Technical Description & User's Manual (2008). Lithuania

[29] R. E. Walpole, R. H. Myers, S. L. Myers, K. Ye. *Probability & Statistics for Engineers & Scientists* (8th ed.). Pearson Prentice Hall. (2007)

[30] Microsoft. *Microsoft Excel*. Redmond, Washington: Microsoft, Computer Software, (2007).

[31] A. B. Voges, G. Y. Stokes, J. M. Gibbs-Davis, R. B. Lettan II, P. A. Bertin, R. C. Pike, S. T. Nguyen, K. A. Scheidt, and F. M. Geiger. *Insight into heterogeneous atmospheric oxidation chemistry: Development of a Tailor-Made Synthetic Model for Studying Tropospheric Surface Chemistry.* J. Phys. Chem. C 111, 1567-1578, (2007)

[32] WaveMetrics, Inc. *Manual: IGOR Pro* Version 6.0, (2009)

[33] W.H. Whiffen. *Intensities in the Raman Spectrum of Benzene*. Proc. Phys. Soc. London Sect. A 69, 375, (1956)

[34] Z. Chen. *Investigating buried polymer interfaces using sum frequency generation vibrational spectroscopy*. Prog Polym Sci. (2010), 35(11): 1376–1402

Appendix 1

The procedure that was used to fit the experimental data is a code written by Voges et al.[31] in Igor Pro. The code is as follows:

```
// This function is meant to fit an SFG spectra with three peaks
// it includes the three peaks, a nonreasonant term, the cross terms for those three peaks and the NR term,
// as well as phases for the three peaks and the NR term

#pragma rtGlobals=1		// Use modern global access method.

Function Lor3peakNRphase(w,freq) : FitFunc
	Wave w
	Variable freq

	//CurveFitDialog/ These comments were created by the Curve Fitting dialog. Altering them will
	//CurveFitDialog/ make the function less convenient to work with in the Curve Fitting dialog.
	//CurveFitDialog/ Equation:
	//CurveFitDialog/ End of Equation
	//CurveFitDialog/ Independent Variables 1
	//CurveFitDialog/ freq
	//CurveFitDialog/ Coefficients 14
	//CurveFitDialog/ w[0] = freqcenter1
	//CurveFitDialog/ w[1] = amplitude1
	//CurveFitDialog/ w[2] = gamma1
	//CurveFitDialog/ w[3] = freqcenter2
```

```
//CurveFitDialog/ w[4] = amplitude2
//CurveFitDialog/ w[5] = gamma2
//CurveFitDialog/ w[6] = freqcenter3
//CurveFitDialog/ w[7] = amplitude3
//CurveFitDialog/ w[8] = gamma3
//CurveFitDialog/ w[9] = Chi_NR
//CurveFitDialog/ w[10] = Phase1
//CurveFitDialog/ w[11] = Phase2
//CurveFitDialog/ w[12] = Phase3
//CurveFitDialog/ w[13] = PhaseNR


        variable x1, x2, x3, t1, t2, t3, t4, t5, t6, t7, t8, t9, t10, p1, p2, p3, pNR
        x1 = freq-w[0]
        x2 = freq-w[3]
        x3 = freq-w[6]
        p1 = w[10]*Pi/180
        p2 = w[11]*Pi/180
        p3 = w[12]*Pi/180
        pNR = w[13]*Pi/180

    t1=w[1]^2/(x1^2+w[2]^2)
    t2=w[4]^2/(x2^2+w[5]^2)
    t3=2*w[1]*w[4]*(x1*x2*cos(p1-p2)+w[2]*w[5]*cos(p1-p2)+x1*w[5]*sin(p2-
p1)+x2*w[2]*sin(p1-p2))/((x1^2+w[2]^2)*(x2^2+w[5]^2))
    t4= w[7]^2/(x3^2+w[8]^2)
    t5=2*w[1]*w[7]*(x1*x3*cos(p1-p3)+w[2]*w[8]*cos(p1-p3)+x1*w[8]*sin(p3-
p1)+x3*w[2]*sin(p1-p3))/((x1^2+w[2]^2)*(x3^2+w[8]^2))
    t6=2*w[7]*w[4]*(x3*x2*cos(p2-p3)+w[8]*w[5]*cos(p2-p3)+x2*w[8]*sin(p3-
p2)+x3*w[5]*sin(p2-p3))/((x3^2+w[8]^2)*(x2^2+w[5]^2))
```

```
    t7=w[9]^2
    t8=2*w[9]*w[1]*(x1*cos(p1-pNR)+w[2]*sin(p1-pNR))/(x1^2+w[2]^2)
    t9=2*w[9]*w[4]*(x2*cos(p2-pNR)+w[5]*sin(p2-pNR))/(x2^2+w[5]^2)
    t10=2*w[9]*w[7]*(x3*cos(p3-pNR)+w[8]*sin(p3-pNR))/(x3^2+w[8]^2)


return t1+t2+t3+t4+t5+t6+t7+t8+t9+t10


End
```